Oncology and Translational Medicine

Volume 7 • Number 4 • August 2021

Oncology and Translational Medicine Volume 7 • Number 4 • August 2021 pp 149-194

邮发代号：38-121
ISSN 2095-9621

GENERAL INFORMATION
≫otm.tjh.com.cn

ISSN 2095-9621
CN 42-1865/R

Oncology and Translational Medicine

肿瘤学与转化医学（英文）

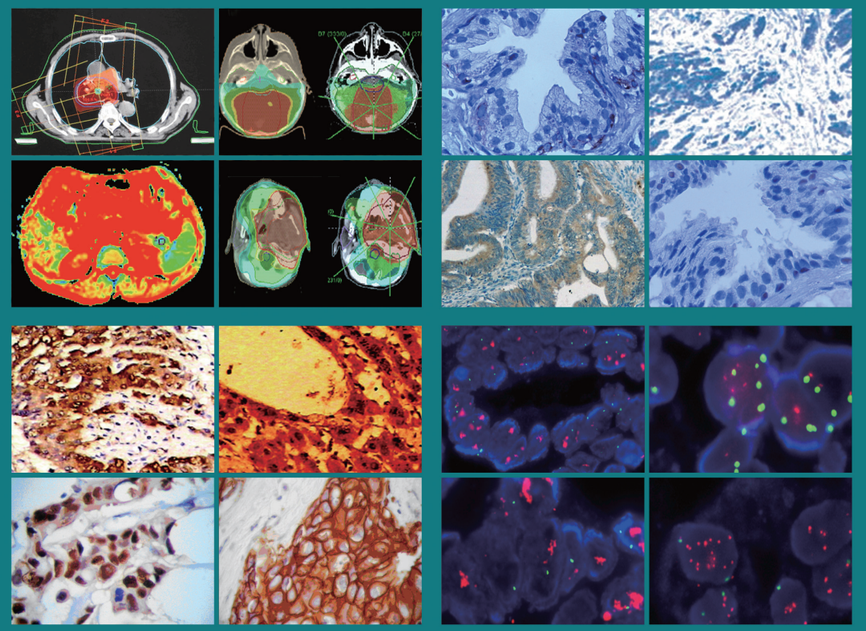

Volume 7
Number 4
August 2021

Oncology and Translational Medicine

Oncology and Translational Medicine
August 2021 Volume 7 Number 4

Contents

Oncology and Translational Medicine

Volume 7 • Number 4 • August 2021

Aims & Scope

Oncology and Translational Medicine is an international professional academic periodical. The Journal is designed to report progress in research and the latest findings in domestic and international oncology and translational medicine, to facilitate international academic exchanges, and to promote research in oncology and translational medicine as well as levels of service in clinical practice. The entire journal is published in English for a domestic and international readership.

Copyright

Supervised by

Ministry of Education of the People's Republic of China.

Administered by

Tongji Medical College, Huazhong University of Science and Technology.

Submission information

Manuscripts should be submitted to:
http://otm.tjh.com.cn
dmedizin@sina.com

Subscription information

ISSN edition: 2095-9621
CN: 42-1865/R

■ Subscription rates
Subscription may begin at any time. Remittances made by check, draft or express money order should be made payable to this journal. The price for 2021 is as follows: US $ 30 per issue; RMB ￥28.00 per issue.

Database

Oncology and Translational Medicine is abstracted and indexed in EMBASE, Index Copernicus, Chinese Science and Technology Paper Citation Database (CSTPCD), Chinese Core Journals Database, Chinese Journal Full-text Database (CJFD), Wanfang Data; Weipu Data; Chinese Academic Journal Comprehensive Evaluation Database.

Business correspondence

All matters relating to orders, subscriptions, back issues, offprints, advertisement booking and general enquiries should be addressed to the editorial office.

Mailing address
Editorial office of
Oncology and Translational Medicine
Tongji Hospital
Tongji Medical College
Huazhong University of Science and Technology
Jie Fang Da Dao 1095
430030 Wuhan, China
Tel.: +86-27-69378388
Email: dmedizin@sina.com

Printer
Changjiang Spatial Information Technology Engineering Co., Ltd. (Wuhan) Hangce Information Cartorgraphy Printing Filial, Wuhan, China
Printed in People's Republic of China

Editors-in-Chief

Managing director

Executive editors

Oncology and Translational Medicine
DOI 10.1007/s10330-020-0407-7
August 2021, Vol. 7, No. 4, P149–P154

ORIGINAL ARTICLE

The expression of vascular endothelial growth factor (VEGF)/ endostatin (ES) and VEGF receptor 2 (VEGFR2)/ES is associated with NSCLC prognosis*

Yuan Yang[1], Baohua Lu[1] (Co-first author), Baolan Li[1] (✉), Weiying Li[2], Mei Jiang[2], Wentao Yue[2], Qunhui Wang[1], Tongmei Zhang[1]

[1] General Department of Medicine, Beijing Chest Hospital, Capital Medical University, Beijing 101149, China
[2] Laboratory of Cell Biotechnology, Beijing Tuberculosis and Thoracic Tumor Research Institute, Beijing 101149, China

Abstract

Objective The aim of our study was to detect the expression of angiogenesis inhibitory proteins and angiogenesis promotive proteins in the postoperative tumor tissue of non-small cell lung cancer (NSCLC) patients. We also investigated the relationship of protein expression with clinical characteristics and prognosis.

Methods We examined the expression of vascular endothelial growth factor (VEGF), VEGF receptor 2 (VEGFR2), and endostatin (ES) proteins in 255 specimens resected from NSCLC patients, using immune histochemistry (IHC). We then evaluated the relationships between the expression of the three proteins and clinical characteristics such as stage, histological type, differentiation, gender, tobacco use, and age. According to the value of VEGF/ES, we divided the cohort into angiogenesis-promoting group A, angiogenesis-inhibiting group A, and balance group A. The survival differences in the three groups were evaluated to determine the prognostic value of VEGF/ES. Similarly, we tested the prognostic value of VEGFR2/ES.

Results VEGF-positive expression was observed in 93 patients (36.4%). VEGF expression was not correlated with the clinical characteristics. VEGFR2-positive expression was observed in 103 patients (40.4%). The expression of VEGFR2 was correlated with the clinical stage (χ^2 = 21.414, P = 0.045) and histological type (χ^2 = 26.911, P = 0.008). ES-positive expression was observed in 140 patients (54.9%). The expression of ES was correlated with the clinical stage (χ^2 = 26.504, P = 0.009). When evaluating the prognostic values of VEGF/ES and VEGFR2/ES, the prognosis of the angiogenesis balance group was similar to that of the angiogenesis-inhibiting group. The minimum survival time was observed in the angiogenesis-promoting group.

Conclusion VEGF/ES and VEGFR2/ES in resected tumors have prognostic value in postoperative NSCLC patients. The survival time of the population with predominant angiogenic factors was short.

Key words: non-small cell lung cancer (NSCLC); angiogenesis; clinical characteristics; prognosis

List of abbreviations VEGF (vascular endothelial growth factor); VEGFR2 (vascular endothelial growth factor receptor 2); ES (endostatin); NSCLC (non-small cell lung cancer); IHC (immunohistochemical); EGFR (epidermal growth factor receptor); ALK (anaplastic lymphoma kinase); ROS1 (c-ros oncogene 1 receptor kinase); TNM (tumor, lymphnode, metastasis); HR (hazard ratio); SCLC (small cell lung cancer); SFDA (State Food and Drug Administration); ERK (extracellular regulated protein kinases); MAPK (mitogen-activated protein kinase)

Received: 25 February 2020
Revised: 23 January 2021
Accepted: 15 March 2021

Lung cancer is the most common cancer worldwide. In both sexes combined, lung cancer is the most commonly diagnosed cancer (11.6% of the total cases) and the leading cause of cancer death (18.4% of the total cancer deaths)[1]. Lung cancer is the most life-threatening cancer in China[2]. Non-small cell lung cancer (NSCLC) is the most common type of lung cancer.

As early as 1971, Folkman proposed that the growth

✉ Correspondence to: Baolan Li. Email: fuseagull@163.com
* Supported by the Natural Science Foundation of China (No. 81602531).

and metastasis of tumors depended on neovascularization within tumors [3]. Since then, many studies have been devoted to the treatment of tumors by blocking neovascularization.

Tumor angiogenesis is regulated by both anti-angiogenic and pro-angiogenic factors. The growth and metastasis of tumors require sustained angiogenesis to provide oxygen and nutrients and to excrete metabolites. Tumor tissue induces an "angiogenesis shift," which is why pro-angiogenic factors are often overexpressed in tumor tissue, while the expression of anti-angiogenic factors is limited [4].

Vascular endothelial growth factor-A (VEGF-A, also known as VEGF) is the most important pro-angiogenic factor that promotes the proliferation, migration, infiltration, and survival of endothelial cells. A study showed that serum VEGF levels might be a predictor of disease prognosis in different types of cancers [5]. VEGF receptor 2 (VEGFR2) is the most important VEGF receptor [4]. Many drugs are used in clinical practice to effectively inhibit the downstream signaling of the VEGF-VEGFR2 pathway, such as bevacizumab (the monoclonal antibodies targeting VEGF) and ramucirumab and apatinib [6] (the receptors of VEGFR2).

Endostatin (ES) is an important anti-angiogenesis factor that was isolated from mouse endothelial cell tumors for the first time in 1997 [7]. Endostatin has an intense and complete inhibitory effect on tumor-induced angiogenesis, showing strong anti-tumor activity. Endostar is an artificially modified vascular endothelial inhibitor that was extracted by Chinese scholars through the *E. coli* expression system in 1999 [8]. Endostar combined with chemotherapy showed good antitumor effects [9].

We hypothesized that the expression of angiogenesis-promoting and angiogenesis-inhibiting factors is imbalanced in patients with NSCLC. To date, many angiogenic promoters and inhibitors have been found to be involved in the regulation of tumors; however, VEGF-VEGFR2 and ES are amongst the most important factors; they play positive and negative regulatory roles in angiogenesis, respectively.

We designed this retrospective cohort study to evaluate the balance between VEGF and the inhibition of endothelial growth factor in resectable NSCLC.

Materials and methods

Patients and tissue specimens

We included 255 patients who underwent surgery for NSCLC at the Beijing Chest Hospital, Capital Medical University, China, between July 2008 and October 2009. Pathological surgical staging was performed according to the 8th edition TNM staging classification for lung cancer. Our study included patients with stage IA–IIIA disease, a small proportion of stage IIIB patients who were diagnosed locally or after surgery, and stage IV patients with single brain or adrenal metastasis. Previous studies have reported that the expression of VEGF, VEGFR2, and ES is significantly higher in tumor tissues and plasma than in normal tissues [8–13]; therefore, we did not establish a healthy control group. None of the patients received radiotherapy, chemotherapy, orangiogenesis inhibitors before surgery. Patients who died during the perioperative period were excluded.

The experiment was completed in 2010, and the deadline for follow-up was from May 2018 to June 2018. The median observation period of these patients was 10 years.

Reagents

Primary VEGF antibody and primary VEGFR2 antibody were purchased from Fuzhou MaiXin Biotechnology Company, China. Primary ES antibody was purchased from Beijing Biosynthesis Biotechnology Company, China. The Novolink™ polymer detection system was purchased from Novocastra Laboratories, USA.

Immunohistochemical analysis

Tumor tissue sections (4–6 μm thick) were fixed in formalin, paraffin-embedded, and dried for 1 h at 60 °C. The sections were washed with phosphate buffered Saline, incubated with hydrogen peroxide for 5 min at room temperature, washed again with phosphate buffered Saline, incubated with protein blocker for 5 min at room temperature. Primary antibodies against VEGF, VEGFR2, and ES were incubated with the same tissue sections at 4 °C. The sections were washed, incubated with Post Primary Block for 15 min, and then incubated with Novolink™ polymer for 15 min. The sections were stained with DAB (3,3-diaminobenzidine) working solution for approximately 5 min and counterstained with hematoxylin for 5 min.

Evaluation of immunohistochemical analysis

We used as emi-quantitative method to assess the expression of VEGF, VEGFR2, and ES. We estimated a weighted average of the percentage of tumor cells stained on whole tumor slides (0 = positive staining in 0–10% of the tumor cells, 1 = positive staining in 11%–25% of the tumor cells, 2 = positive staining in 26%–50% of the tumor cells, and 3 = positive staining in more than 51% of the tumor cells). The staining intensity was also evaluated in a semi-quantitative manner, representing the average intensity of the tumor cells (0 = no staining, 1 = weak staining, 2 = moderate staining, and 3 = strong staining, equivalent to the positive control, which showed clear, well-defined, and strong staining). The intensity and

proportion scores were then multiplied to obtain a total score ranging from 0 to 9, with 0 = no staining (–), 1–3 = weak positive (+), 4–6 = moderate positive (++), and 7–9 = strong positive (+++). We defined (–, +) as negative expression, which could also be defined as low expression, and we defined (++, +++) as positive expression, which could also be defined as high expression.

Statistical analysis

Statistical analysis was performed using SPSS version 19.0 (IBM Corp., Armonk, NY, USA), and the groups were compared using Chi-Square tests. The survival rate was calculated using the Kaplan-Meier method and compared using the log-rank test. We used the Cox step-back regression model to understand the multivariate analysis related to overall survival, which yielded hazard ratios (HRs) of $P < 0.05$, which were considered significant in all of our analyses.

Results

The expression of VEGF, VEGFR2, and ES

The demographic features of the patients included in this study are presented in Table 1. The expression levels of VEGF, VEGFR2, and ES are summarized in Table 2.

Correlations between VEGF staining and clinical features

VEGF staining of the cytoplasm of malignant cells accounted for 36.4% of high expression, and 93 of the 255 specimens showed moderate/strong staining, as shown in Fig. 1a (adenocarcinoma cells) and 1d (squamous cell carcinoma cells). Regarding the percentage of positively stained malignant cells in the tumor tissue, the expression of VEGF did not show significant differences in terms of the clinical stage ($\chi^2 = 10.083$, $P = 0.609$), histological type ($\chi^2 = 17.425$, $P = 0.134$), differentiation ($\chi^2 = 12.175$, $P = 0.432$), sex ($\chi^2 = 2.182$, $P = 0.902$), tobacco use ($\chi^2 = 5.735$, $P = 0.453$), and age ($\chi^2 = 1.872$, $P = 0.765$).

Correlations between VEGF2 staining and clinical features

VEGFR2 staining of the cytoplasm of malignant cells accounted for 40.4% of high expression, and 103 of the 255 specimens showed moderate/strong staining. Staining was mainly observed in the cytoplasm, and a few tumors stained positively on the cell membrane, as shown in Fig. 1b (adenocarcinoma cells) and 1e (squamous cell carcinoma cells).

The percentage of positive tumor cells was different between the clinical stage ($\chi^2 = 21.414$, $P = 0.045$) and histological type ($\chi^2 = 26.911$, $P = 0.008$), and the cells did not show a significant difference in terms of differentiation ($\chi^2 = 11.616$, $P = 0.478$), sex ($\chi^2 = 7.619$, $P = 0.267$), tobacco use ($\chi^2 = 5.056$, $P = 0.537$), and age ($\chi^2 = 1.971$, $P = 0.715$).

Table 1 The demographic features of these patients

Patient demographics	No. of patients	%
Total	255	
Gender		
Male	177	69.4
Female	78	30.6
age (year)		
< 65	176	69.0
≥ 65	79	31.0
Histological type		
Adenocarcinoma	110	43.2
Squamous carcinoma	127	49.8
Adeno-squamous cell carcinoma	8	3.1
Large-cell carcinoma	2	0.8
Bronchioloalveolar-carcinoma	8	3.1
Differentiation		
Poorly	37	14.5
Poorly-moderately	54	21.2
Moderately	141	55.3
Moderately-well differentiated	18	7.1
Well differentiated	5	1.9
Clinical stage		
I	91	35.6
II	50	19.6
III	95	37.3
IV	19	7.5
Tobacco use		
Yes	135	52.9
No	120	47.1

Table 2 The IHC expression of VEGF, VEGFR2 and ES [*n* (%)]

Expression	–	+	++	+++
VEGF	44 (17.2)	118 (46.3)	76 (29.8)	17 (6.7)
VEGFR2	23 (9.0)	129 (50.6)	88 (34.5)	15 (5.9)
ES	47 (18.4)	68 (26.7)	127 (49.8)	13 (5.1)

Note: IHC, immunohistochemical; VEGF, vascular endothelial growth factor; VEGFR2, VEGF receptor 2; ES, endostatin

Correlation between ES staining and clinical features

ES staining of the cytoplasm of malignant cells accounted for 54.9% of high expression, and 140 of the 255 specimens showed moderate/strong staining. The cytoplasm was stained, as shown in Fig. 1c (adenocarcinoma cells) and 1f (squamous cell carcinoma cells).

The percentage of positive tumor cells differed among the clinical stages ($\chi^2 = 26.504$, $P = 0.009$), and there was no significant difference observed in terms of the histological type ($\chi^2 = 8.344$, $P = 0.758$), differentiation ($\chi^2 = 11.839$, $P = 0.459$), sex ($\chi^2 = 3.024$, $P = 0.806$), tobacco use ($\chi^2 = 3.378$, $P = 0.760$), and age ($\chi^2 = 3.946$, $P = 0.139$).

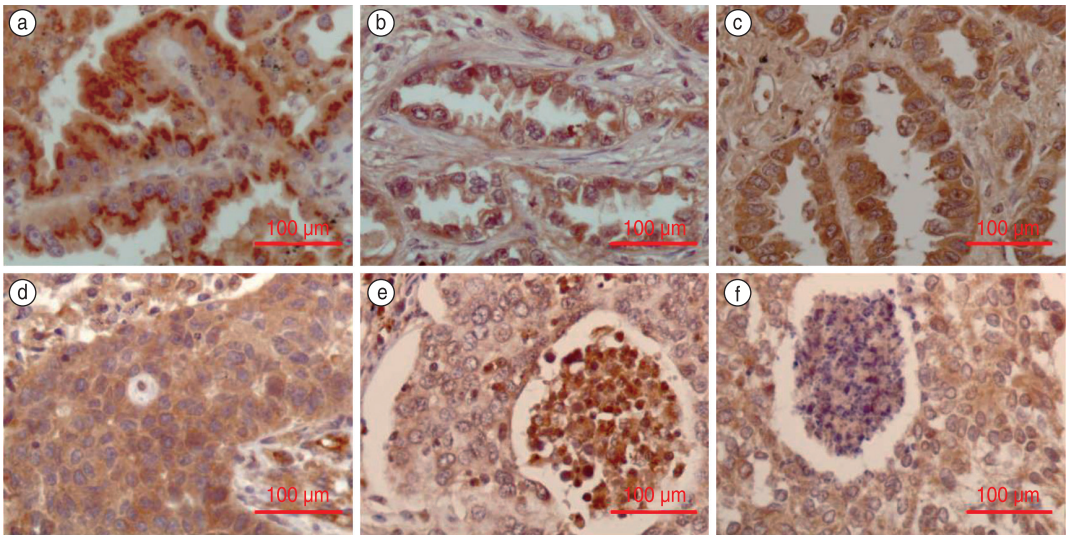

Fig. 1 (a) positive VEGF staining in adenocarcinoma; (b) positive VEGFR2 staining in adenocarcinoma; (c) positive ES staining in adenocarcinoma; (d) positive VEGF staining in squamous cell carcinoma; (e) positive VEGFR2 staining in squamous cell carcinoma; (f) positive ES staining in squamous cell carcinoma. Note: VEGF, Vascular endothelial growth factor; VEGFR2: VEGF receptor 2; ES, Endostatin (Immunohistochemistry staining, 40 × optical microscopy)

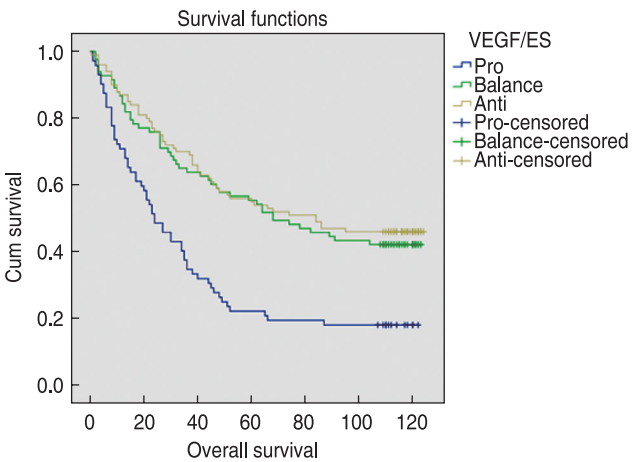

Fig. 2 Survival curves in pro-angiogenesis group A, balance-angiogenesis group A and anti-angiogenesis group A

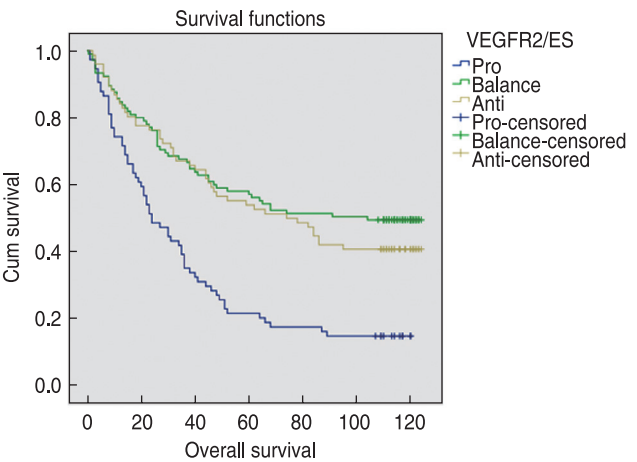

Fig. 3 Survival curves in pro-angiogenesis group B, balance-angiogenesis group B and anti-angiogenesis group B

The survival differences among the anti-angiogenesis group, pro-angiogenesis group, and balance group

According to the IHC score, when the VEGF score was greater than the ES score, it was placed in the pro-angiogenesis group A (pro-A, including 72 patients); when the VEGF score was equal to the ES score, it was placed in the balance group A (bal-A, including 83 patients); and when the VEGF score was less than the ES score, it was placed in the anti-angiogenesis group A (ant-A, including 100 patients).

Similarly, when the VEGFR2 score was greater than the ES score, it was placed in the pro-angiogenesis group B (pro-B, including 74 patients); when the VEGFR2 score was equal to the ES score, it was placed in the balance group B (bal-B, including 105 patients); and when the VEGFR2 score was less than the ES score, it was placed in the anti-angiogenesis group B (ant-B, including 76 patients).

The median survival time of the pro-A group was 24 months (first quartile, 9 and third quartile, 49 months). The median survival time of the bal-A group was 68 months (first quartile, 26 and third quartile, 115 months). The median survival time of the ant-A group was 84 months (first quartile, 26 and third quartile, 116 months). The difference was statistically significant ($P < 0.001$).

Table 3 Univariate and multivariate analysis of overall survival

Factors	Univariate analysis			Multivariate analysis		
	P-value	HR	95% CI	*P*-value	HR	95% CI
Age (< 65 years *vs*. ≥ 65 years)	0.244	1.214	0.876–1.682			
Gender (male *vs*. female)	0.712	1.064	0.764–1.484			
Histology types (non-SCC *vs*. SCC)	0.097	1.301	0.953–1.776			
Tumor differentiation (poorly *vs*. poorly-moderately *vs*. moderately *vs*. moderately-well differentiated *vs*. well differentiated)	0.011	0.794	0.664–0.949	0.042	0.825	0.685–0.993
TNM stage (stage I *vs*. stage II *vs*. stage III *vs*. stage IV)	< 0.001	1.756	1.501–2.054	< 0.001	1.720	1.465–2.020
Smoking status (smoker *vs*. nonsmoker)	0.848	1.031	0.756–1.404			
VEGF/ES (pro-group *vs*. balance-group *vs*. anti-group)	< 0.001	0.650	0.534–0.791	< 0.001	0.671	0.554–0.814
VEGFR2/ES (pro-group *vs*. balance-group *vs*. anti-group)	< 0.001	0.654	0.528–0.810	0.069	0.779	0.595–1.020

Note: SCC, squamous cell carcinoma; TNM, tumor-node-metastasis; VEGF, vascular endothelial growth factor; ES, endostatin; VEGFR2, VEGF receptor 2; HR, hazard ratio; 95% CI, 95% confidence interval

The survival curves are shown in Fig. 2.

The median survival time of the pro-B group was 24 months (first quartile, 10 and third quartile, 51 months). The median survival time of the bal-B group was 104 months (first quartile, 26 and third quartile, 118 months). The median survival time of the ant-B group was 76 months (first quartile, 27 and third quartile, 114 months). The difference was statistically significant ($P < 0.001$). The survival curves are shown in Fig. 3.

The Cox proportional hazard model was used to determine multiple factors related to OS. The results showed that smoking, sex, age, and histological type were not correlated with survival, while the disease stage ($P < 0.001$), degree of differentiation ($P = 0.042$), and VEGF/ES ($P < 0.001$) were independent factors related to survival (Table 3).

Discussion

Since Folkman proposed the theory of tumor angiogenesis [13–14], "starvation of tumors" has become the fourth major treatment for tumors, in addition to surgery, chemotherapy, and radiotherapy.

From the molecule to the cell and then to the organ – there is a process of regulation in organisms to achieve system balance. Angiogenesis is also a process of confrontation between promoters and inhibitors. Angiogenesis and inflammation are involved in the process of wound healing. Tissue injury activates angiogenesis factors that promote the growth of granulation tissue and tissue repair. This process is strictly regulated by angiostatin, to avoid excessive scar formation [15]. Tissue wounds are ultimately repaired or scarred; however, the proliferation and invasiveness of tumors are different processes compared to the tissue/wound healing process. Tumors are chronic stimuli that result in "never-healing wounds" [16].

Our research showed that postoperative NSCLC patients with higher levels of anti-angiogenic factors had longer survival times than patients with pro-angiogenic factors, according to the expression of VEGF/ES and VEGFR2/ES.

The balance group included patients with anti-angiogenic factors that were similar to pro-angiogenic factors. Patients in the balance group had a survival time that was close to or even longer than those in the anti-angiogenesis group. We infer that in the process of tumor angiogenesis, when angiogenesis factors are strong, feedback leads to an increase in the levels of angiogenesis-inhibiting factors. When the factors promoting and inhibiting angiogenesis reach a relatively stable state, tumor growth slows down. Systemic homeostasis prolongs the overall survival of patients. This may also explain the accelerated progression of tumors when anti-angiogenic drugs are withdrawn.

We further hypothesized that there would be a more suitable population for anti-angiogenesis therapy, which may benefit more from anti-angiogenesis therapy with a high expression of the angiogenesis promoter. The effect of anti-angiogenesis therapy may be limited in patients with strong tumor inhibitors and in patients with a balance of promotion and inhibition factors. This is an inference that needs to be confirmed by further research. This phenomenon may also explain why some multicenter clinical studies have shown that anti-angiogenesis therapy can prolong the survival of patients, but its efficacy is limited [17].

At present, many pro-angiogenic and anti-angiogenic factors have been identified. VEGF and ES are the most important factors. VEGF/VEGFR2 promotes endothelial cell proliferation and migration, which increases vascular permeability and angiogenesis. When VEGF is combined with VEGFR2, it activates signaling pathways, including the MAPK, ERK, and ATK pathways, leading to endothelial cell proliferation and angiogenesis. ES can inhibit angiogenesis through many signaling pathways, including the VEGF-triggered signaling pathway [18]. In contrast, ES leads to the up-regulation of VEGF. In a

murine lung cell line transfected with the ES gene, ES protein was secreted, and the expression of VEGF protein was increased [19]. The test showed that ES upregulates the VEGF protein. Thus, we concluded that we should combine these two important indicators (VEGF and ES) to evaluate the status of angiogenesis.

Abdollahi *et al* [20] established the concept of "direct" angiogenesis inhibitor ES and "indirect" anti-angiogenic inhibitor VEGFR2-TKI. The difference between direct and indirect agents is whether their target is microvascular endothelial cells. VEGFR2 is the most important and specific receptor for VEGF. They confirmed that the combination of low-dose ES and VEGFR2-TKI could remarkably reduce tumor growth when compared tomono-agent therapy in diverse human xenograft models. Niu *et al* [21] established an animal model and treated subcutaneously-implanted tumors in mice with ES, bevacizumab, or a combination of the two drugs. They found that combining bevacizumab with ES resulted in better results than the use of a single drug.

Based on these studies, we speculated that the combined use of direct angiogenesis ES and indirect anti-angiogenic bevacizumabin NSCLC could achieve better efficacy. We chose patients with strong angiogenic factors and then treated them with bevacizumab and ES to achieve better results.

However, more clinical trials are needed to confirm this as our research is retrospective, and we only observed that people with high levels of angiogenesis-promoting factors have the worst prognosis. Therefore, more prospective clinical studies are required to verify our findings.

Ethics approval and consent to participate

All procedures performed in this study that involved human participants were in accordance with the ethical standards of the Institutional and National Research Committee and with the 1964 Declaration of Helsinki and its later amendments or comparable ethical standards. Informed consent was obtained from all the participants enrolled in this study.

Conflicts of interest

The authors indicated no potential conflicts of interest.

References

1. Bray F, Ferlay J, Soerjomataram I, *et al*. Global cancer statistics 2018: GLOBOCAN estimates of incidence and mortality worldwide for 36 cancers in 185 countries. CA Cancer J Clin, 2018, 68: 394–424.
2. Chen WQ, Zheng RS, Baade PD, *et al*. Cancer statistics in China, 2015. CA Cancer J Clin, 2016, 66: 115–132.
3. Folkman J. Tumor angiogenesis: therapeutic implications. N Engl J Med, 1971, 285: 1182–1186.
4. Alevizakos M, Kaltsas S, Syrigos KN. The VEGF pathway in lung cancer. Cancer Chemother Pharmacol, 2013, 72: 1169–1181.
5. Lin YC, Zeng D, Wang HB, *et al*. Clinical significance of serum vascular endothelial growth factor in advanced malignant tumors. Chinese-German J Clin Oncol, 2008, 7: 611–614.
6. Wang L, Lu J, Liu Y, *et al*. A retrospective analysis of the safety and efficacy of apatinib in treating advanced metastatic colorectal cancer. Oncol Transl Med, 2017, 3: 210–216.
7. O'Reilly MS, Boehm T, Shing Y, *et al*. Endostatin: an endogenous inhibitor of angiogenesis and tumor growth. Cell, 1997, 88: 277–285.
8. Carrillo de Santa Pau E, Arias FC, Caso Peláez E, *et al*. Prognostic significance of the expression of vascular endothelial growth factors A, B, C, and D and their receptors R1, R2, and R3 in patients with nonsmall cell lung cancer. Cancer, 2009, 115: 1701–1712.
9. Ming PP, Ge W, Liu L, *et al*. 117 cases of advanced malignancies treated with recombinant human endostatin plus chemotherapy. Chinese-German J Clin Oncol, 2013, 12: 61–64.
10. Szarvas T, László V, Vom Dorp F, *et al*. Serum endostatin levels correlate with enhanced extracellular matrix degradation and poor patients' prognosis in bladder cancer. Int J Cancer, 2012, 130: 2922–2929.
11. Woo IS, Kim KA, Jeon HM, *et al*. Pretreatment serum endostatin as a prognostic indicator in metastatic gastric carcinoma. Int J Cancer, 2006, 119: 2901–2906.
12. Feldman AL, Pak H, Yang JC, *et al*. Serum endostatin levels are elevated in patients with soft tissue sarcoma. Cancer, 2001, 91: 1525–1529.
13. Folkman J. Antiangiogenesis in cancer therapy – endostatin and its mechanisms of action. Exp Cell Res, 2006, 312: 594–607.
14. Gordon MS, Margolin K, Talpaz M, *et al*. Phase I safety and pharmacokinetic study of recombinant human anti-vascular endothelial growth factor in patients with advanced cancer. J Clin Oncol, 2001, 19: 843–850.
15. Abdollahi A, Hlatky L, Huber PE. Endostatin: the logic of antiangiogenic therapy. Drug Resist Updat, 2005, 8: 59–74.
16. Dvorak HF. Tumors: wounds that do not heal-redux. Cancer Immunol Res, 2015, 3: 1–11.
17. Vokes EE, Salgia R, Karrison TG. Evidence-based role of bevacizumab in non-small cell lung cancer. Ann Oncol, 2013, 24: 6–9.
18. Ling Y, Yang Y, Lu N, *et al*. Endostar, a novel recombinant human endostatin, exerts antiangiogenic effect via blocking VEGF-induced tyrosine phosphorylation of KDR/Flk-1 of endothelial cells. Biochem Biophys Res Commun, 2007, 361: 79–84.
19. Cui R, Takahashi K, Takahashi F, *et al*. Endostatin gene transfer in murine lung carcinoma cells induces vascular endothelial growth factor secretion resulting in up-regulation of *in vivo* tumorigenecity. Cancer Lett, 2006, 232: 262–271.
20. Abdollahi A, Lipson KE, Sckell A, *et al*. Combined therapy with direct and indirect angiogenesis inhibition results in enhanced antiangiogenic and antitumor effects. Cancer Res, 2003, 63: 8890–8898.
21. Niu N, Li BL, Liu CY, *et al*. Combining bevacizumab with endostatin gets better antitumor efficacy *in vivo* in lung cancer animal model. Chin J Lung Cancer (Chinese), 2013, 16: 61–66.

DOI 10.1007/s10330-020-0407-7
Cite this article as: Yang Y, Lu BH, Li BL, *et al*. The expression of vascular endothelial growth factor (VEGF)/ endostatin (ES) and VEGF receptor 2 (VEGFR2)/ES is associated with NSCLC prognosis. Oncol Transl Med, 2021, 7: 149–154 .

Oncology and Translational Medicine
DOI 10.1007/s10330-020-0440-0

August 2021, Vol. 7, No. 4, P155–P159

ORIGINAL ARTICLE

Relationship between molecular changes in epidermal growth factor receptor (*EGFR*) and anaplastic lymphoma kinase (*ALK*) mutations in lung adenocarcinoma*

Rina Na[1], Wei Luan[2] (Co-first author), Yinzai He[3], Yanwei Gao[3], Nier Cha[3], Baoqin Jia[3] (✉)

[1] Department of General Surgery, Inner Mongolia People's Hospital, Hohhot 010017, China
[2] Department of Oncology, Inner Mongolia People's Hospital, Hohhot 010017, China
[3] Department of Surgical Oncology, Inner Mongolia People's Hospital, Hohhot 010017, China

Abstract

Objective This study aimed to analyze the relationship between the mutations in epidermal growth factor receptor (*EGFR*) and anaplastic lymphoma kinase (*ALK*) and their impact on the prognosis and treatment of lung adenocarcinoma.

Methods A total of 158 cases of lung adenocarcinoma reported between January 2007 and January 2014 were retrospectively analyzed. These tumors were resected using radical pneumonectomy and underwent pathology-based diagnosis at our institution (Inner Mongolia People's Hospital, Hohhot, China). The tissue sections were evaluated using the updated World Health Organization classification of lung adenocarcinomas (2015 version), with each histological component recorded in 5% increments. The histological subtypes were classified, and any surviving cases were followed up. The reverse transcription-polymerase chain reaction (RT-PCR) and direct DNA sequencing were used to evaluate mutations in exons 18, 19, 20, and 21 in the *EGFR* gene, and the echinoderm microtubule-associated protein-like 4 gene-ALK variant (*EML4-ALK*) fusions were detected using sequencing.

Results Our cohort included 25 patients with pre-invasive adenocarcinoma, 13 patients with lepidic, 66 patients with acinar, 13 patients with papillary, and 25 patients with solid infiltrative adenocarcinoma with the remaining cases presenting with a variety of pathological subtypes. The prognosis of each histological subtype was different with the 5-year disease-free survival and 5-year overall survival (OS) of pre-invasion adenocarcinoma at 100%; the 5-year OS of lepidic, acinar, and papillary adenocarcinoma patients was only 84.6%, 72.7%, and 76.9%, respectively. The 5-year OS of solid and mucinous adenocarcinomas were 32.0% and 36.4%, respectively. *EGFR* mutation was detected in 69 cases with a mutation rate of 43.7% and majority of these mutations were found in exons 19 (50.6%) and 21 (37.9%), with women and non-smokers shown to experience a higher mutation rate ($P < 0.05$). However, histological subtype analysis showed that *EGFR* mutations were primarily found in adenocarcinomas. Most of these mutations were found in lepidic (53.8%) or acinar adenocarcinomas (50.0%), whereas these mutations were rare in both solid (28.0%) and mucinous adenocarcinoma (27.2%). The fusion mutation rate in the *EML4-ALK* gene was 5.69%, and was most common in young, nonsmoking patients ($P < 0.05$).

Conclusion The prognosis of patients in each lung adenocarcinoma subtype is different, and these outcomes are likely related to mutations in the *EGFR* and *EML4-ALK* genes. *EGFR* mutation rates are higher in lepidic and acinar adenocarcinomas, whereas *EML4-ALK* gene fusion mutations are more common in solid and mucinous adenocarcinoma. *EGFR* mutations are more common in female and non-smoking patients, whereas *EML4-ALK* fusions are more common in young, non-smoking patients.

Received: 21 June 2020
Revised: 6 June 2021
Accepted: 28 June 2021

Key words: lung cancer; histological subtypes; prognosis; the echinoderm microtubule-associated protein-like 4 gene-ALK variant (*EML4-ALK*); epidermal growth factor receptor (*EGFR*)

✉ Correspondence to: Baoqin Jia. Email: 13604715646@qq.com
* Supported by a grant from the Sciences Foundation of Health Commission of Inner Mongolia Autonomous Region (No. 201701008).

More than half of all newly diagnosed non-small cell lung cancer is lung adenocarcinoma that has variable genetic and morphological patterns and presents with a variety of clinicopathological characteristics. The World Health Organization (WHO) published a new classification system for lung tumors in 2015 which relies on histology-based classification terms [1]. Epidermal growth factor receptor (*EGFR*) and anaplastic lymphoma kinase (*ALK*) have been identified as the critical genetic drivers for lung adenocarcinoma, and both act as critical prognostic factors in this disease. This study aimed to explore the relationship between the various histological types of lung adenocarcinoma and common gene mutations, as well as the clinicopathological characteristics of these patients in an effort to provide new insights into individualized treatments for this disease.

Materials and methods

Tissue samples

We collected the data from 158 cases of lung adenocarcinoma treated at the Department of Oncology, Inner Mongolia People's Hospital, Hohhot, China, between January 2007 and January 2014. All patients signed an informed consent and both the clinical and pathological data of the patients were reviewed, and the relevant information was recorded, including gender, age, smoking history, tumor size, tumor location, and tumor stage. Any patients receiving preoperative adjuvant radio- or chemotherapy were excluded, and staging (tumor, lymph node, and metastasis) was performed according to the guidelines established in the 7th edition of the United States Joint Committee on lung cancer staging system. The follow-up information collected for surviving patients included preoperative staging, surgical methods and the treatment outcome of patients after operation, etc.

Pathological examinations

Hematoxylin and eosin (H&E)-stained sections from each of the tissue samples were re-examined by two experienced pathologists and classified using the new WHO lung adenocarcinoma classification system (2015). These reexaminations included a reevaluation of the e morphological standard and the histological subtype of the tumor which were then classified as: *in situ* adenocarcinoma (AIS), minimal invasive adenocarcinoma (MIA), lepidic adenocarcinoma (LPA), acinar adenocarcinoma, papillary adenocarcinoma, solid adenocarcinoma with mucus formation, micropapillary adenocarcinoma, invasive mucinous adenocarcinoma, enteric adenocarcinoma, and colloidal carcinoma. Each histological component was recorded in 5% increments and the degree of tumor differentiation, tumor thrombus, mitotic number (/10 hpf), necrosis and the relationship between the tumor and pleura were evaluated and recorded. All diagnostic criteria were then omitted.

Specimen preparation

All samples were fixed in neutral formaldehyde and embedded in paraffin. The blocks with tumor tissue were selected and each paraffin block was cut into 4-micron-thick sections, subjected to H&E staining and evaluated under a microscope. A block with a tumor component ratio of greater than 75% was selected for each case. Four to five 5 μM thick sections were placed into a 1.5 mL tube and then subjected to genetic evaluation. Genetic analysis of the tumor was performed in 158 patients. *EGFR* mutations were detected by Sanger sequencing or amplification refractory mutation system, as previously described. *ALK* alterations were detected by fluorescence *in situ* hybridization with ALK break apart probes and/or immunohistochemistry (IHC) staining with Ventana anti-ALK antibody as previously described. Mutations in exons 18, 19, 20 and 21 of the *EGFR* gene and the echinoderm microtubule-associated protein-like 4 gene-ALK variant *(EML4-ALK)* fusions were analyzed by reverse transcription-polymerase chain reaction (RT-PCR) and direct DNA sequencing.

Statistical analysis

SPSS 22.00 (IBM Corp., Armonk, NY, USA) was used to analyze the data. Chi-square analysis was used to evaluate the correlation between *EGFR* and *ALK* mutations and associated information, and the log-rank test was used to evaluate the survival rate in each group. A P value of < 0.05 was set as statistically significant.

Results

Our cohort comprised of 70 males and 88 females at an average age of 59.1 years (30–77 years), with these 158 participants including 120 nonsmokers (75.9%). Our participants spanned various tumor types and stages, with 63 participants in stage I, 44 in stage II, 41 in stage III, and 10 cases at stage IV. These included 25 cases of pre-invasion adenocarcinomas, including lepidic adenocarcinoma (13 cases), acinar adenocarcinoma (66 cases), papillary adenocarcinoma (13 cases), solid adenocarcinoma (25 cases), and other pathological subtypes. The follow-up time spanned between 22–112 months, and four cases (one lepidic, two acinar, one papillary) were lost to follow up. A total of 119 patients survived their initial disease with 13 experiencing tumor recurrence and metastasis, and 35 dying before the end of the study. The prognosis of each histological subtype was different (Table 1), with the 5-year disease-free survival and overall survival (OS) at 100% for *in situ* and minimally invasive adenocarcinoma, and 84.6%, 72.7%, and 76.9% for lepidic, acinar, and

papillary adenocarcinoma, respectively. The 5-year OS rates in solid and mucinous adenocarcinoma were only 32.0% and 36.4%, respectively.

Of the 158 samples, 69 exhibited detectable mutations in the *EGFR* gene, making the overall mutation rate for this gene 43.7%. The majority of these mutations were found in exons 19 (50.6%) and 21 (37.9%), and these mutation rates were significantly higher in female patients (54.5% for women and 30% for men; $P < 0.05$). The mutation rate in the non-smoking group (49.2%) was higher than that of the smoking group (26.3%), with this difference also demonstrating statistical significance ($P < 0.05$). However, age, tumor size, stage, pleural involvement, and lymph node metastasis were

Table 1 Survival and histological subtype of lung adenocarcinomas

Histological subtype	*n*	5-year DFS (%)	5-year OS (%)
Precancerous adenocarcinoma			
Adenocarcinoma *in situ*	5	100	100
Minimal invasive adenocarcinoma	20	100	100
Infiltrating adenocarcinoma			
Mainly lepidic	13	69.2	84.6
Mainly acinar	66	51.5	72.7
Mainly papillary	13	53.8	76.9
Micropapillary	5	0	60.0
Mainly solid	25	0	32.0
Mucinous adenocarcinoma	11	36.4	36.4

Note: DFS, disease-free survival; OS, overall survival

Table 2 Mutational analysis of 158 cases of lung adenocarcinoma [*n* (%)]

Item	*n*	*EGFR* (+)	*EGFR* (–)	*P*	*ALK* (+)	*ALK* (–)	*P*
Gender				0.0000			0.2701
Male	70	21 (30.0)	49 (70.0)		4 (5.7)	66 (94.3)	
Female	88	48 (54.5)	40 (45.5)		5 (5.7)	83 (94.3)	
Age (years)				0.5944			0.0000
< 55	60	26 (43.3)	34 (56.7)		6 (10.0)	54 (90.0)	
≥ 55	98	42 (42.9)	56 (57.1)		3 (3.1)	95 (96.9)	
Smoking status				0.0000			0.0049
Non smoking	120	59 (49.2)	99 (40.8)		8 (6.7)	112 (93.3)	
Smoking	38	10 (26.3)	28 (73.7)		1 (2.6)	37 (97.4)	
Histological subtype				0.3369			0.0019
Precancerous adenocarcinoma							
AIS	5	3 (60.0)	2 (40.0)		0 (0.0)	5 (100.0)	
MIA	20	9 (45.0)	11 (55.0)		1 (5.0)	19 (95.0)	
Infiltrating adenocarcinoma							
Lepidic	13	7 (53.8)	6 (46.2)		0 (0.0)	13 (100.0)	
Acini	66	33 (50.0)	33 (50.0)		2 (3.1)	64 (96.9)	
Papillae	13	5 (38.5)	8 (61.5)		0 (0.0)	13 (100.0)	
Mainly solid	25	7 (28.0)	18 (72.0)		3 (12.0)	22 (88.0)	
Micro nipple	5	2 (40.0)	3 (60.0)		0 (0.0)	5 (100.0)	
Mucous adenocarcinoma	11	3 (27.2)	8 (92.8)		3 (27.2)	8 (92.8)	
Tumor size (cm)				0.0311			
≤ 3	107	51 (47.7)	56 (52.3)				
> 3	51	14 (27.5)	37 (72.5)				
Pleural invasion				0.6771			
Yes	88	34 (38.7)	54 (61.3)				
No	70	29 (41.4)	41 (58.6)				
Lymph node metastasis				0.8313			
Yes	40	16 (40.0)	24 (60.0)				
No	118	52 (44.1)	66 (55.9)				
Tumor stage				0.9121			
Stage I	63	36 (57.1)	27 (42.9)				
Stage II	44	25 (56.8)	19 (43.2)				
Stage III	41	18 (43.9)	23 (56.1)				
Stage IV	10	6 (60.0)	4 (40.0)				

Note: *EGFR*, epidermal growth factor receptor; *ALK*, anaplastic lymphoma kinase; AIS, *in situ* adenocarcinoma; MIA, minimal invasive adenocarcinoma

not found to be related to *EGFR* mutation rates in these patients. Histological subtype analysis showed that *EGFR* mutation was more common in lepidic (53.8%) and acinar type adenocarcinomas (50.0%), whereas these mutations were rarer in solid tumors (28.0%) and mucinous adenocarcinomas (27.2%). Fusion mutation, *EML4-ALK*, was identified in 5.69% of the samples and was found to be more common in young and non-smoking patients (all $P < 0.05$). This fusion was also more common in mucinous and solid adenocarcinomas (Table 2).

Discussion

This study demonstrates that the new classification method for lung adenocarcinomas may be predictive for curative effect, prognosis, and tumor metabolism [2–5], and suggests that this new classification method can be used to supplement clinical treatment decision-making using tumor staging. The prognosis of each histological subtype of lung adenocarcinoma is different. Both *in situ* and minimally invasive adenocarcinoma have a 5-year disease-free survival of 100% and a 5-year total survival of 100%, suggesting that these patients may only need surgical resection without adjuvant treatment; the prognosis of lepidic, acinar, and papillary adenocarcinoma is moderate; however, solid and mucinous adenocarcinomas have a 5-year OS of 32.0% and 36.4%, respectively, with very poor prognosis. This suggests that some of these patients may need adjuvant treatment after surgery and a growing number of studies have confirmed that both the micro papilla and solid components are directly related to poorer prognosis [6–7], which has the added value of helping to predict the survival odds of patients independent of tumor stage. The appearance of solid components also indicates that the tumor is more invasive, rendering it necessary to include the micropapillary and solid elements in the pathological report using 5% increments.

Recent evaluations have continued to expand our understanding of the genetic origins and drivers of lung cancer and molecular typing, based on genetic characteristics, helps to take the treatment of advanced lung cancer into the realm of individualized treatment. *EGFR* mutations are an important predictor of targeted therapy in lung adenocarcinoma and have been widely applied in clinical intervention trials. The *EGFR* mutation rate in lung cancers in Caucasian patients is approximately 10%, whereas in Asian patients, it can be as high as 30% to 40% [8]. Most of these mutations occur in young, female, non-smokers and the majority of these *EGFR* mutations have been linked to the clinical characteristics of the tumor, including histology, race, gender, etc. The results of this study showed that the *EGFR* mutation rate in this cohort was 43.7%, with majority of mutations in exons 19 and 21. Women and non-smokers had a higher mutation rate, which is similar to other reports, but there were no correlations between *EGFR* mutation and age, tumor size, stage, pleural involvement or lymph node metastasis. Histological subtype analysis showed that majority of *EGFR* mutations were identified in lepidic and acinar adenocarcinoma, whereas these mutations were rarer in the solid and mucinous adenocarcinoma samples. Histological features such as lepidic structure and acinar structure may predict *EGFR* mutation better than other clinical parameters. It was also found that the *EGFR* mutation rate in mucinous adenocarcinoma was lower (27.2%) than that of non-mucinous adenocarcinomas with lepidic structure (53.8%).

ALK fusions have been shown to define a unique molecular subtype in lung adenocarcinomas. Our data revealed a 5.69% occurrence of *ALK* fusion mutations in the lung adenocarcinomas of this cohort, with the average age of these patients being significantly lower than the *ALK*-negative group, which was consistent with other results in the literature [9]. The relationship between smoking history and *ALK* fusions is controversial, with several studies suggesting that *ALK* fusions are more common in nonsmokers, but several other papers reporting that smoking history is not a significant factor in *ALK* fusion mutations. This study shows that *ALK* fusions were significantly more common in nonsmokers in this cohort, but the specific mechanism underlying this correlation requires further study. There was no significant difference in the *ALK* fusion rate between the sexes which is significantly different from the *EGFR* gene, where these mutations are generally believed to be more common in women. Studies from western countries have suggested that *ALK* fusion-positive cases are more common in acinar like tumors [10], whereas others have found that Japanese patients with mucus secretion and cribriform-like lung adenocarcinomas have higher *ALK*-positive rates [11]. However, studies in China show that the *ALK* mutation rates are significantly higher in infiltrating mucinous and solid infiltrating adenocarcinomas in Chinese patients. There were no fusion mutations in pre-invasion adenocarcinomas, suggesting that these fusions may be a late event in the development of lung cancer. Early detection is one of the most relevant limiting factors in the treatment of lung cancer. This work may contribute to the early detection of lung cancer.

Conflicts of interest

The authors indicated no potential conflicts of interest.

References

1. Travis WD, Brambilla E, Nicholson AG, *et al*. The 2015 World Health Organization Classification of Lung Tumors: Impact of genetic, clinical and radiologic advances since the 2004 Classification. J Thorac

Oncol, 2015, 10: 1243–1260.
2. Kadota K, Colovos C, Suzuki K, *et al*. FDG-PET SUVmax combined with IASLC/ATS/ERS histologic classification improves the prognostic stratification of patients with stage I lung adenocarcinoma. Ann Surg Oncol, 2012, 19: 3598–3605.
3. Chiu CH, Yeh YC, Lin KH, *et al*. Histological subtypes of lung adenocarcinoma have differential ^{18}F-fluorodeoxyglucose uptakes on the positron emission tomography/computed tomography scan. J Thorac Oncol, 2011, 6: 1697–1703.
4. Kadota K, Nitadori JI, Sarkaria IS, *et al*. Thyroid transcription factor-1 expression is an independent predictor of recurrence and correlates with the IASLC/ATS/ERS histologic classification in patients with stage I lung adenocarcinoma. Cancer, 2013, 119: 931–938.
5. Warth A, Muley T, Meister M, *et al*. The novel histologic International Association for the study of Lung Cancer/American Thoracic Society/European Respiratory Society classification system of lung adenocarcinoma is a stage-independent predictor of survival. J Clin Oncol, 2012, 30: 1438–1446.
6. Nakashima H, Jiang SX, Sato Y, *et al*. Prevalent and up-regulated vimentin expression in micropapillary components of lung adenoeareinomas and its adverse prognostic significance. Pathol Int, 2015, 65: 183–192.
7. Nagano T, Ishii G, Nagai K, *et al*. Structural and biological properties of a papillary component generating a micropapillary component in lung adenocarcinoma. Lung Cancer, 2010, 67: 282–289.
8. Shi Y, Au JS, Thongprasert S, *et al*. A prospective, molecular epidemiology study of *EGFR* mutations in Asian patients with advanced non-small-cell lung cancer of adenocarcinoma histology (PIONEER). J Thorac Oncol, 2014, 9: 154–162.
9. Wu YL, Fukuoka M, Mok TSK, *et al*. Tumor response and health-related quality of life in clinically selected patients from Asia with advanced non-small-cell lung cancer treated with first-line gefitinib: post hoc analyses from the IPASS study. Lung Cancer, 2013, 81: 280–287.
10. Inamura K, Takeuchi K, Togashi Y, *et al*. EML4-ALK lung cancers are characterized by rare other mutations, a TTF-1 cell lineage, an acinar histology, and young onset. Mod Pathol, 2009, 22: 508–515.
11. Sakairi Y, Nakajima T, Yasufuku K, *et al*. *EML4-ALK* fusion gene assessment using metastatic lymph node samples obtained by endobronchial ultrasound-guided transbronchial needle aspiration. Clin Cancer Res, 2010, 16: 4938–4945.

DOI 10.1007/s10330-020-0440-0
Cite this article as: Na RN, Luan W, He YZ, *et al*. Relationship between molecular changes in epidermal growth factor receptor (*EGFR*) and anaplastic lymphoma kinase (*ALK*) mutations in lung adenocarcinoma. Oncol Transl Med, 2021, 7: 155–159.

Oncology and Translational Medicine
DOI 10.1007/s10330-020-0468-8

August 2021, Vol. 7, No. 4, P160–P164

ORIGINAL ARTICLE

Efficacy and adverse reactions of apatinib as second-line or later-line treatment in advanced lung cancer

Tao Ren[1], Yan Wu[2] (✉)

[1] Department of Oncology, The First People's Hospital of Nanning, Nanning 530022, China
[2] Department of Pharmacy, The First Affiliated Hospital of Xi'an Medical University, Xi'an 710077, China

Abstract

Objective The objective was to investigate the prognostic factors of advanced lung cancer treated with apatinib by log-rank regression analysis.

Methods Sixty patients with advanced stage lung cancer confirmed at The First People's Hospital of Nanning between January 2018 and December 2018 who had received a second-line treatment or a treatment above this level were included. All patients were treated with 425 mg/d apatinib orally for a 28-day course of treatment. Log-rank regression analysis of remission rates, disease control rates, adverse events, and prognostic factors in all patients was performed.

Results After treatment, the total remission rate was 6.7%, and the disease control rate was 61.7% (37/60). Progression-free survival was 3.2 ± 0.1 months, and overall survival was 5.3 ± 0.5 months. The overall incidence of grade 3–4 adverse reactions was 15.0% (9/60), and these adverse reactions were significantly relieved by reducing the drug dose or suspending drug use. Differentiation degree, Eastern Cooperative Oncology Group (ECOG) score, and adverse reactions were all important and independent risk factors affecting the prognosis of patients ($P < 0.05$).

Conclusion Apatinib treatment could effectively inhibit the progress of the disease for patients with advanced lung cancer and prolong their survival with relatively mild toxicity and side effects, which is beneficial to patient tolerance. Moreover, the degree of differentiation, ECOG score, and adverse reactions could affect the prognosis of patients.

Received: 10 October 2020
Revised: 4 March 2021
Accepted: 10 April 2021

Key words: Log-rank regression analysis; apatinib; advanced lung cancer; prognostic factors

Lung cancer is a malignant tumor with relatively high morbidity and mortality worldwide, and most patients are at the advanced stage of lung cancer at the time of diagnosis, resulting in a low 5-year survival rate [1]. When lung cancer develops to an advanced stage, lymph nodes and cancer cells infiltrate into adjacent tissues and metastasize to distant tissues and organs; thus, the best opportunity for surgery is often missed upon diagnosis [2]. Currently, patient conditions are effectively alleviated through radiotherapy, chemotherapy, and targeted therapy. Platinum-combined chemotherapy can effectively kill cancer cells, prolong the disease-free life of patients, and significantly improve their quality of life; however, recurrence is frequent after one year of treatment [3]. Radiotherapy can effectively control tumors; however, there are still limitations in the treatment of patients with advanced lung cancer whose tumors have metastasized [4]. As the first generation of oral anti-angiogenic drugs in China, apatinib, whose main target is vascular endothelial growth factor receptor (VEGFR)-2, has shown significant efficacy in the treatment of advanced stomach cancer, significantly prolonging the total survival of patients with advanced gastric cancer for whom second-line treatment has failed [5–6]. Researchers have also found that apatinib combined with conventional chemotherapy has a good effect on patients with advanced non-small cell lung cancer [7]. However, the clinical efficacy of apatinib alone for the treatment of patients with advanced lung cancer for whom second-line treatment has failed has not been reported. In this study, patients with advanced lung cancer for whom second-line treatment or a treatment above this level failed were treated with 425 mg/d of apatinib administered orally in a 28-day course of treatment, to explore the efficacy and safety of this treatment.

✉ Correspondence to: Yan Wu. Email: wuyan57968@163.com

Materials and methods

Patient population

In this study, a total of 60 patients with advanced lung cancer were included. The enrolled patients received therapy at The First People's Hospital of Nanning between January 2018 and December 2018. The patients included 38 males and 22 females; their age was 39–75 years (average 64.1 ± 4.6), 12 patients had small cell lung cancer, 48 patients had non-small cell lung cancer; 28 cases showed poor differentiation, 22 showed moderate differentiation, and 10 showed high differentiation. The inclusion criteria were as follows: (1) patients for whom second-line treatment or a treatment above this level failed, (2) all patients who presented with pathologically confirmed advanced lung cancer, and (3) patients with a life expectancy of at least 3 months. The exclusion criteria were as follows: (1) patients with severe cardiac dysfunction, (2) mental disorders that lead to an inability to cooperate with the researchers, (3) pregnant and lactating women, and (4) patients who had received surgical treatment. This study was approved by the Ethics Committee of The First People's Hospital of Nanning. Written informed consent was obtained from all patients for the use of their clinical information and for obtaining their blood and DNA samples.

Methods

All patients were treated with apatinib alone as follows: oral administration of 425 mg apatinib (Jiangsu Hengrui Pharmaceutical Co., Ltd., China) once a day, 30 min after a meal for 28 days (28-day course). During the treatment period, if the patients showed adverse reactions, the dosage could be reduced to 250 mg/d.

Observational index

Clinical efficacy evaluation

Patients were evaluated for clinical efficacy, mainly using the solid tumor efficacy evaluation criteria, which were mainly divided into progressive disease (PD), stable disease (SD), partial remission (PR), and complete remission (CR). The total response rate = (PR + CR)/total number of cases, and the disease control rate = (PR + CR + SD)/total number of cases. Progression-free survival refers to the time from the patient's further disease development or from being enrolled to drug intolerance. The overall survival is the time from enrollment to death.

Adverse reaction monitoring

The occurrence of adverse reactions in patients was observed and classified into grade 1, 2, 3, or 4, depending on the severity of the adverse reactions, according to the World Health Organization criteria for the evaluation of the toxic side effects of antineoplastic drugs, with higher grades indicating that the adverse reactions are relatively serious.

Factor analysis

Single and multifactorial analyses of factors affecting patient prognosis, including patient age, gender, pathology type, degree of tissue differentiation, tumor diameter, tumor stage, Eastern Cooperative Oncology Group (ECOG) score, and grade of adverse events, were performed.

Statistical analyses

The data were analyzed by SPSS 21.0, and the χ^2 (%) test was used for counting. The log rank method was used for univariate analysis, and prognostic factors were screened. The Cox regression model was used for multivariate analysis to confirm the independent influencing factors. $P < 0.05$ showed significant differences.

Results

Clinical efficacy

After treatment, CR accounted for 0.0% (0/60), PR accounted for 6.7% (4/60), SD accounted for 55.0% (33/60), PD accounted for 38.3% (23/60), the total remission rate was 6.7%, and the disease control rate was 61.7% (37/60). The progression free survival was 3.2 ± 0.1 months, and the overall survival was 5.3 ± 0.5 months.

Occurrence of adverse effects

The overall incidence of grade 3–4 adverse reactions was 15.0% (9/60), which was significantly improved by either dose reduction or suspension of drug administration, as shown in Table 1.

Single-factor analysis of the prognosis of patients with advanced lung cancer

The degree of differentiation, ECOG score, and adverse effects were all important factors ($P < 0.05$) affecting patient prognosis, as shown in Table 2.

Table 1 Occurrence of adverse effects

Adverse reactions	Proteinuria	Hand-foot syndrome	Diarrhea	Hypertension	Myelosuppression
Gread 1–2	11	8	9	13	14
Gread 3–4	0	2	1	4	2
Total case	11	10	10	17	16
Total Incidence	18.3	16.7	16.7	28.3	26.7

Table 2 Single-factor analysis of the prognosis of patients with advanced lung cancer (eg)

Parameter	No. of patients	Progression-free survival			Mean survival time		
		Median	95% CI	*P*	Median	95% CI	*P*
Age (years)							
< 65	38	3.5	3.41–5.53	> 0.05	4.9	4.69–5.69	> 0.05
≥ 65	22	3.1	1.39–5.15		4.5	3.60–5.53	
Sex							
Male	38	3.9	2.07–4.35	> 0.05	3.8	3.97–5.70	> 0.05
Female	22	3.0	1.45–4.74		4.4	3.79–5.37	
Histology							
SCLC	12	3.3	2.30–4.97	> 0.05	4.4	3.76–5.88	> 0.05
NSCLC	48	3.4	2.29–5.19		5.2	4.49–6.45	
Degree of tissue differentiation							
Low	28	2.8	2.89–3.25	< 0.05	4.3	3.89–5.97	< 0.05
Middle	22	4.2	2.27–6.77		5.6	5.69–6.67	
High	10	5.8	4.30–8.71		6.0	6.75–6.50	
Pathological type							
Squamous carcinoma	32	2.7	2.75–3.13	> 0.05	3.9	2.75–3.13	> 0.05
Adenocarcinoma	19	4.2	3.51–5.43		5.8	5.53–6.58	
Adeno-squamous carcinoma	9	5.4	4.89–6.03		4.1	3.87–6.11	
Diameter of tumor (cm)							
≥ 3	35	3.3	2.89–4.63	> 0.05	4.8	4.05–5.60	> 0.05
< 3	25	3.9	2.79–6.07		5.6	4.75–6.69	
Stage							
III	24	4.4	3.74–5.75	> 0.05	5.7	5.17–6.89	> 0.05
IV	36	2.8	2.49–3.54		3.8	3.39–5.15	
ECOG (score)							
< 2	37	3.9	3.18–5.30	< 0.05	5.4	4.90–6.07	< 0.05
≥ 2	23	2.9	1.39–4.15		3.5	1.77–5.75	
Adverse effects (gread)							
> 2	9	1.8	2.35–3.07	< 0.05	4.1	2.99–5.59	< 0.05
≤ 2	55	3.5	2.47–5.09		4.9	4.21–6.17	

Multifactorial analysis of the prognosis of patients with advanced lung cancer

The degree of tissue differentiation, ECOG score, and adverse events were all independent risk factors for patient prognosis ($P < 0.05$; Table 3).

Discussion

Lung cancer is a serious threat to human life and health, and the incidence rate in male patients is higher than that in women [1]. Traditional chemotherapy can kill tumor cells as well as normal tissue cells, resulting in serious adverse reactions in the body [3]. The index of chemotherapy is relatively narrow, the specificity is poor, and drug resistance leads to disease recurrence, which is why targeted therapy is gradually replacing treatment using chemical drugs [2]. In recent years, targeted epidermal growth factor receptor tyrosine kinase inhibitors (EGFR-TKIs), which are relatively well tolerated by patients with few side effects, have been widely used. Relevant studies have shown that the use of EGFR-TKIs can be applied to the treatment of patients with a positive EGFR gene mutation, and a good therapeutic effect can be obtained [8]. Despite the significant initial efficacy of targeted drug therapy, drug resistance occurs in this treatment as well, similar to chemotherapy. With the progressing drug administration time, the likelihood of developing resistance increases, reducing the effectiveness of later treatment and eventually leading to further development of the disease [9]. Apatinib is a first-generation oral anti-angiogenic drug invented in China that targets VEGFR-2 and receptor tyrosine kinases (RTKs), such as c-kit, RET, and c-src [10]. VEGF-2 has now been found to promote endothelial cell proliferation during angiogenesis by activating the mitogen-activated protein kinase signaling pathway [11]. By blocking VEGFR-2, apatinib can inhibit

Table 3 Multifactorial analysis of the prognosis of patients with advanced lung cancer (eg, %)

Parameter	SE	B	Wald	Sig.	Exp (B)
Degree of tissue differentiation	0.399	-1.127	7.279	0.007	0.299
ECOG score	0.589	1.307	5.096	0.029	4.199
Adverse effects	0.506	1.215	8.800	0.000	3.989

endothelial cell proliferation, which ultimately leads to anti-angiogenesis, and this has been shown to have anti-tumor effects in a variety of cancers [12]. This also provides the theoretical basis for the treatment of lung cancer with apatinib. The present study, which assessed the effect of apatinib treatment by log-rank analysis, found that patients were treated with an overall remission rate of 6.7% and a disease control rate of 61.7%. Progression-free survival (3.2 ± 0.1 months) and overall survival (5.3 ± 0.5 months) were observed. Therefore, the use of apatinib for patients with advanced lung cancer could effectively control the disease. Because apatinib is an angiogenesis inhibitor with high affinity, it can effectively block the transmission of downstream signaling pathways with a significant inhibitory effect on the neovascularization of endothelial cells [13]. Sun Lu *et al*. showed that apatinib effectively regulates and contributes to the process of kinase phosphorylation by inhibiting extracellular signals downstream of the signaling pathway [14]. In recent years, several clinical trials have confirmed that apatinib effectively exerts its unique antitumor effect in the treatment of breast [15], gastric [16], and colorectal cancer [17], as well as other malignant cancers. Chemotherapeutic drugs have a more general cytotoxic effect, and they can cause damage to normal tissue cells of the body while killing cancer cells, thus leading to patient intolerance and relatively poor treatment compliance. Apatinib, in contrast, makes it easier for patients to tolerate and accept the treatment [18–19]. The present study showed that the overall incidence of grade 3-4 adverse reactions was 15.0%, and the adverse reactions were significantly reduced after dose reduction or suspension of drug administration. Thus, apatinib has a relatively mild adverse reaction profile in the treatment of patients with advanced lung cancer, which is more conducive to treatment acceptance by patients. In this study, data were analyzed separately for regression using the log-rank method. The results showed that the degree of differentiation, ECOG score, and adverse reactions could influence patient prognosis, and all the three were independent risk factors. This shows that the factors that affect the prognosis of patients with advanced lung cancer are mainly the degree of tissue differentiation, ECOG score, and severity of adverse reactions. However, the influence of other factors on the prognosis of patients with advanced lung cancer needs further confirmation via a larger sample size in order to make the results of the study more accurate and reliable.

In summary, the treatment of patients with advanced lung cancer using apatinib could effectively inhibit the progression of the disease and prolong the survival of patients, with relatively mild toxic side effects that could be well tolerated by patients. In addition, the degree of differentiation, ECOG score, and adverse effects could have an impact on patient prognosis.

Conflicts of interest

The authors indicated no potential conflicts of interest.

References

1. Siegel RL, Miller KD, Jemal A. Cancer statistics, 2020. CA Cancer J Clin, 2020, 70: 7–30.
2. Li DH, Yao Y, Geng Q. Chinese society of clinical oncology lung cancer diagnosis and treatment guidelines (2018 edition) updated interpretation. J Clin Surg (Chinese), 2019, 27: 36–39.
3. Lund-Iversen M, Scott H, Erik H Strøm, *et al*. Expression of estrogen receptor-α and survival in advanced-stage non-small cell lung cancer. Anticancer Res, 2018, 38: 2261–2269.
4. Chen HX, Lin WH, Dai PL, *et al*. Advances in radiotherapy for locally advanced non-small cell lung cancer. Electron J Integr Chin Western Med Cardiovasc Dis (Chinese), 2020, 8: 20.
5. Liya L, Hao Y, Lihong H, *et al*. Progression-free survival as a surrogate endpoint for overall survival in patients with third-line or later-line chemotherapy for advanced gastric cancer. Oncol Targets Ther, 2015, 8: 921–928.
6. Yang Y, Zhang W, Yao J, *et al*. First-line treatment of apatinib in elderly patient of advanced gastric carcinoma: A case report of NGS-driven targeted therapy. Cancer Biol Ther, 2018, 19: 10–13.
7. Jiang Y. Efficacy and adverse reactions of apatinib mesylate combined with conventional chemotherapy in the treatment of advanced non-small cell lung cancer. Contemp Med (Chinese), 2020.
8. Yang X B, Chai X S, Wu WY, *et al*. Gefitinib plus Fuzheng Kang'ai formula in patients with advanced non-small cell lung cancer with epidermal growth factor receptor mutation: A randomized controlled Trial. Chin J Integr Med (Chinese), 2018, 24: 734–740.
9. Ippolito E, Floreno B, Rinaldi C G, *et al*. Efficacy of a propolis-based Syrup (FARINGEL) in preventing radiation-induced esophagitis in locally advanced lung cancer. Chemotherapy, 2018: 76.
10. Tian S, Quan H, Xie C, *et al*. YN968D1 is a novel and selective inhibitor of vascular endothelial growth factor receptor-2 tyrosine kinase with potent activity *in vitro* and *in vivo*. Cancer Sci, 2011, 102: 1374–1380.
11. Takahashi T, Yamaguchi S, Chida K, *et al*. A single autophosphorylation site on KDR/Flk-1 is essential for VEGF-A-dependent activation of PLC-gamma and DNA synthesis in vascular endothelial cells. EMBO J, 2001, 20: 2768–2778.
12. Kang JP, Xiao YB, Dong SW, *et al*. Clinical application of apatinib mesylate in the treatment of advanced refractory bone and soft tissue sarcoma. Chin Clin Oncol (Chinese), 2019, 46: 615–621.
13. Liang S K, Lee M R, Liao W Y, *et al*. Prognostic factors of afatinib as a first-line therapy for advanced EGFR mutation-positive lung adenocarcinoma: A real-world, large cohort study. Oncotarget, 2018, 9: 23749–23760.
14. Sun L, Liu XY, Yu H, *et al*. Efficacy analysis of apatinib mesylate in the treatment of epithelial ovarian cancer with second-line chemotherapy failure. Chin Clin Oncol (Chinese), 2019, 46: 627–630.
15. Dong D, Liu YZ, Li WG, *et al*. Analysis of efficacy and Adverse reactions of apatinib mesylate in the treatment of advanced breast cancer. Tumor Pharmacol (Chinese), 2019, 9: 754–757+762.
16. Han RB. Clinical efficacy and side effects of apatinib in the treatment of advanced gastric cancer. Electron J Integr Chin Western Med Cardiovasc Dis (Chinese), 2020, 8: 180–181.
17. Zhao YF, Wen FG. Clinical observation of single drug Apatinib in the treatment of advanced colorectal cancer. Chin J Metall Ind Med

(Chinese), 2019, 36: 279–280.
18. Wang HL, Gong TX, Zhou SX, *et al*. Efficacy and safety of apatinib mesylate in third-line treatment of patients with advanced non-small cell lung cancer. Chin J Clin Pharmacol Ther (Chinese), 2019, 24: 567–572.
19. Pi C, Xu CR, Zhang MF, *et al*. EGFR mutations in early-stage and advanced-stage lung adenocarcinoma: Analysis based on large-scale data from China. Thorac Cancer, 2018, 9: 814–819.

DOI 10.1007/s10330-020-0468-8
Cite this article as: Ren T, Wu Y. Efficacy and adverse reactions of apatinib as second-line or later-line treatment in advanced lung cancer. Oncol Transl Med, 2021, 7: 160–164.

Oncology and Translational Medicine
DOI 10.1007/s10330-021-0485-5

August 2021, Vol. 7, No. 4, P165–P171

ORIGINAL ARTICLE

Enhancing the treatment effects of tumor cell purified autogenous heat shock protein 70-peptide complexes on HER-3-overexpressing breast cancer*

Xia Chen[1], Xiaoming Zhang[2], Xiangji Lu[3], Meng Ren[4], Rina Su[4], Weishi Gao[4], Yanwei Gao[4] (✉)

[1] Department of Apheresis, Inner Mongolia Red Cross Blood Center, Hohhot, Inner Mongolia 010010, China
[2] Department of Ultrasound medicine, Inner Mongolia People's Hospital, Hohhot, Inner Mongolia 010017, China
[3] Department of General Surgery, Inner Mongolia Armed Police Hospital, Hohhot, Inner Mongolia 010010, China
[4] Department of Surgical Oncology, Inner Mongolia People's Hospital, Hohhot, Inner Mongolia 010017, China

Abstract

Objective The aim of this study was to enhance the treatment effect of tumor purified autogenous heat shock protein 70-peptide complexes (HSP70-PCs) on HER-3-overexpressing breast cancer.

Methods In this study, we first studied the expression of HER-3 in breast cancer tissues and its relationship with patient characteristics. We then purified HSP70-PCs from primary breast cancer cells with different HER-2 and HER-3 expression profiles and determined the cytotoxicity of autogenous dendritic cells (DCs) and CD8+ T cells induced by these complexes. Third, recombinant human HSP70-HER-3 protein complexes were used to inhibit the autogenous HSP70-PCs purified from HER-3–overexpressing breast cancer cells, and the resulting immunological response was examined.

Results The results show that HSP70-PCs can be combined with recombinant HSP70-HER-3 protein complexes to induce stronger immunological responses than autogenous HSP70-PCs alone and that these treatments induce autogenous CD8+ T cell killing of HER-3-positive breast cancer cells.

Conclusion These findings provide a new direction for HSP70-DC-based immunotherapy for patients with HER-3-overexpressing breast cancer.

Received: 24 February 2021
Revised: 25 April 2021
Accepted: 15 May 2021

Key words: heat shock protein 70 peptide complexes (HSP70-PCs); HER-3 protein; recombinant protein; dendritic cells (DCs); cellular immunotherapy

Breast cancer is the most common cancer in women, and the incidence of breast cancer increases every year. The Globocan 2012 data, released by the International Agency for Research on Cancer, reports that there are approximately 1,671,000 new cases of breast cancer reported worldwide each year, with 522,000 reported deaths from breast cancer [1].

HER-2 is the most important therapeutic target in breast cancer, with several novel therapeutics showing a high degree of efficacy for HER-2-positive breast cancers. These include Herceptin. However, no effective treatment has been identified for HER-2-negative breast cancer. Therefore, current research is focused on identifying novel therapeutic targets for HER-2-negative breast cancer and developing effective treatment strategies for these malignancies [2–3].

Cellular immunotherapy, a form of biological tumor therapy, is one of the most effective treatments for breast cancer. These therapies use biological agents to isolate, activate, and transfuse the patient's own or allogeneic tumor-specific and nonspecific killer cells. Many approaches for cellular immunotherapy targeting tumors have been developed and dendritic cell (DC)-based active immunotherapy shows good potential as a novel strategy for breast cancer. DCs are the most powerful antigen presenting cells (APCs) and can activate cytotoxic T lymphocytes [4–5].

Heat shock protein 70 (HSP70) is an important

✉ Correspondence to: Yanwei Gao. Email: gaoyw0518@163.com
*Supported by a grant from the National Natural Science Foundation of China (No. 81260392).

molecular chaperone that binds to tumor antigen peptides in tumor cells to form HSP70-peptide complexes (PCs). Tumor-derived HSP70-PCs can specifically interact with DCs and drive their antigen presentation. Once the antigen is presented, the immune response will produce a series of antigen-specific cytotoxic CD8+ T cells. Our previous study showed that we could purify HSP70 complexes from HER2-2-overexpressing breast cancers (HSP70-HER-2-PCs), and that these HSP70-HER-2-PCs produced more comprehensive tumor antigen peptides and induced stronger immune activity against the tumor cells from which the complex was derived [6–7]. However, this method did not achieve decent results in HER-2-negative breast cancers. Recent studies have shown that HER-3 may be a potential target for many kinds of tumors; however, this result remains controversial [8–9].

In this study, we evaluated whether HER-3 can be used as a target for HSP70-DC-based cell immunotherapy. We also explored whether our established method could be used against breast cancers with high HER-3 expression.

Materials and methods

Patient selection and postoperative tumor tissue treatment

We selected 70 patients with breast cancer who were scheduled to undergo radical surgery at the Oncology Department of the Inner Mongolia People's Hospital between January 2017 and December 2018. No patient had received preoperative chemotherapy or radiotherapy. The age of the patients ranged from 27 to 68 years, and all patients were females; all pathological types were diagnosed as invasive breast cancer by fine needle puncture and cytological examination. Postoperative tumor tissues were divided into two sections: one section was used for postoperative pathology and immunohistochemical examination (HER-2 and HER-3 staining), and the other section was used for primary cell culture. The study was approved by the Human Research Ethics Committee at the Inner Mongolia People's Hospital and all of the patients provided informed consent for the collection of the tissue samples. In cases where primary tumor cell culture was successful we went on to isolate peripheral blood mononuclear cells (PBMCs) from the peripheral blood samples of the same patients.

Immunohistochemistry

Tissue samples from primary tumors were fixed in 10% neutral buffered formalin and embedded in paraffin. Serial sections (4 μm) were stored in a deep freezer (-20℃) until immunostaining could be completed. For antigen retrieval, the sections were immersed in citrate buffer (pH 6.0), and samples were heated in a pressure cooker. The primary antibodies were mouse anti-human HER-2 monoclonal antibody and rabbit anti-human HER-3 monoclonal antibody. Isotype-matched rabbit IgG or mouse IgG was used as a negative control. Following incubation with primary antibody, sections were incubated with horseradish peroxidase (HRP)-labeled goat anti mouse or rabbit antibody and immunoreactions were visualized using diaminobenzidine.

HER-2 expression was scored using the following parameters: (a) the intensity of the membrane staining (score 0: no staining, score 1: +, score 2: ++, score 3: +++), and (b) the percentage of HER-2-positive cells (score 1: 1–25%, score 2: 26–50%, score 3: 51–75%, and score 4: > 75%). The total score was calculated as the sum of the two separate scores and ranged from 0 to 7. A score of 3 or higher was considered positive for HER-2 immunostaining and marked as HER-2 (+).

The HER-3 sections were scored as follows: (a) the intensity of the cytoplasmic staining (score 0: no staining, score 1: +, score 2: ++, score 3: +++), (b) the percentage of HER-3-positive cells (score 1: 0–25%, score 2: 26–50%, score 3: 51–75%, and score 4: >75%), and (c) the presence or absence of membrane staining (score 0: absent; score 1: present). The total score was calculated as the sum of these three scores and ranged from 0 to 8. A score of 4 or higher was considered positive for HER-3-immunostaining and marked as HER-3 (+).

Breast cancer primary cell culture

The breast cancer primary cell culture was completed as previously described, with some modifications [10]. The resected breast cancer tissues were immediately placed in ice-cold RPMI-1640 medium containing 100 U/mL penicillin G and 100 μg/mL streptomycin, and transported to the laboratory within 10 min. After the removal of the necrotic tissues, the samples were rinsed twice in phosphate buffered saline (PBS) and cut into small fragments. These fragments were then incubated with 1% collagenase type II in a gently shaking water bath for 1 h at 37°C before being passed through a 38-μm mesh sieve. The resulting cell suspension was then washed twice and centrifuged at 300 × *g* for 10 min before the cells were diluted to 5×10^5 cells/mL and incubated in RPMI-1640 supplemented with 10% heat inactivated fetal calf serum (FCS) at 37°C and 5% CO_2. The fibroblasts were removed by reducing the FCS concentration to 5% during the second week of culture and then returned to 10% in the third week. Cells were passaged at 75% confluency.

Grouping

Patients and their corresponding breast cancer primary cells were divided into four groups based on their HER-2 and HER-3 immunohistochemistry results: Group A was HER-2 (+) and HER-3 (+), group B was HER-2 (+) and

HER-3 (-), Group C was HER-2 (-) and HER-3 (+) and Group D was HER-2 (-) and HER-3 (-). Six cases were randomly selected from each group for analysis.

Purification of autogenous HSP70-PCs

Purifications of the autogenous HSP70-PCs were performed as previously described [7]. The breast cancer primary cells were heated in a water bath at 42°C for 12 h, and then allowed to recover for 2 h at 37°C and 5% CO_2. After heat shock, the tumor cells were digested using 0.02% trypsin, and then 5×10^6 cells from each cell line were homogenized for 15 min on ice in a hypotonic buffer consisting of 50 mM Tris-HCl, 150 mM NaCl, 1 mM phenylmethylsulfonyl fluoride, 1 mM sodium fluoride, and 5 mM 3-[(3-cholamidopropyl) dimethylammonio]-1-propanesulfonate (CHAPS) at pH 7.2. After ultrasonication at 0°C for 30 min, the homogenate was centrifuged at 10,000 × *g* for 90 min at 4°C before the supernatant was dialyzed against buffer A (20 mM Tris-HCl, 150 mM NaCl, 1 mM $CaCl_2$, 1 mM $MnCl_2$, 0.5 mM phenylmethylsulfonyl fluoride, and 15 mM β-mercaptoethanol, pH 7.4) overnight at 4°C. The sample was then loaded onto a ConA-Sepharose column and unbound protein was collected at a flow rate of 12 mL/h. The fraction of interest was then dialyzed against buffer B (20 mM Tris-HCl, 20 mM NaCl, 3 mM $MgCl_2$, 1 mM $MnCl_2$, 0.5 mM phenylmethylsulfonyl fluoride and 15 mM β-mercaptoethanol, pH 7.4) overnight at 4°C before being applied to an ADP-agarose column equilibrated with buffer B at a flow rate of 12 mL/h. The column was washed with buffer B containing 0.5 M NaCl until no protein could be detected by the Bradford assay. The target protein was then eluted using buffer B supplemented with 3 mM ADP. The endotoxin level in the preparations was determined using the limulus amebocyte lysate assay.

The amounts of HER-2 and HER-3 protein in the purified products were quantified using HER-2 and HER-3 ELISA kits according to the manufacturer's instructions.

Preparation of DCs and CD8+ T cells

DCs were generated as previously described [11]. Briefly, PBMCs were isolated from the hepa¬rinized venous blood of the patients using density gradient centrifugation and Ficoll-Hypaque and cultured in RPMI-1640 medium containing 10% FCS for 2 h. Non-adherent cells were collected and used to generate CD8+ T cells, and the adherent cells were cultured for 7 days in RPMI-1640 medium containing 10% FCS, 800 U/mL recombinant human granulocyte-macrophage colony stimulating factor, and 500 U/mL recombinant human interleukin (IL)-4 to generate DCs. Half the media volume was replaced every other day, and 50 U/mL of tumor necrosis factor-α was added to the culture medium on the sixth day.

CD8+ T cells were harvested from the non-adherent fraction as previously described. Briefly, non-adherent cells were resuspended in RPMI-1640 medium containing 10% FCS, 100 U/mL penicillin G, and 100 μg/mL streptomycin. Recombinant human interferon (IFN)-γ (1,000 IU/mL) was added on day 0. Then 50 ng/mL mouse anti-human monoclonal antibody against CD3, 100 U/mL recombinant human IL-1β, and 300 U/mL recombinant IL-2 were added to the culture and the cells were incubated at 37°C in a humidified atmosphere with 5% CO_2 and subcultured every third day in fresh complete medium with 300 U/mL IL-2 at 2×10^6 cells/mL.

Induction of CD8+ T cells by DCs pulsed with autogenous HSP70-PCs and *in vitro* cytotoxicity testing

An LDH release assay was used to determine the specific cytolytic activities of the CD8+ T cells as previously reported [7]. DCs from each of the four groups (1×10^5 each) were pulsed with their autogenous HSP70-PCs (10 μg) for 12 h and then washed in PBS before being co-cul¬tured with autogenous CD8+ T cells at a ratio of 1:10. The co-cultures were treated with 300 U/mL IL-2 in a 96-well plate for 1 week and then the four groups of CD8+ T cells were used as effector cells in the cytotoxicity assays evaluated using an LDH cytotoxicity detection kit. The corresponding primary breast cancer cells were used as the target. Target and effector cells were resuspended in assay medium (RPMI-1640 with 1% BSA), and then target cells (1×10^4 cells/well) were co-cultured with effector cells at a 1:10 ratio in a 96-well round-bottomed culture plate at 37°C. After incubation for 4 h, the cells were centrifuged at 50 × *g* for 10 min, and the supernatant was collected and transferred to another 96-well plate for the LDH assay. The LDH detection mixture (100 μL/well) was added and the plates were then incubated in the dark for 30 min at room temperature (15–25°C). These reactions were stopped following the addition of 50 μL of stop solution and the absorbance of the samples was measured at 490 nm using a microplate reader.

Preparation of recombinant human HSP70-HER-3 protein complexes and their application in the immunoprecipitation binding analysis

The recombinant protein complexes were prepared as previously described [7]. The recombinant HSP70-HER-3 protein complex was generated by incubating recombinant human HSP70 and recombinant human HER-3 protein at a 1:1 molar ratio at 43°C for 30 min and then at 37°C for 1 h. Binding was evaluated by co-immunopre¬cipitation and western blot analysis. Briefly, the HSP70-HER-3 protein mixture was incubated with rabbit anti-human mono¬clonal antibody against HER-3

(1:100) at room temperature for 2 h. The complex was then precipitated by incuba¬tion with protein A-Sepharose CL-4B (20 μl/mL) and rotating for 8 h on ice. Samples were then washed eight times with washing buffer (1 M Tris-HCl, 5 M NaCl, 0.5 M EDTA and 0.1% Triton X-100, pH 7.4) at 4°C to remove any nonspecific binding of the recombinant proteins to the protein A-Sepharose and then the beads were mixed with 2X SDS sample buffer, boiled for 5 min, and subjected to SDS-PAGE. Samples were transferred to a nitrocellulose membrane and then probed with the mouse anti-human monoclonal antibody against HSP70 (1:100) at room temperature for 1 h. Membranes were then incubated with HRP-conjugated goat anti-mouse IgG (1:10,000) and then proteins were visualized by autoradiography.

Immunological activity of DCs pulsed with the autogenous HSP70-PCs combined with the recombinant HSP70-HER-3 protein complexes

Each group of DCs was divided into three parts (1×10^5 cells in each part) and each part was pulsed using different antigens for 12 h. Antigen a was 10 μg of autogenous HSP70-PCs. Antigen b was 10 μg of the *in vitro* generated antigen complex: autogenous HSP70-PCs and recombinant human HSP70-HER-3 protein complexes mixed at a 1:1 ratio. Antigen c was 10 μg of the recombinant human HSP70-HER-3 protein complex. The pulsed DCs were then co-cultured with autogenous CD8+ T cells at a ratio of 1:10 and the cytolytic activities of the CD8+ T cells were determined using LDH release as described above.

Statistical analysis

Values are expressed as the mean ± standard deviation (SD) or as a percentage. The correlations between the study variables were investigated using the Spearman's correlation coefficient and all analyses were conducted using SPSS18.0 software. *T*-test and chi square test are applied. The results were considered statistically significant at $P < 0.05$.

Results

Correlation between HER-3 expression and the clinical parameters of patients

A total of 70 patients with breast cancer were included in this study. Patient characteristics are listed in Table 1. We used the scoring approach described in the Methods section to categorize HER-2 and HER-3 expression in the tumor samples from the patient cohort as follows: 37 cases (53%) were HER-3-positive, 33 cases (47%) were HER-3-negative, 29 cases (41%) were HER-2-positive, and 41 cases (59%) were HER-2-negative. The expression of HER-3 was positively correlated with tumor size, histological type, lymph node metastasis, and the HER-2 expression status of the patients. There was no significant association between HER-3 expression and the age of onset in these patients (Table 2).

Table 1 Characteristics of breast cancer patients included in this study (70 cases)

Characteristics	*n*	%
Age (years)	48 ± 11	
Tumor size		
< 2 cm	24	34
2–5 cm	32	46
> 5 cm	14	20
Histological grade		
1	8	11
2	28	40
3	34	49
Axillary lymph node metastasis status		
Absence	22	31
Presence	48	69
HER-2 status		
Positive	29	41
Negative	41	59
HER-3 status		
Positive	37	53
Negative	33	47

Table 2 Correlations between HER-3 immunohistochemical expression and clinicopathological characteristics of the breast cancer patients

Variable	*P* value	*R* value
Age	0.301	0.274
Tumor size	0.029	0.172
Histological grade	0.042	0.187
Axillary lymph node metastasis status	0.025	0.201
HER-2 status	0.037	0.146

Primary breast cancer cell culture and grouping

Of the 70 primary breast cancer cell cultures obtained from the surgical specimens, three became contaminated during culture and four developed senescence. The remaining cultures were passaged 4–5 times until we achieved sufficient cell density (1×10^7 cells) to complete the preparation of the autogenous HSP70-PCs and populate the target cell quota in the further experiments. We categorized the 63 tumor cell cultures into four groups as described in Methods: Group A was HER-2 (+) and HER-3 (+) ($n = 17$), group B was HER-2 (+) and HER-

3 (-) (n = 8), Group C was HER-2 (-) and HER-3 (+) (n = 16), and Group D was HER-2 (-) and HER-3 (-) (n = 22).

Quantitative detection of autogenous HSP70-PCs

We then randomly selected six cases from each of the four groups and purified autogenous HSP70-PCs from the primary breast cancer cells (5×10^6 cells for each case). Protein was then quantified using the Bradford method and the standard curve showed that the total protein in the autogenous HSP70-PCs was 165.89 ± 20.77 μg (n = 24). We performed quantitative analysis of HER-2 and HER-3 expression using ELISA kits and found that the amount of HER-2 protein in the HER-2 (+) groups (A and B) was 1.35 ± 0.24 μg (n = 12) and that the HER-3 content in the HER-3 (+) groups (A and C)was very low, at only 5.21 ± 1.16 ng (n = 12). The endotoxin levels in the preparations were lower than 0.03 EU/mg as determined by the LAL assays.

In vitro cytotoxicity tests

We next induced autogenous CD8+ T cells by co-culturing these cells with the four groups of autogenous DCs pulsed with their autogenous HSP70-PCs. The specific cytolytic activities of each of the four groups of CD8+ T cells were then examined using an LDH release assay following 4 h of co-culture of the effector (CD8+ T cells) and target cells (primary breast cancer cells) at a 10:1 ratio. There were no significant differences in the amount of LDH released in groups A and B (HER-2 (+)/HER-3 (+) and HER-2 (+)/HER-3 (-), respectively), but there was a significant increase in LDH in groups C and D (HER-2 (-)/HER-3 (+) and HER-2 (-)/HER-3 (-), respectively) (P < 0.05; Fig. 1). There was no significant difference between groups C and D. This result suggests that the HER-3 protein in the autogenous HSP70-PCs purified from HER-3-positive primary breast cancer cells did not exhibit any specific immunological activity when inducing autogenous CD8+ T cells.

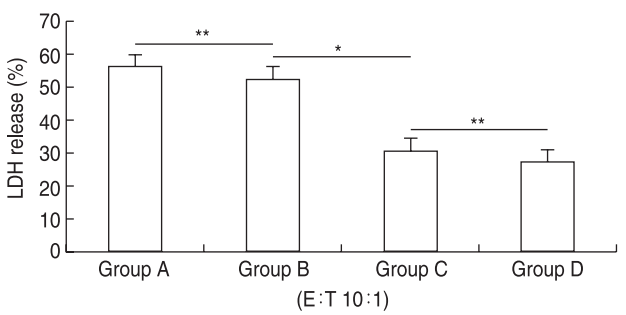

Fig. 1 LDH release assays using CD8+ T cells induced with autogenous HSP70-PCs. The HSP70-PC induced CD8+ T cells were used as effector cells, and the primary breast cancer cells from which the antigen was derived were used as target cells. Group A is HER-2 (+) and HER-3 (+), group B is HER-2 (+) and HER-3 (-), Group C is HER-2 (-) and HER-3 (+), Group D is HER-2 (-) and HER-3 (-). Assays were performed in triplicate. Results are expressed as the mean ± SD (n = 6). $^*P$ < 0.05, $^{**}P$ > 0.05.

Fig. 2 Co-immunoprecipitation-based analysis of the recombinant human HSP70-HER-3 protein complexes. Recombinant human HSP70 and HER-3 proteins were mixed and then immunoprecipitation was performed using HER-3 antibody, before being evaluated by western blot.

Recombinant human HSP70-HER-3 protein complex prepared *in vitro*

Recombinant human HSP70 was incubated with recombinant human HER-3 protein at a 1:1 molar ratio at 43˚C for 30 min, and then at 37˚C for 1 h. The complex was then evaluated by co-immunoprecipitation and western blot. The protein A-Sepharose-immune complex was found to bind to a mouse anti-human monoclonal antibody against HSP70. We then used a chemiluminescence reagent to demonstrate the successful *in vitro* preparation of the recombinant human HSP70-HER-3 protein complexes (Fig. 2).

Immunological activity of DCs pulsed with autogenous HSP70-PCs combined with recombinant HSP70-HER-3 protein complexes

Finally, we examined the immunological activity of autogenous HSP70-PCs combined with recombinant HSP70-HER-3 protein complexes against breast cancer cells. Each of the four groups of DCs was pulsed using different antigens: the autogenous HSP70-PCs alone (antigen a), the autogenous HSP70-PCs and the recombinant HSP70-HER-3 protein complexes (antigen b), or the recombinant human HSP70-HER-3 protein complexes alone (antigen c). The pulsed DCs were then used to induce autogenous CD8+ T cells, and the cytolytic activities of these T cells against primary breast cancer cells were evaluated by LDH release assays.

Groups A and C, which were positive for HER-3 expression (HER2+/HER3+ and HER2-/HER3+, respectively), presented with significantly higher levels of LDH in response to antigen b when compared with antigens a and c (P < 0.05). In group B and D, the LDH release level was not significantly different between antigens a and b, but significantly increased in response

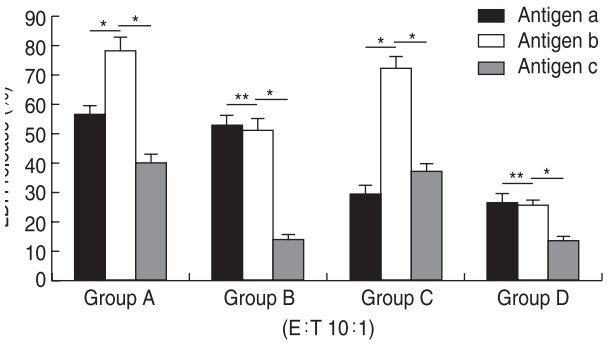

Fig. 3 Immunological activity using the recombinant human HSP70-HER-3 protein complex and autogenous HSP70-PCs. Group A is HER-2 (+) and HER-3 (+), group B is HER-2 (+) and HER-3 (-), Group C is HER-2 (-) and HER-3 (+), Group D is HER-2 (-) and HER-3 (-). Antigen a is the autogenous HSP70-PC alone. Antigen b is a 1:10 ratio of the autogenous HSP70-PCs and the recombinant human HSP70-HER-3 protein complex. Antigen c is the recombinant human HSP70-HER-3 protein complex alone. Assays were performed in triplicate and results are expressed as the mean ± SD (n = 6). $^{*}P < 0.05$, $^{**}P > 0.05$.

to antigen c ($P < 0.05$; Fig. 3). This result suggests that the combination of autogenous HSP70-PCs and recombinant HSP70-HER-3 protein complexes produces stronger immunological activity than autogenous HSP70-PCs alone and increase the killing capacity of autogenous CD8+ T cells targeting HER-3-positive breast cancer cells.

Discussion

DCs are powerful APCs, with an almost 1000 fold higher antigen-presenting capacity when compared to other APCs, such as macrophages and B lymphocytes. Many studies have shown that DCs effectively stimulate initial T cell activation, which is considered the main initiator of the body's anti-tumor immune response. This means that DC-based cellular immunotherapy is an important component in tumor biotherapy. For this reason, this strategy is widely used in China when producing comprehensive treatments for a variety of malignant tumors, including breast cancer, and has been shown to achieve good therapeutic effect [12–13].

HSP70 is an important intracellular molecular chaperone and acts as an important cytoprotective agent via its binding of misfolded proteins preventing their denaturation during cellular stress. HSP70 is highly expressed in multiple kinds of tumor cells and can bind to a large number of tumor antigenic peptides via a noncovalent bond. Immunization with autogenous HSP70-PCs purified from cancer cells provides protection against tumors derived from the same type of cancer cells from which they were purified. The anti-tumor immunogenic mechanism underlying these effects relies on the fact that tumor-derived HSP70-PCs may produce specific antigens for processing by APCs such as DCs, which may then induce antigen-specific cytotoxic CD8+ T cells which target and eradicate these specific tumor cells [14–15].

The human epidermal growth factor receptor (EGFR) family consists of four members: HER-1, HER-2, HER-3 and HER-4. All four family members are transmembrane glycoproteins and closely associated with the development and progression of breast cancer. Among these proteins the role of HER-2 in cancer pathogenesis is the best established. Previous studies have shown that the overexpression of HER-2 in breast cancer patients is associated with estrogen receptor and progesterone receptor negativity, increased histological grade, high rates of cell proliferation, lymph node involvement and poor prognosis. HER-2 has thus become an important target in the targeted treatment and cell therapy protocols developed for breast cancer [16].

In our previous study, we established a new method using CHAPS to purify HSP70-PCs containing more efficient tumor peptides with an increased proportion of membrane tumor-associated peptides from human breast cancer cells. CD8+ cells induced with DCs pulsed using these products demonstrate better anti-tumor activity against the HER-2 overexpressing breast cancer cells from which the complex is derived. However, this method did not achieve good results for HER-2-negative breast cancers because of the absence of an accurate target. Many studies have shown that overexpression of HER-3 is also linked to HER-2 positivity and lymph node involvement. These results suggest that HER-3 may be a potential target for breast cancer treatment, although this hypothesis remains controversial [17].

Given this, we used immunohistochemical methods to determine the expression status of HER-3 in breast cancer in the samples for this study. We identified 37 cases (53%) of HER-3-positive tumors in this cohort and demonstrated that the expression of HER-3 was positively correlated with tumor size, histological type, lymph node metastasis and HER-2 expression status. These results suggest that HER-3 may be a potential target for breast cancer patients, although the correlations between HER-3 expression and various prognostic factors, such as progression-free survival (PFS) and overall survival (OS), are not yet confirmed.

We went on to produce autogenous HSP70-PCs from HER-3-overexpressing breast cancer cells. However, the *in vitro* cytotoxicity results showed that these HSP70-PCs did not exhibit good anti-tumor activity against the HER-3-overexpressing breast cancer cells from which the complexes were purified. Given this we speculated that the HER-3 protein content in these autogenous HSP70-PCs (as quantified by ELISA) was too low to induce a sufficient anti-tumor response. Several aspects

might explain the low levels of HER-3 protein content, including a loss of HER-3 protein during the purification process or denaturation of the HER-3 protein during the purification process.

Thus, to address this issue, we prepared recombinant human HSP70-HER-3 protein complexes and combined these with the autogenous HSP70-PCs in an effort to circumvent the negative effects of reduced HER-3 expression. We compared the immune activity of these new products to those of the autogenous HSP70-PCs or recombinant human HSP70-HER-3 protein complexes on their own. The new protein complex had stronger immunocompetence and induced both autogenous DCs and CD8+ T cells which were able to specifically kill HER-3-overexpressing breast tumor cells whether they were HER-2 positive or negative. This result suggests that the HER-3 protein can be used as a target for HSP70-DC-based cellular immunotherapy and that the anti-tumor immune activity of autogenous HSP70-PCs from breast cancer patients with increased HER-3 expression can be significantly increased using *in vitro* modifications.

In summary, we demonstrated that HER-3 protein can act as a target for cellular immunotherapies against breast cancer. We also demonstrated a new treatment method for HER-3-overexpressing breast cancers. Our future research will focus on the following aspects: (1) we plan to follow the HER-3-positive patients to determine the relationship between HER-3 expression and OS and PFS; (2) we would like to conduct larger clinical trials to evaluate the therapeutic efficacy of this approach and (3) we want to examine the relationship between each of the HER family proteins and breast cancer. We firmly believe that our evaluations will facilitate more effective individualized immunotherapy for breast cancer patients in the future.

Conflicts of interest

The authors indicated no potential conflicts of interest.

References

1. Fahad Ullah M. Breast cancer: current perspectives on the disease status. Adv Exp Med Biol, 2019, 1152: 51–64.
2. Sharifi M, Wisinski KB. Advance in the treatment of early-stage HER2-positive breast cancer. Clin Adv Hemator Oncol, 2020, 8: 482–492.
3. Schutz F, Domschke C and Schneeweiss A. Targeted therapy of HER2-negative breast cancer. Oncol Res Treat, 2016, 39: 118–121.
4. Yanwei Gao, Xia Chen, Weishi Gao, *et al*. A study on melanoma treatment using dendritic cells loaded with antigens purified from melanoma cell lines. Oncol Transl Med, 2020, 1: 21–25.
5. Stein JV. T cell motility as modulator of interactions with dendritic cells. Front Immunol, 2015, 6: 559.
6. Zarema Albakova, Grigoriy A Armeev, Leonid M Kanevskiy, *et al*. HSP70 multi-functionality in cancer. Cells. 2020, 3: 587.
7. Gao Y, Chen X, Gao W, *et al*. A new purification method for enhancing the immunogenicity of heat shock protein 70-peptide complexes. Oncol Rep,2012, 28: 1977–1983.
8. Conradi LC, Spitzner M, Metzger AL, *et al*. Combined targeting of HER-2 and HER-3 represents a promising therapeutic strategy in colorectal cancer. BMC Cancer, 2019, 19: 880.
9. Li Q, Yuan Z and Cao B. The function of human epidermal growth factor receptor-3 and its role in tumors. Oncol Rep, 2013, 30: 2563–2570.
10. Meng Ren, Huixia Xu, Xiangji Lu, *et al*. The study of selective primary culture and determinationof a breast cancer cell line *in vitro*. Oncol Transl Med, 2020, 2: 68–71.
11. Lee YS, Radford KJ. The role of dendritic cells in cancer. Int Rev Cell Mol Biol, 2019, 348: 123–178.
12. Wculek SK, Cueto FJ, Mujal AM, *et al*. Dendritic cells in cancer immunology and immunotherapy. Nat Rev Immunol, 2020, 20: 7–24.
13. Lin M, Liang S, Jiang F, *et al*. 2000-2013, a valuable study: Autologous tumor lysate-pulsed dendritic cell immunotherapy with cytokine-induced killer cells improves survival in stage IV breast cancer. Immunol Lett, 2017, 183: 37–43.
14. Kumar S, StokesJ 3rd, Singh UP, *et al*. Targeting HSP70: a possible therapy for cancer. Cancer Lett, 2016, 374:156–166.
15. Tagliamonte M, Petrizzo A, Tornesello ML, *et al*. Antigen-specific vaccines for cancer treatment. Hum Vaccin Immunother, 2014, 10: 3332–3346.
16. Eccles SA. The epidermal growth factor receptor/Erb-B/HER family in normal and malignant breast biology. Int J Dev Biol, 2011, 55: 685–696.
17. Bae SY, La Choi Y, Kim S, *et al*. Her3 status by immunohistochemistry is correlated with poor prognosis in hormone receptor-negative breast cancer patients. Breast Cancer Res Treat, 2013, 139: 741–750.

DOI 10.1007/s10330-021-0485-5
Cite this article as: Chen X, Zhang XM, Lu XJ, *et al*. Enhancing the treatment effects of tumor cell purified autogenous heat shock protein 70-peptide complexes on HER-3-overexpressing breast cancer. Oncol Transl Med, 2021, 7: 165–171.

Oncology and Translational Medicine
DOI 10.1007/s10330-021-0477-7
August 2021, Vol. 7, No. 4, P172–P176

ORIGINAL ARTICLE

The clinical efficacy of percutaneous ethanol-lipiodol injection (PEI) combined with high-intensity focused ultrasound (HIFU) for small hepatocellularcarcinoma in special or high-risk locations*

Xiaoli Zou[1], Changzhi Zhao[2], Tao Wang[2], Li Jia[1], Zhongyi Feng[2], Xiaoguang Wang[2], Lei Wei[2], Xiaobei Liu[2] (✉)

[1] Department of Ultrasound Imaging, The Affiliated Dalian Municipal Friendship Hospital of Dalian Medical University, Dalian 116001, China
[2] Department of Hepatobiliary Surgery, The Affiliated Dalian Municipal Friendship Hospital of Dalian Medical University, Dalian 116001, China

Abstract

Objective The objective of this study was to explore the short-term effects and postoperative complications of ultrasound-guided percutaneous ethanol-lipiodol injection (PEI) combined with high-intensity focused ultrasound (HIFU) for the treatment of small hepatocellular carcinoma in a special or high-risk location.

Methods Forty patients with small liver cancer in a special or high-risk location were randomly divided into two groups: 20 patients were treated with PEI combined with HIFU (P + H group), and 20 patients were treated with HIFU alone (H group). There were no significant differences in average age, liver function, tumor location, tumor number, or tumor size between the two groups ($P > 0.05$).

Results Significant differences were observed in ablation parameters between the two groups ($P < 0.05$). Under the same power, ablation rates of the P + H group were significantly higher than those in the H group, and postoperative complications in the P + H group were significantly lower than those in the H group ($P < 0.05$).

Conclusion The combination of PEI and HIFU has better clinical value than HIFU alone for small-cell liver cancer in special or high-risk locations.

Received: 8 January 2021
Revised: 21 February 2021
Accepted: 21 May 2021

Key words: hepatocellular carcinoma; special location; high-intensity focused ultrasound (HIFU); percutaneous ethanol-lipiodol injection (PEI); ethanol; lipiodol

Cancer can occur in any part of the liver, and 23.4%–34.7% of hepatocellular carcinoma is located in a special or high-risk location (caudate lobe, adjacent to the top of the diaphragm, gallbladder fossa, hepatic portal, main blood vessels, heart, gastrointestinal organs, etc.) [1–2]. Due to the specificity of its location, it is difficult to operate on small liver cancer in high-risk locations, and radiofrequency and microwave ablation in clinical practice have serious postoperative complications that are regarded as refractory disease or taboo by many scholars [3]. In recent years, with the rapid development of ultrasound therapy, high-intensity focused ultrasound (HIFU) has played an important role in the treatment of *in situ* ablation of hepatocellular carcinoma, especially for small liver cancer in special or high-risk areas. However, due to the influence of tumor structure, location, and "thermal toxicity", the effect of HIFU on tumors with rich blood supplies or in special areas is not ideal. To improve the effects of HIFU, we used an ethanol-lipiodol injection combined with HIFU in the treatment of small liver cancer in special or high-risk areas, and compared the results to using to HIFU alone. We observed the short-term efficacy and evaluated the safety of this method.

✉ Correspondence to: Xiaobei Liu. Email: 13942077177@139.com
* Supported by the research grant from Dalian Health and Family Planning Commission of China (No. 1611020).

Clinical records and methods

General data

This was a prospective study carried out in a single tertiary referral center. Ethical approval was obtained from the local ethics committee. Forty patients who presented with pathologically and clinically confirmed small liver cancer in special or high-risk areas (the maximum diameter of a single lesion or the sum of the diameters of multiple lesions ≤ 5.0 cm [4]) were randomly selected (50 lesions included) and divided into two groups: the HIFU group (H group) and the percutaneous ethanol-lipiodol injection (PEI) combined with HIFU group (P + H group). Each group consisted of 20 patients of various ages and sexes. Twenty-one cases were not treated with other methods [Transcatheter arterial chemoembolization (TACE) was not effective and the operation was refused], eight cases recurred, and eleven cases metastasized. According to the Child-Pugh classification, the numerical scores of all the cases were Child-B or Child-A, without contraindications.

The main reagents used were anhydrous alcohol injection (Tianjin Kemiou Chemical Reagent Co., China), ethanol content ≥ 99.7%, and iodinated oil injection.

Instruments and equipment

Instruments and equipment used included: (1) PEIT needles with three holes, diameter of 21G and length of 200 mm, and 1 cm calibrations (HAKKO Medical, Japan); (2) Acuson S2000 Diagnostic Ultrasound Systemprobe with a frequency of 3.5 MHz anda guide frame (Siemens Medical Solutions, USA); (3) Model JC focused ultrasound tumor therapeutic system (Chongqing HIFU Medical Technology Co., Ltd, China), which was mainly composed of a treatment table (high-frequency generator, integrated transducer and six-dimension motion devices), therapeutic control part, ultrasound monitoring device, water handling system, and a safety protecting device. The therapeutic transducer had a diameter of 200 mm, a therapeutic frequency of 0.8 MHz, and a focal length of 170 mm.

Methods

Preoperative preparation

Routine blood, urine, stool, liver and renal function, electrolyte, blood glucose, blood group, and alpha fetoprotein tests, as well as coagulogram, electrocardiogram, echocardiography, upper abdominal ultrasound, chest CT, plain scan, and contrast-enhanced MRI of the upper abdomen were performed for all patients to ensure the location, size, shape, blood supply, and adjacent organs of the tumors, and the bowel and skin were prepared. No history of alcohol allergy or negative iodine test results were shown for the patients in the P + H group. Informed consent was obtained from all patients before the operations.

Percutaneous ethanol-lipiodol injection

Via local anesthesia with 2% lidocaine, the patients in the P + H group were placed in the treatment position, disinfected, and paved with a sterile sheet 30 min before HIFU. In order to avoid major blood vessels and bile ducts under ultrasound guidance, 21G PEIT needles were inserted into the lesions, and the margins between treated and untreated tissue could be as narrow was 0.5–1.0 cm. An injection of 1.5 mL of amixture of anhydrous alcohol and iodinated oil (proportion of 8:1) was administered slowly due to the size of the tumor, and the needle body was rotated to disperse it evenly. The needle was quickly removed after the operation.

High-intensity focused ultrasound

Surgeries on both the H and P+H groups were performed under general anesthesia. The gastric tube was placed prior to the operation (although no gastric tube was placed when the tumor was far from the gastrointestinal site). When the lesion was on the top of the diaphragm, "artificial pleural effusion" was required prior to the operation [5]. Combined with preoperative MRI and intraoperative ultrasound localization, the injection trace in the target area of the patients in the P + H group could be clearly displayed (hyperechoic reflection); accordingly, the therapeutic effect of HIFU was evaluated based on the gray scale of the target tissue during the treatment. When hyperechoic changes in the target area or overall gray scale increased, the treatment was considered to be effective [6].

Observed contents

(1) Efficacy index: Contrast-enhanced MRI was performed one month after the HIFU operation to evaluate ablation volume and rate of the tumors. Ablation volume (cm^3) = $4/3\pi \times$ R1 (cm) × R2 (cm) × R3 (cm) (R1 = longest diameter/2; R2 = shortest diameter/2; R3 = height/2); ablation rate = ablation volume/target volume × 100%. (2) Safety index: Complications were statistically analyzed according to the classification developed by the Society of Interventional Radiology [7].

Statistical analysis

All data were expressed as $\bar{\chi} \pm s$ and compared with a *t*-test or chi-square test using the SPSS 20.0 software package (SPSS Inc., New York, USA). Statistical significance was defined as a two-tailed *P*-value < 0.05.

Results

Comparison of general condition

No significant difference was observed in average age, liver function, tumor size, tumor number, or tumor location between the H and P + H groups ($P > 0.05$), which showed that the treatment conditions between

Table 1 The comparison of general condition between H and P + H groups ($\bar{\chi} \pm s$)

Groups	Cases	Sex		Average age (years)	Child-Pugh grades			Average volume of tumor (cm^3)
		Male	Female		Grade A	Grade B	Grade C	
H group	20	16	4	63.50 ± 8.96	15	5	0	28.90 ± 19.31
P + H group	20	17	3	62.85 ± 9.89	17	3	0	26.73 ± 16.23

Table 2 The comparison of the location of the lesions between H and P + H groups (*n*)

Groups	Lesion numbers	Location						
		Diaphragm top	Main blood vessels	Gallbladder fossa	Hepatic portal organs	Heart	Gastrointestinal	Caudate lobe
H group	23	3	8	3	3	2	3	1
P + H group	27	4	7	4	4	2	4	2

Table 4 The comparison of the complications between H and P + H groups [*n* (%)]

Groups	Fever (°C)		Liver function	Skin injury			Postoperative local pain			
	≥ 38	< 38	ALT/AST slight increase	I°	II°	III°	Grade 0	Grade I	Grade II	Grade III
H group	1 (5)	2 (10)	6 (30)	14 (70)	2 (10)	2 (10)	0	2 (10)	14 (70)	4 (20)
P + H group	2 (10)*	3 (15)*	8 (40)*	13 (65)	0*	0*	3 (15)*	5 (25)*	11 (55)*	1 (5)*

Note: Postoperative pain was classified by verbal rating scale (VRS) of World Health Organization (WHO): Grade 0 (no pain), Grade I (mild pain), Grade II (moderate pain), Grade III (severe pain). *, Comparison between H and P + H groups, $P < 0.05$. ALT/AST: Alanine aminotransferase/Aspartate aminotransferase

the two groups were consistent and could be compared (Tables 1 and 2).

Comparison of ablation parameters in HIFU

Significant differences in ablation parameters between the H and P + H groups ($P < 0.05$) were observed, which showed that under the same power, ablation rates of the P + H group were significantly greater than those in the H group (Table 3).

Comparison of postoperative complications

No treatment-related deaths, intestinal perforation, bile leakage, liver failure, tumor implantation, ormetastasis were observed in either group. Slight differences existed in fever and liver function damage when the condition returned to normal within one week ($P < 0.05$). No significant difference was observed in skin injury I° (local swelling and erythema) between the two groups ($P > 0.05$). However, in the H group, two patients had blisters and two had skin necrosis. Postoperative local pain in the H group was more severe than that in the P + H group ($P < 0.05$; Table 4).

Table 3 The comparison of ablation parameters between H and P + H groups ($\bar{\chi} \pm s$)

Groups	Ablation volume (cm^3)	Ablation rate (%)
H group	11.66 ± 7.26	40.35
P + H group	18.46 ± 13.12	69.01*

Note: *, Comparison between H and P + H groups, $P < 0.05$

Discussion

HIFU is a non-invasive local therapy technique that has been widely used in the treatment of solid tumors, such as those in liver and pancreatic cancers. Compared with traditional techniques, such as surgery, radiofrequency therapy, microwave therapy, and intervention therapy, HIFU has more advantages, such as a more accurate curative effect, less trauma and pain, faster recovery, and repeatability of treatment [8]. HIFU is also a safer and more effective non-invasivetreatment for small liver cancer in special or high-risk areas. However, due to the differences in tumor shape, location, and "thermal toxicity", in our study, the energy subsidence of HIFU in the focal region was reduced, and the risk of comlications increased. At the cost of reducing acoustic power and prolonging treatment time, the ablation rate was reduced, and the chances of tumor residual and recurrence and complications increased.

The safe and effective improvement of the energy deposition and therapeutic effect of HIFU for liver cancer in special or high-risk regions is an important topic worldwide. Both physical and chemical methods can be used to change the acoustic properties and environment of target tissues (AET) [9], such as intratumoral injection of anhydrous alcohol or TACE, before HIFU. This method affects the mechanism that controls the coagulation and denaturation of tissue protein and vascular embolism, and can improve thermal toxicity and accelerate irreversible

coagulative necrosis. Since anhydrous alcohol disperses poorly and has a limited solidification range, iodinated oil is used because of its high acoustic impedance, which can easily stimulate an increase in temperature [10], as well as act as an anti-proliferative cytotoxin. Intratumoral injection [11–12] of iodinated oil can block material exchange between tumor cells and tissue fluid, especially the acquisition of oxygen, which directly leads to the necrosis of tumor cells. The higher the percentage of iodinated oil deposition, the higher the necrosis rate of the tumor and the better the therapeutic effect. One study reported [13] that when anhydrous alcohol and iodinated oil are mixed, they can strengthen each other and reduce the threshold power of the cavitation effect. In other words, the cavitation effect can occur easily under low acoustic power with ethanol-lipiodol injection during HIFU, which causes the temperature at the focal regionto rise, and also increases the volume of coagulative necrosis covering the entire tumor; thus, the chance of tumor recurrence is reduced. This may be an important rationale for the use of PEI prior to HIFU in the treatment of liver cancer. In addition, iodinated oil also has "tracing" characteristics which make it easier to determine the treatment region and evaluate the postoperative effect of HIFU.

Our study showed that, under the same acoustic power, the ablation rates in the P + H group were significantly higher than those in the H group, which indicated that the intratumoral ethanol-lipiodol injection had significantly changed the AET, which improved the therapeutic effect of HIFU.

Due to the even dispersion of anhydrous alcohol and iodinated oil, which form a "sound beam barrier" that increases the acoustic impedance and local heat deposition, it becomes easier and faster to form a conglomerate gray scale change. When sound waves are reflected into the necrotic zone to reduce the energy deposition in the ectopic area, they effectively protect the normal tissue around the tumor, thus reducing the complications of HIFU for small liver cancer in high-risk or special regions. This was consistent with the results in the P + H group in this study. No serious complications, such as gastrointestinal perforation orbile leakage, were observed in this study, although minor ones, such as transient fever and liver function damage, were slightly more severe in the P + H group. However, these were considered to be reversible and related to the toxic absorption effect of anhydrous alcohol and iodinated oil. The skin damage in the P + H group was mostly seen as local mild swelling, while in the H group some individual patients had blisters, and two patients had skin injuries classified as III°. The classified scores of postoperative pain in P + H group were significantly lower compared to the H group.

Because of the abundant blood supply of hepatocellular carcinoma, the injection speed should be slow in order to prevent the drugs from becoming diluted, entering the blood vessels orbiliary tract, or returning to the abdominal cavity. For lesions in special or high-risk locations, it is extremely challenging for ultrasound-guided puncture to ensure one-time success when the patients are holding their breath. Core needle puncture, while tracking the tip of the needle, is recommended to ensure that the tip can reach the deep part of the tumor and that the drug evenly diffuses. Therefore, it is necessary to push and rotate the needle body during the injection process. At the same time, early injection prior to HIFU reduces the coagulation range for tumor tissues, thus reducing the synergistic effect of the drug during HIFU. Therefore, ethanol-lipiodol injection 1 h before HIFU plays a synergistic role and is beneficial for intraoperative localization.

The ethanol-lipiodol injection has both a direct chemical effect on the tumor and a synergistic effect on HIFU in the treatment of hepatocellular carcinoma, which can improve the efficacy of HIFU in clinical therapy.

Conflicts of interest

The authors indicated no potential conflicts of interest.

References

1. Bureau of Medical Administration, National Health Commission of the People's Republic of China. Guidelines for diagnosis and treatment of primary liver cancer in China (2019 edition). J Clin Hepatol (Chinese), 2020, 36: 277–292.
2. Liu LL, Pan HM. The development of radiofrequency ablation of hepatic carcinoma in high-risk locations. Chin Clin Oncol (Chinese), 2012, 17: 475–478.
3. Teratani T, Yoshida H, Shiina S, *et al*. Radiofrequency ablation for hepatocellular carcinoma in so-called high-risk locations. Hepatology, 2006, 43: 1101–1108.
4. Liu Q, Wang WQ. Hepatocellular carcinoma. 1st ed. Beijing: People's Medical Publishing House, 2000. 379–380.
5. Wu GM, Min S. Efficacy and security of high-intensity focused ultrasound (HIFU) for liver cancer with the aid of artificial hydrothorax under general anesthesia. Chin J Modern Med (Chinese), 2011, 21: 227–229.
6. Chinese Medical Association. The guidelines of high intensity focused ultrasound tumor therapeutic system in clinical practice (Trial). Natl Med J China (Chinese), 2005, 85: 796–797.
7. Sacks D, McClenny TE, Cardella JF, *et al*. Society of Interventional Radiology clinical practice guidelines. J Vasc Interv Radiol, 2003, 14 (9 Pt 2): S199–S202.
8. Zou XL, Sun BX, Jia L, *et al*. The clinical study of ultrasound-guided intra-hysteromyoma injection of ethyl alcohol absolute combined with HIFU in the treatment of uterine fibroids. Oncol Transl Med, 2018, 4: 203–207.
9. Wu F, Wang ZB, Chen WZ, *et al*. Advanced hepatocellular carcinoma: treatment with high-intensity focused ultrasound ablation combined

with transcatheter arterial embolization. Radiology, 2005, 235: 659–667.
10. Zou JZ, Ou X. Research progress on the therapeutic dosimetry of high intensity focused ultrasound. Sci Technol Review (Chinese), 2010, 28: 95–100.
11. Li H, Zu MH. Experimental study of the effect of Lipiodol intratumorally injected on hepatocellular carcinoma cells. Chin J Interv Imaging Ther (Chinese), 2007, 4: 383–387.
12. Durand-Fontanier S, Simon A, Duroux JL, *et al*. Lipiodol ultra-fluid: an antitumor agent-*in vitro* study. Anticancer Res, 1999, 19: 4357–4361.
13. Chen C, Liu Y, Maruvada S, *et al*. Effect of ethanol injection on cavitation and heating of tissues exposed to high-intensity focused ultrasound. Phys Med Biol, 2012, 57: 937–961.

DOI 10.1007/s10330-021-0477-7
Cite this article as: Zou XL, Zhao CZ, Wang T, *et al*. The clinical efficacy of percutaneous ethanol-lipiodol injection (PEI) combined with high-intensity focused ultrasound (HIFU) for small hepatocellularcarcinoma in special or high-risk locations. Oncol Transl Med, 2021, 7: 172–176.

Oncology and Translational Medicine
DOI 10.1007/s10330-021-0493-3

August 2021, Vol. 7, No. 4, P177–P182

ORIGINAL ARTICLE

Relationship between miR-7-5p expression and ^{125}I seed implantation efficacy in pancreatic cancer and functional analysis of target genes*

Tingting Hao[1], Chaoqi Wang[2] (Co-first author), Yingjie Song[3] (Co-first author), Wanyan Wu[1], Xuetao Li[1], Tao Fan[1] (✉)

[1] Department of Oncology, The People's Hospital of China Three Gorges University, The First People's Hospital of Yichang, Yichang 443000, China
[2] Department of Urinary Surgery, Affiliated Hospital of Inner Mongolia University for the Nationalities, Tongliao 028007, China
[3] General Surgery, The People's Hospital of China Three Gorges University, The First People's Hospital of Yichang, Yichang 443000, China

Abstract

Objective The aim of this study was to investigate the relationship between miR-7-5p expression and intertissue-^{125}I irradiation sensitivity in pancreatic cancer tissues and to analyze the function of target genes.

Methods Thirty-seven patients with unresectable pancreatic ductal adenocarcinoma (PDAC) treated with radioactive ^{125}I seed implantation were enrolled. RT-PCR was used to detect the expression level of miR-7-5p in cancer tissues and analyze the relationship between miR-7-5p expression and ^{125}I radiation sensitivity. Bioinformatic software and online tools were used to predict the miR-7-5p target genes and analyze their functional annotation and pathway enrichment.

Results Radioactive ^{125}I seed implantation was followed up for 2 months. The objective response rate of the miR-7-5p high expression group was 65.0% (13/20), whereas the objective response rate of the miR-7-5p low expression group was 5.88% (1/17), and the difference between the two groups was statistically significant (χ^2 = 13.654, P < 0.001). A total of 187 target genes were predicted using three databases. GO functional annotation showed that target genes were mainly involved in cellular response to insulin stimulus, regulation of gene expression by genetic imprinting, cytosol, peptidyl-serine phosphorylation, bHLH transcription factor binding, cargo loading into vesicles, cellular response to epinephrine stimulus, and nucleoplasm. KEGG pathway enrichment analysis showed that target genes were mainly involved in the ErbB signaling pathway, HIF-1 signaling pathway, axon guidance, longevity regulatory pathway, endocrine resistance, glioma, choline metabolism in cancer, and EGFR tyrosine kinase inhibitor drug resistance. Molecular complex detection analysis by Cytoscape revealed that PIGH, RAF1, EGFR, NXT2, PIK3CD, PIK3R3, ERBB4, TRMT13, and C5orf22 were the key modules of miR-7-5p target gene clustering.

Conclusion The expression of miR-7-5p in pancreatic cancer tissues positively correlated with the radiosensitivity of ^{125}I seeds. Via targeted gene regulation, miR-7-5p acts on the network of multiple signaling pathways in PDAC and participates in its occurrence and development. Thus, miR-7-5p may become a predictive index of ^{125}I seed implantation therapy sensitivity in PDAC patients.

Key words: miR-7-5p; pancreatic cancer; ^{125}I; radioactive seed implantation

Received: 7 May 2021
Revised: 16 July 2021
Accepted: 21 August 2021

The relationship between miRNAs and tumors is similar to that of tumor suppressor genes and cancer activators. The miRNAs are directly or indirectly involved in regulating the expression of one or more target genes. Abnormal expression of miRNAs plays an important role in the occurrence and development of tumors as well

✉ Correspondence to: Tao Fan. Email: 1601340054@qq.com
* Supported by grants from the health commission of Hubei Province scientific research project (No. WJ2019H510) and the Natural Science Foundation of Inner Mongolia Autonomous Region (No. 2021MS8071), China.

as drug efficacy evaluation [1–3]. Therefore, miRNAs are increasingly being considered potential biomarkers for disease diagnosis, curative effect judgment, and prognosis evaluation [4]. We studied the effect of ^{125}I seed implantation on unresectable pancreatic ductal adenocarcinoma (PDAC) and the expression level of miR-7-5p in cancer tissue, to explore the relationship between the expression of miR-7-5p and the irradiation sensitivity of radioactive ^{125}I seeds. Bioinformatic software and online tools were used to predict miR-7-5p target genes, perform their functional annotation and pathway enrichment analysis, and analyze the key modules of the target gene network.

Materials and methods

This study was conducted at the People's Hospital of China Three Gorges University, China, from January 2017 to March 2019. The research was conducted after approval from the Committee on Human Research and Ethics. Thirty-seven patients with unresectable PDAC undergoing radioactive ^{125}I seed implantation were enrolled in the study. Complete follow-up data were collected. The ^{125}I isotope, activity 0.5–0.9 mCi, half-life 59.43 days, gross tumor volume (GTV) prescription dose 115–130 Gy (at least D90 reached the prescription dose).

The expression of miR-7-5p in pancreatic carcinoma was detected by real-time PCR. The total mRNA kit from Takara Company was used to extract total cellular RNA. cDNA was prepared as described in the instructions of the Prime Script®RT Kit with gDNA Eraser (Perfect Real Time) reverse transcription kit. Real-time PCR amplification was conducted using cDNA as a template and U6 as an internal reference. The miR-7-5p upstream primer was 5'-CCACGTTGGAAGACTAGTGATTT-3', and the downstream primer was 5'-TATGGTTGTTCT GCTCTCTGTCTC-3'. U6 upstream primer: 5'-CTCGC TTCGGCAGCACA-3'; downstream primer: 5'-AACGC TTCACGAATTTGC GT-3'. The reaction mixture consisted of 10.0 μL of 2 × SYBR Premix Ex Taq™ II, 0.8 μL of each of the upstream and downstream primers, 2.0 μL of cDNA, 0.4 μL of ROX reference dye (50 ×), and DEPC water to a total of 20.0 μL. The reaction conditions were as follows: denaturation at 95°C for 30 s, annealing at 62°C for 40 s, repeating the above steps for 40 cycles, and finally a hold at 4°C for preservation. After the end of PCR amplification, the analyzer displayed the standard curve, amplification curve, and melting curve. The amplification factor was calculated using the $2^{-\Delta\Delta Ct}$ method.

Three online tools, TargetScan, miRDB, and miRWalk, were used to predict the target genes of hsa-miR-7-5p, and to obtain a more accurate target gene by creating a Venny map (https:// bioinfogp.cnb.csic.es/tools/venny/index.html) and taking the intersection. An online platform (https:// cloud.oebiotech.cn/task/detail/arrayenrichment/) was used to perform Gene Ontology (GO) functional annotation and Kyoto Encyclopedia of Genes and Genomes (KEGG) was used to perform pathway enrichment analysis. The online tool STRING (https://string-db.org/) and miRNet 2.0 database (www.mirnet.ca/Faces/home.xhtml) were used to obtain the miRNA-Gene network graph and matrix list, which was then imported using Cytoscape 3.6.1 software. The Molecular Complex Detection (MCODE) plugin was used for module clustering analysis to detect the potential functional modules in the network. In the MCODE process, the cut-off value of a degree was set to 2, and the cut-off value of the node score was set to 0.2.

SPSS version 20.0, was used for statistical analysis of the data. Cancerous tissue miR-7-5p relative expression was measured using the $2^{-\Delta\Delta Ct}$ value measure, divided into high- and low-level groups. Measurement data are expressed as mean ± SD. An independent sample *t*-test was used for comparison between the two groups. All *P* values were bidirectional and $P < 0.05$ was considered to be significant.

Results

Among the 37 patients who received CT-guided radioactive ^{125}I seed inter-tissue implantation therapy, 20 patients had high miR-7-5p expression (miR-7-5p High) and 17 patients had low miR-7-5p expression. Thirty-seven patients were treated with inter-tissue implantation of radioactive ^{125}I seeds. After 2 months of follow-up, 14 patients achieved PR, 23 achieved SD, and no patients achieved CR or PD. The objective response rate of the miR-7-5p high group was 65.0% (13/20) whereas that of the miR-7-5p low group was 5.88% (1/17), and there was a significant difference between the two groups ($\chi^2 = 10.347$, $P = 0.001$; Fig. 1). The results showed that the

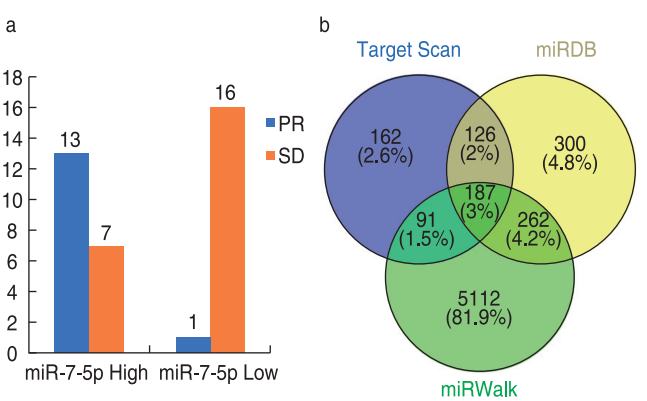

Fig. 1 (a) Relationship between miR-7-5p expression level and therapeutic response; (b) Venn diagrams of TargetScan, miRDB, and miRWalk predicting miRNA-7-5p target genes

expression of miR-7-5p positively correlated with the irradiation sensitivity to radioactive ^{125}I seeds. Patients with high expression of miR-7-5p were relatively sensitive to radiotherapy with high objective efficiency, while patients with low expression were relatively insensitive to radiotherapy with low objective efficiency.

The online tools TargetScan, miRDB, and miRWalk were used to predict target genes of miR-7-5p and a total of 187 target genes were identified by all three tools (Fig. 1). Through online tools, mirDIP 4.1 (http://ophid.utoronto.ca/ mirDIP/index confirm JSP) filtering. The lowest reliability of setting parameters was selected as very high, and 25 prediction software packages, such as filter source RNA22, Mirtar, RNAHybrid, Mircode, MBStar, TargeRank, Microrna.org, Pita, TargetScan, PicTar, and MirBase were selected, and the frequency of occurrence of target genes was at least 1. The results showed that the 187 intersection target genes were all target genes of very high credibility.

There were 135 biological process (BP) annotated genes, 146 cellular component (CC) annotated genes, and 129 molecular function (MF) annotated genes. A bar chart for the top 10 most significant functions of BP, CC, and MF genes identified through the GO enrichment analysis is shown in Fig. 2.

Through the BP, CC, and MF functional annotation of GO, we found that target genes were mainly involved in cellular response to insulin stimulus, regulation of gene expression by genetic imprinting, cytosol, peptidyl-serine phosphorylation, bHLH transcription factor binding, cargo loading into vesicles, cellular response to epinephrine stimulus, and nucleoplasm. KEGG pathway enrichment analysis showed that target genes were mainly involved in the ErbB signaling pathway, HIF-1 signaling pathway, axon guidance, longevity regulatory pathway, multiple species, endocrine resistance, glioma, choline metabolism in cancer, and EGFR tyrosine kinase inhibitor drug resistance (Fig. 3).

Seven potential functional modules in the network were identified using module clustering (Table 1). PIGH, RAF1, EGFR, NXT2, PIK3CD, PIK3R3, ERBB4, TRMT13, and C5orf22 were the key modules in the hsa-miR-7-5p target gene cluster.

Discussion

MiR-7-5p has been reported to play an anti-tumor role in human colorectal cancer [5], NSCLC [6], nasopharyngeal carcinoma [7], gastric cancer [8], hepatocellular carcinoma

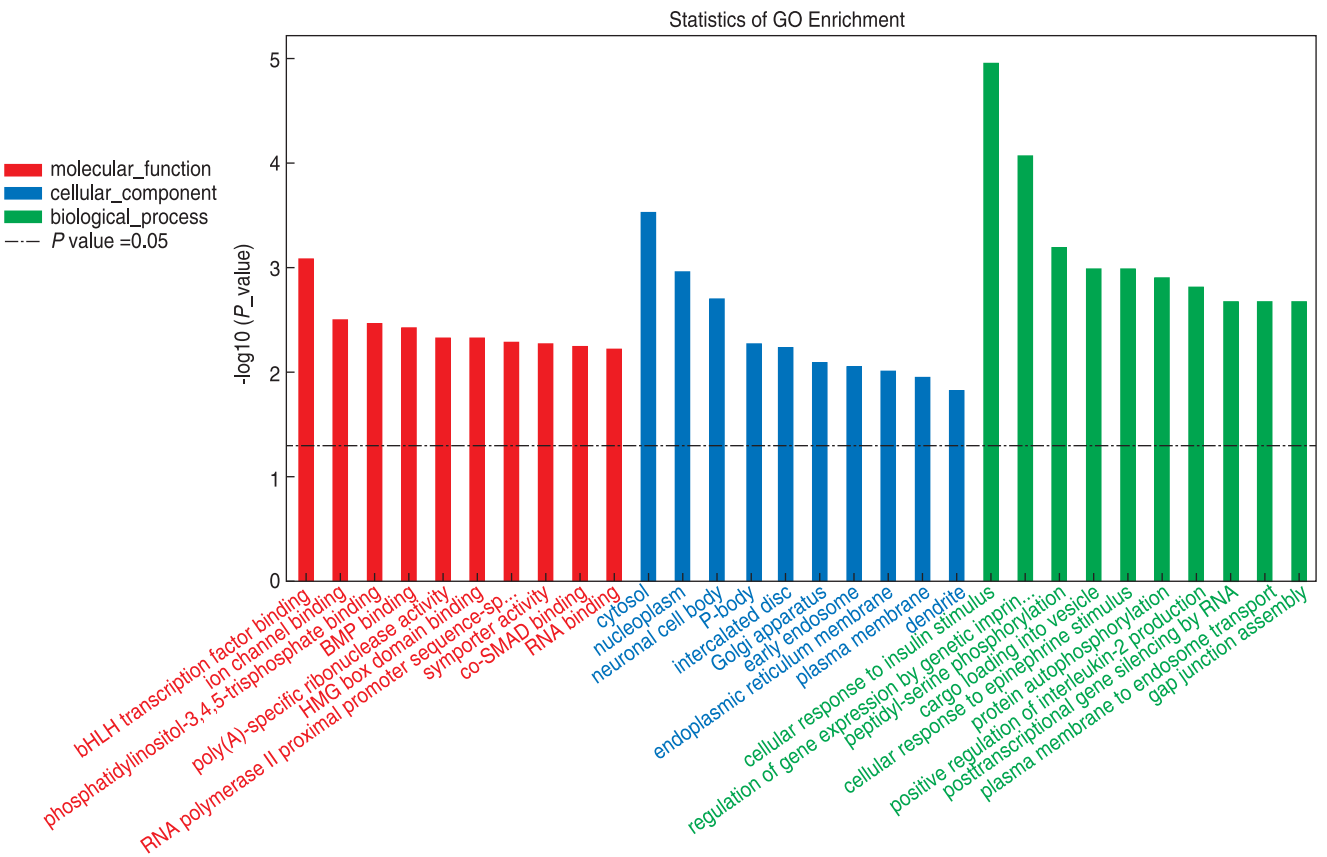

Fig. 2 GO bar graph. Y-axis is - log10 (*P* value). The higher the bar graph height, the greater the significance

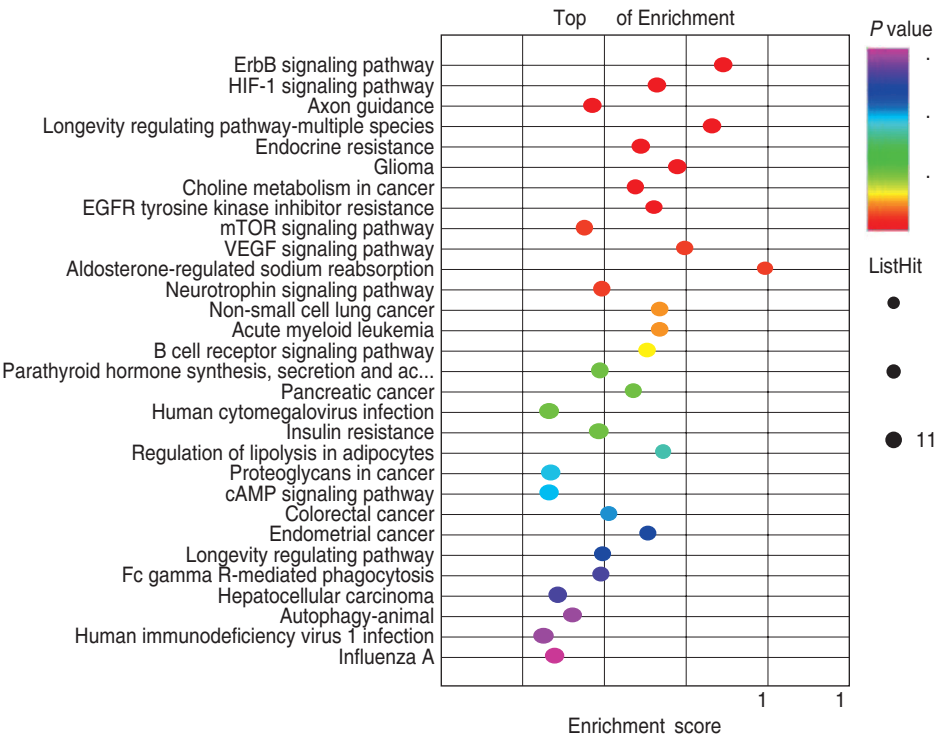

Fig. 3 KEGG bubble chart: the y-axis corresponds to the KEGG entries, the x-axis corresponds to the enrichment score, the size of the point corresponds to the number of intersection genes in the KEGG entries, and the smaller the *P* value of KEGG enrichment, the greater the significance

Table 1 Seven functional modules of MCODE module cluster analysis

Cluster	Score	Nodes	Edges	Node IDs
1	5.111	10	23	PIGH, RAF1, EGFR, NXT2, PIK3CD, PIK3R3, ERBB4, TRMT13, C5orf22, hsa-mir-7-5p
2	4.5	5	9	ADCY9, PDE4B, CAMK2D, CACNB4, PDE4D
3	4	4	6	EIF4EBP2, SGK1, MAPKAP1, AKT3
4	3.333	4	5	SP1, GATA6, PAX6, KLF4
5	3.333	4	5	PICALM, SORT1, TFRC, RAB5B
6	3	3	3	STRN3, CCT4, STRN
7	3	3	3	IPO11, XPO7, KPNA1

[9], cervical cancer [10], breast cancer [11], small cell lung cancer [12], and other tumors. However, its expression and function are sometimes contradictory. The expression of miR-7-5p is significantly lower in lung cancer tissues. *In vivo* and *in vitro* studies have shown that miR-7-5p targeting NOVA2 inhibits the proliferation, migration, and invasion of lung cancer cells [6]. In esophageal cancer tissues, miR-7-5p is highly expressed compared to para-cancerous tissues and is negatively correlated with the survival rate of patients with esophageal cancer. The downregulation of miR-7-5p *in vivo* can inhibit the occurrence and development of esophageal cancer by inactivating the MAPK signaling pathway [13]. Nevertheless, the high expression level of miR-7-5p can significantly inhibit the growth, migration, and colony formation of human hepatocellular carcinoma cells [14].

In addition, miR-7 modulates the chemoradiotherapy sensitivity of some tumors. In terms of chemotherapy resistance, Lai *et al.* revealed that miR-7 is downregulated in doxorubicin-resistant small cell lung cancer cells, and miR-7 enhancement inhibits doxorubicin-induced homologous recombination repair by inhibiting the expression of Rad51 and BRCA1, thereby improving the sensitivity of doxorubicin-resistant small cell lung cancer cells to doxorubicin [12]. In temozolomide (TMZ)-resistant gliomas, miR-7 can increase the sensitivity of cells to TMZ by downregulating YY1 and hindering the stemness of TMZ-resistant glioblastoma cells [15]. In terms of radiation resistance, studies have found that high expression of miR-7-5p can promote radiation resistance in cervical

cancer and liver cancer cells after radiation (5 Gy and 10 Gy) [16]. However, other studies have found that miR-7-5p inhibitor can significantly enhance the radiation resistance of nasopharyngeal carcinoma cells by promoting the proliferation, migration, and invasion of NPC cells, inhibiting cell apoptosis, and improving the sensitivity of nasopharyngeal carcinoma cells to radiotherapy [17]. The role of miR-7-5p in the radiosensitivity of human pancreatic cancer has not yet been studied. In this study, we found that the expression of miR-7-5 was positively correlated with the radiosensitivity of pancreatic cancer. Thirty-seven patients with unresectable pancreatic cancer were treated with ^{125}I seeds under the guidance of spiral CT. After 2 months of follow-up, 14 patients achieved PR, 23 patients achieved SD, and no patients achieved CR or PD. The objective response rate (ORR) of the miR-7-5p high group was 65.0% (13/20) whereas the ORR of the miR-7-5p group was 5.88% (1/17), and there was a significant difference between the two groups (χ^2 = 13.654, P < 0.001). The results showed that the high expression of miR-7-5p was relatively sensitive to radiotherapy with a high objective effective rate, while the low expression of miR-7-5p was relatively insensitive to radiotherapy with a low objective effective rate.

The tumorigenicity and tumor inhibition of miRNA are achieved by binding to the 3' noncoding region of the corresponding target gene to degrade or inhibit the translation of the target gene miRNA [18]. Because of the diversity of miRNA target genes in type and quantity, the same miRNA may regulate multiple target genes simultaneously, and the same gene may be precisely regulated by multiple miRNAs at the same time. The regulatory mechanisms of target genes are complex. Therefore, it is very important to accurately predict miRNA target genes and correctly understand the regulation mode between miRNA and target genes [19].

Currently, bioinformatics is an important method for predicting miRNA target genes [20] and has the advantage of being able to handle a large amount of data and simple operation. To improve the accuracy of target gene prediction and reduce false results, the results of multiple database prediction are intersected. In this study, 187 miRNA-7-5p target genes were predicted and screened using TargetScan, miRDB, and miRWalk. BP, CC, and MF enrichment analysis of GO showed that target genes were mainly involved in cellular response to insulin stimulus, regulation of gene expression by genetic imprinting, cytosol, peptidyl-serine phosphorylation, bHLH transcription factor binding, cargo loading into vesicles, cellular response to epinephrine stimulus, and nucleoplasm. KEGG pathway enrichment analysis showed that target genes were mainly involved in the ErbB signaling pathway, HIF-1 signaling pathway, axon guidance, longevity regulatory pathway, multiple species, endocrine resistance, glioma, choline metabolism in cancer, and EGFR tyrosine kinase inhibitor drug resistance. Using the mirnet2.0 database and Cytoscape 3.6.1 software, we found that PIGH, RAF1, EGFR, NXT2, PIK3CD, PIK3R3, ERBB4, TRMT13, and C5ORF22 were the key modules in the cluster of hsa-miR-7-5p target gene networks. However, the rationality of miR-7-5p and its target gene as a biomarker of radiotherapy sensitivity in pancreatic cancer requires further study.

Conclusion

This study found that age, sex of and tumor marker level, tumor location, and tumor size in patients with pancreatic cancer were not the main factors affecting the efficacy of radioactive ^{125}I particles. However, the expression of miR-7-5p in pancreatic cancer tissues positively correlated with the radiosensitivity of ^{125}I seeds. Through targeted gene regulation, miR-7-5p acts on the network of multiple signaling pathways of PDAC and participates in its occurrence and development and is thus expected to become a predictive index of ^{125}I seed implantation therapy sensitivity in patients with PDAC.

Conflicts of interest

The authors indicated no potential conflicts of interest.

References

1. Huang JH, Liu HZ, Zhao Y, *et al*. MicroRNAs expression patterns predict tumor mutational burden in colorectal cancer. Front Oncol, 2020, 10: 550986.
2. Ren ZJ, Lv MM, Yu Q, *et al*. MicroRNA-370-3p shuttled by breast cancer cell-derived extracellular vesicles induces fibroblast activation through the CYLD/Nf-κB axis to promote breast cancer progression. FASEB J, 2021, 35: e21383.
3. Grenda A, Krawczyk P, Błach J, *et al*. Tissue microRNA expression as a predictor of response to immunotherapy in NSCLC patients. Front Oncol, 2020, 10: 563613.
4. Otsuka K, Ochiya T. Possible connection between diet and microRNA in cancer scenario. Semin Cancer Biol, 2021, 73: 4–18.
5. Zheng YW, Nie PH, Xu SF. Long noncoding RNA CASC21 exerts an oncogenic role in colorectal cancer through regulating miR-7-5p/YAP1 axis. Biomed Pharmacother, 2020, 121: 109628.
6. Xiao HP. MiR-7-5p suppresses tumor metastasis of non-small cell lung cancer by targeting NOVA2. Cell Mol Biol Lett, 2019, 24: 60.
7. Zhong Q, Huang JC, Wei JW, *et al*. Circular RNA CDR1as sponges miR-7-5p to enhance E2F3 stability and promote the growth of nasopharyngeal carcinoma. Cancer Cell Int, 2019, 19: 252.
8. Xin L, Liu L, Liu C, *et al*. DNA-methylation-mediated silencing of miR-7-5p promotes gastric cancer stem cell invasion via increasing Smo and Hes1. J Cell Physiol, 2020, 235: 2643–2654.
9. Kabir TD, Ganda C, Brown RM, *et al*. A microRNA-7/growth arrest specific 6/TYRO3 axis regulates the growth and invasiveness of sorafenib-resistant cells in human hepatocellular carcinoma. Hepatology, 2018, 67: 216–231.
10. Yang F, Guo L, Cao Y, *et al*. MicroRNA-7-5p promotes cisplatin resistance of cervical cancer cells and modulation of cellular energy

homeostasis by regulating the expression of the PARP-1 and BCL2 genes. Med Sci Monit, 2018, 24: 6506–6516.
11. Gao DF, Zhang XF, Liu BB, *et al*. Screening circular RNA related to chemotherapeutic resistance in breast cancer. Epigenomics, 2017, 9: 1175–1188.
12. Lai JZ, Yang HN, Zhu YY, *et al*. MiR-7-5p-mediated down-regulation of PARP1 impacts DNA homologous recombination repair and resistance to doxorubicin in small cell lung cancer. BMC Cancer, 2019, 19: 602.
13. Shi W, Song JX, Gao ZY, *et al*. Downregulation of miR-7-5p inhibits the tumorigenesis of esophagus cancer via targeting KLF4. Oncol Targets Ther, 2020, 13: 9443–9453.
14. Song XZ, Ren XN, Xu XJ, *et al*. LncRNA RHPN1-AS1 promotes cell proliferation, migration and invasion through targeting miR-7-5p and activating PI3K/AKT/mTOR pathway in hepatocellular carcinoma. Technol Cancer Res Treat, 2020, 19: 1533033820957023.
15. Jia B, Liu W, Gu JT, *et al*. MiR-7-5p suppresses stemness and enhances temozolomide sensi-tivity of drug-resistant glioblastoma cells by targeting Yin Yang 1. Exp Cell Res, 2019, 375: 73–81.
16. Tomita K, Fukumoto M, Itoh K, *et al*. MiR-7-5p is a key factor that controls radioresistance via intracellular Fe(2+) content in clinically relevant radioresistant cells. Biochem Biophys Res Commun, 2019, 518: 712–718.
17. Peng JJ, Liu F, Zheng H, *et al*. lncRNA ZFAS1 contributes to the radioresistance of nasopharyngeal carcinoma cells by sponging hsa-miR-7-5p to upregulate ENO2. Cell Cycle, 2021, 20: 126–141.
18. Cecene G, Ak S, Eskiler GG, *et al*. Circulating miR-195 as a therapeutic biomarker in Turkish breast cancer patients. Asian Pac J Cancer Prev, 2016, 17: 4241–4246.
19. Chen G, Hu J, Huang Z, *et al*. MicroRNA-1976 functions as a tumor suppressor and serves as a prognostic indicator in non-small cell lung cancer by directly targeting PLCE1. Biochem Biophys Res Commun, 2016, 473: 1144–1151.
20. Fan T, Wang CQ, Zhang K, *et al*. Differentially expressed genes analysis and target genes prediction of miR-22 in breast cancer. Oncol Transl Med, 2021, 7: 59–64.

DOI 10.1007/s10330-021-0493-3
Cite this article as: Hao TT, Wang CQ, Song YJ, *et al*. Relationship between miR-7-5p expression and ^{125}I seed implantation efficacy in pancreatic cancer and functional analysis of target genes. Oncol Transl Med, 2021, 7: 177–182.

Oncology and Translational Medicine
DOI 10.1007/s10330-021-0490-0
August 2021, Vol. 7, No. 4, P183–P194

REVIEW ARTICLE

Mechanism of tumor synthetic lethal-related targets

Yuhang Zhang[1], Peng Xu[2] (✉)

[1] Shaanxi University of Traditional Chinese Medicine, Xianyang 712000, China
[2] Shaanxi Academy of Traditional Chinese Medicine, Shaanxi Provincial Hospital of Traditional Chinese Medicine, Xi'an 710003, China

Abstract

Synthetic lethality is becoming more and more important in the precise treatment of oncology. Malignant tumors caused by gene mutations involve a complex DNA signaling process, and inhibition of DNA signaling in different ways may more effectively control the occurrence and development of tumors.

Inhibition of tumor paired lethal genes effectively kills tumor cells, and more and more novel drugs that inhibit tumors are developing in this direction. This article reviews the synthetic lethal theory and discusses selection of drugs to target mutated genes in common solid tumors. The synthetic lethal gene pairs, representative targeted drugs, and related characteristics of four tumor types: lung cancer, breast cancer, colon cancer and prostate cancer, are systematically reviewed.

Received: 13 April 2021
Revised: 26 May 2021
Accepted: 15 July 2021

Key words: synthetic lethal; targeted drug; common tumors

Tumors are a distant effect produced by DNA damage in the body. Inhibition of DNA damage repair in tumor cells has a fatal impact on their development. The principle that tumor cells undergo lethal effects under two or more non-lethal and non-allelic mutations is known as a synthetic lethal. Cancer therapy has gradually developed from interfering with DNA physicochemical synthesis to precise targeting at the genetic level. With the wide application in clinical practice of gene sequencing in patients with mutant carcinogenic tumors, the application of synthetic lethal-related paired gene targeted drugs can more effectively block the proliferation of tumors and improve prospects for cancer therapy. In this review, based on the theory of tumor gene synthesis and lethality, the principle of tumor inhibition by paired genes that initiate related tumorigenesis is summarized, and the drug treatment options for common solid tumors are explored.

Synthetic lethal

Organisms have complex DNA repair systems to protect their integrity, mainly through homologous recombination pathways or non-homologous end joining, to repair double-stranded DNA breaks, and through base excision repair or mismatch repair to repair single-stranded DNA breaks. DNA damage repair is initiated after normal cellular DNA is damaged under the influence of physicochemical, biological, and other carcinogenic factors, and damage repair mechanisms are meticulous and complete to protect it from carcinogenesis.

However, tumor cells themselves have genetic defects; hence, the failure to repair DNA damage leads to fatal effects in cells. Driver mutations are an important factor in thousands of mutations leading to tumorigenesis and have a greater impact in the development of tumors than other passenger genes [1]. Generally, tumors have multiple oncogene mutations, but most tumors are sensitive to the inhibition of a single oncogene, which is known as "oncogene addiction" [2].

The key goal of cancer drugs is to selectively initiate the genetic damage of target and persistent tumor cells. Under the theory of synthetic lethality, the multiple inhibition of enzymes involved in DNA repair and cell cycle control in tumor genetic signaling pathways can block the development of tumors. Synthetic lethality is important in targeted and precise treatment of tumors after chemotherapy [3–4] (Fig. 1).

This inhibition leads to tumor cell apoptosis due to oncogene signaling addiction, collateral vulnerability, and more generally synthetic lethality [5–6]. An attractive strategy for the synthetic lethal treatment of malignant tumors is to target enzyme functions [7] and related proteins that are dispensable in normal cells. This makes gene

✉ Correspondence to: Peng Xu. Email: zxz310@163.com

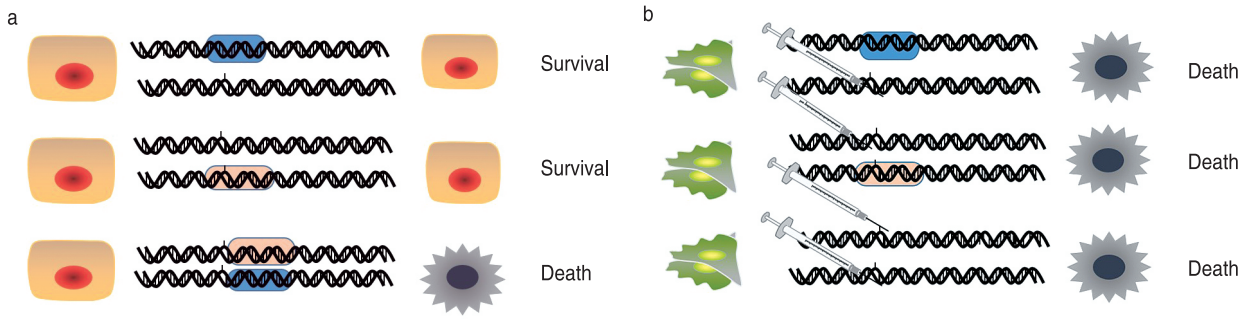

Fig. 1 Cells in synthetic lethal theory

inhibition methods feasible by focusing on enzymes that are essential for the survival of mutant protocancerous cells, such as tyrosine kinases and cell cycle-dependent methionine kinases. Although many drugs that block driver gene addiction have been shown to be successful in the treatment of cancer, multiple inhibition of cancer gene mutations is still challenging in cancer therapy. For example, malignant cells generated by BRCA gene mutations are clinically effective in demonstrating the synthetic lethality of PARP (poly ADP-ribose polymerase) inhibitors [8]. This example encourages modern cancer research to search for synthetic lethal "gene-drug" combinations [9] to target other mutated driver genes in the progression of cancer, toward "gene-gene" patterns.

Tumor synthetic lethal gene mechanism

Lung cancer

Lung cancer is still the most common tumor worldwide.Since the correlation between the occurrence of lung cancer and driver genes has been increasingly confirmed, the application of targeted drugs in the "gene-drug" model of precise treatment of lung cancer has been widely and meaningfully effective.

EGFR-KRAS

Epidermal growth factor (EGF) converts extracellular signals into appropriate cellular responses via epidermal growth factor receptor (EGFR) tyrosine kinase binding ligands and activating multiple signaling steps [10]. EGFR's known ligands include EGF, TGFA/TGF-α, AREG, epigen/EPGN, BTC/betacellulin, HURP/EREG and HBEGF [11]. Ligand binding activates at least four major downstream signaling cascades, including RAS-RAF-MEK-ERK, PI3K-AKT, among others. EGFR may also activate the NF-κB signaling cascade [12] and can also directly phosphorylate other proteins such as RGS16, activating its GTPase activity and may transduce EGF receptor signal to G protein-coupled [13] receptor signal transduction [14]. It phosphorylates MUC1 and increases its interaction with SRC and CTNNB1/β-catenin. Cell migration is positively regulated by interaction with CCDC88A/GIV, which retains EGFR at the cell membrane after ligand stimulation, thereby promoting EGFR signaling and thus triggering cell migration [15]. The KRAS gene belongs to the RAS gene family, in which the Ras protein binds GDP/GTP and has intrinsic GTPase activity. Its related pathways include the common cytokine receptor gamma chain family signaling pathway and the negative regulation of the MAPK pathway. Gene Ontology (GO) annotations related to this gene include GTP binding. An important paralog of this gene is NRAS, which plays an important role in the regulation of cell proliferation [16] and in promoting oncogenic events by inducing transcriptional silencing of tumor suppressor genes (TSG) in lung cancer cells in a ZNF304-dependent manner [17]. KRAS and EGFR proteins produce synthetic lethality when co-expressed in human lung adenocarcinoma (LUAD) cells [18]. The clinical use of KRAS-associated inhibitory drugs in combination with EGFR-TKIs is increasingly widely recommended in the progression of lung cancer treatment (Fig. 2a).

CDK4-RAS

Serine/threonine protein kinase, also known as cell cycle regulatory protein (CDK), is involved in the control of the cell cycle and differentiation, promoting G1/S transition. Phosphorylated pRB/RB1 and NPM1. CDK interacts with D-type G1 cyclins during the interphase of G1 to form the pRB/RB1 kinase and to control cell cycle entry and is also involved in the initiation and maintenance of cell cycle exit during cell differentiation. CDK prevents cell proliferation and negatively regulates cell differentiation and may act in centrosome organization and delay senescence during the cell cycle stage [19]. It plays an important role in cellular regulation, and abnormal expression of this gene in tumor cells leads to continuous malignant proliferation of tumors. CDK1 is a target of miR-34c-3p, which is one of the promising lethal targets for KRAS mutant cancers. In addition, the combination of CDK1 inhibition (mediated by RO3306) and miR-34c-3p overexpression leads to an additive effect on the viability of cells expressing KRASmut [20]. KRAS

a

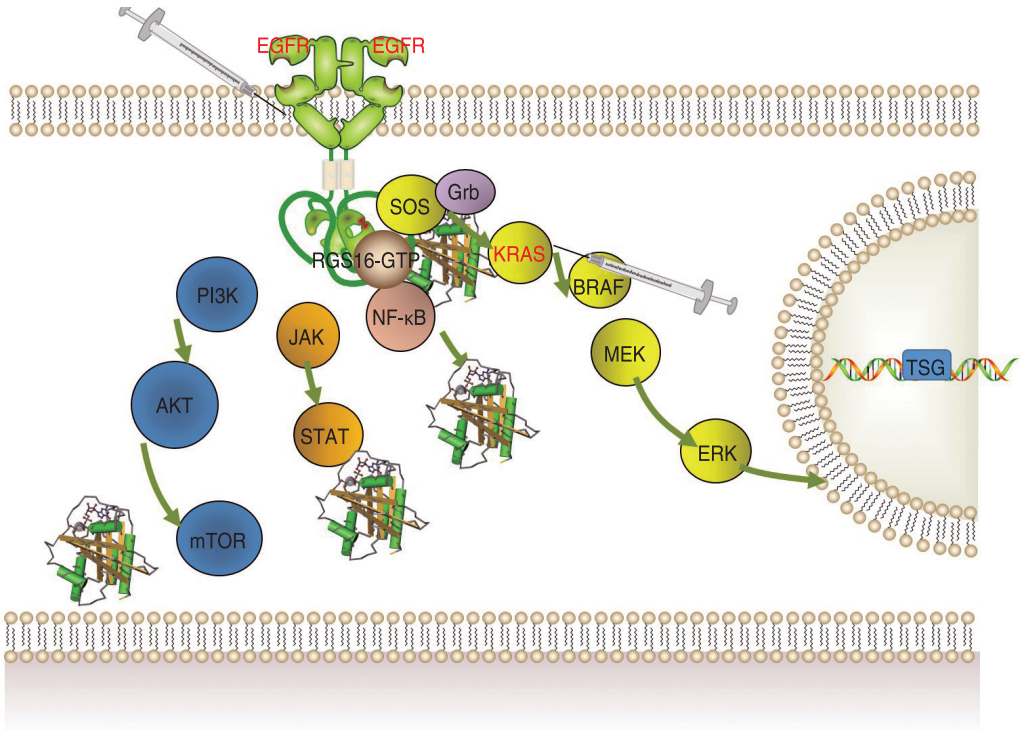
EGFR
EGFR
SOS
Grb
RGS16-GTP
KRAS
BRAF
PI3K
NF-κB
JAK
MEK
TSG
AKT
STAT
ERK
mTOR

b

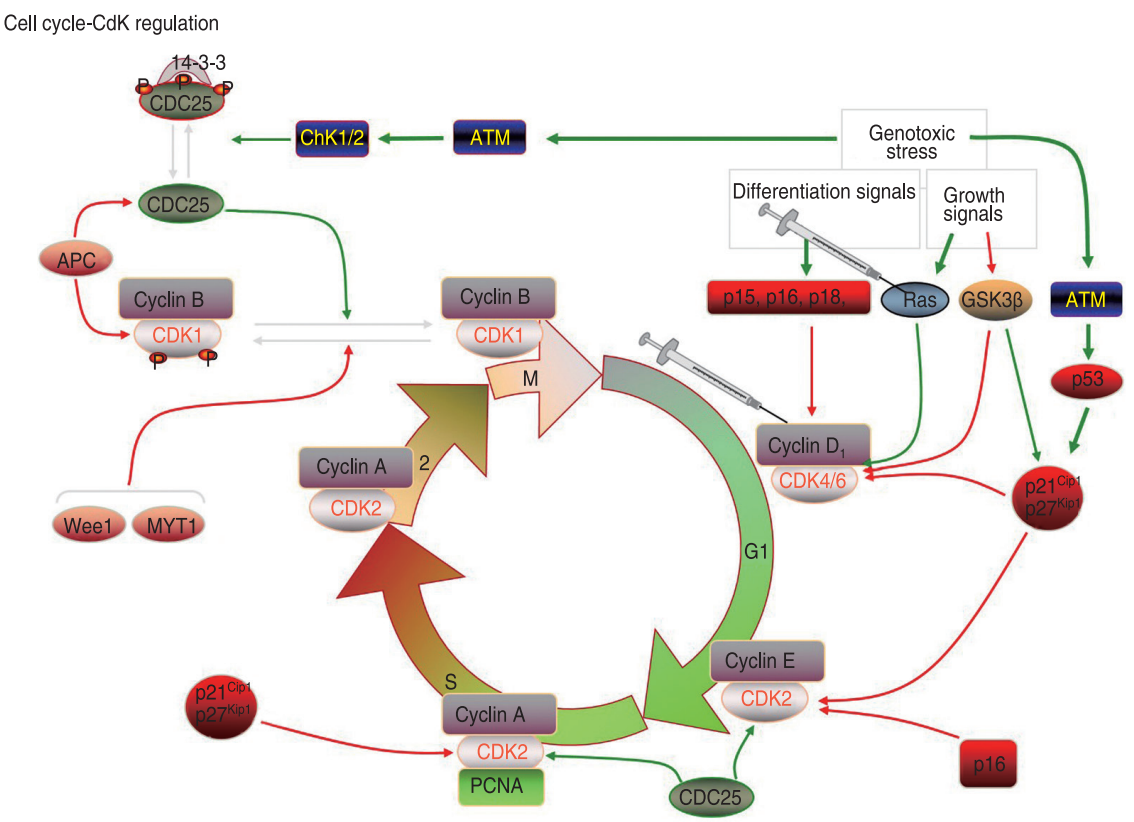
Cell cycle-CdK regulation
14-3-3
CDC25
ChK1/2
ATM
Genotoxic stress
Differentiation signals
Growth signals
CDC25
APC
Cyclin B
CDK1
Cyclin B
CDK1
M
p15, p16, p18
Ras
GSK3β
ATM
p53
Cyclin D1
CDK4/6
p21Cip1 p27Kip1
Cyclin A
2
CDK2
Wee1
MYT1
G1
Cyclin E
CDK2
S
p21Cip1 p27Kip1
Cyclin A
CDK2
PCNA
CDC25
p16

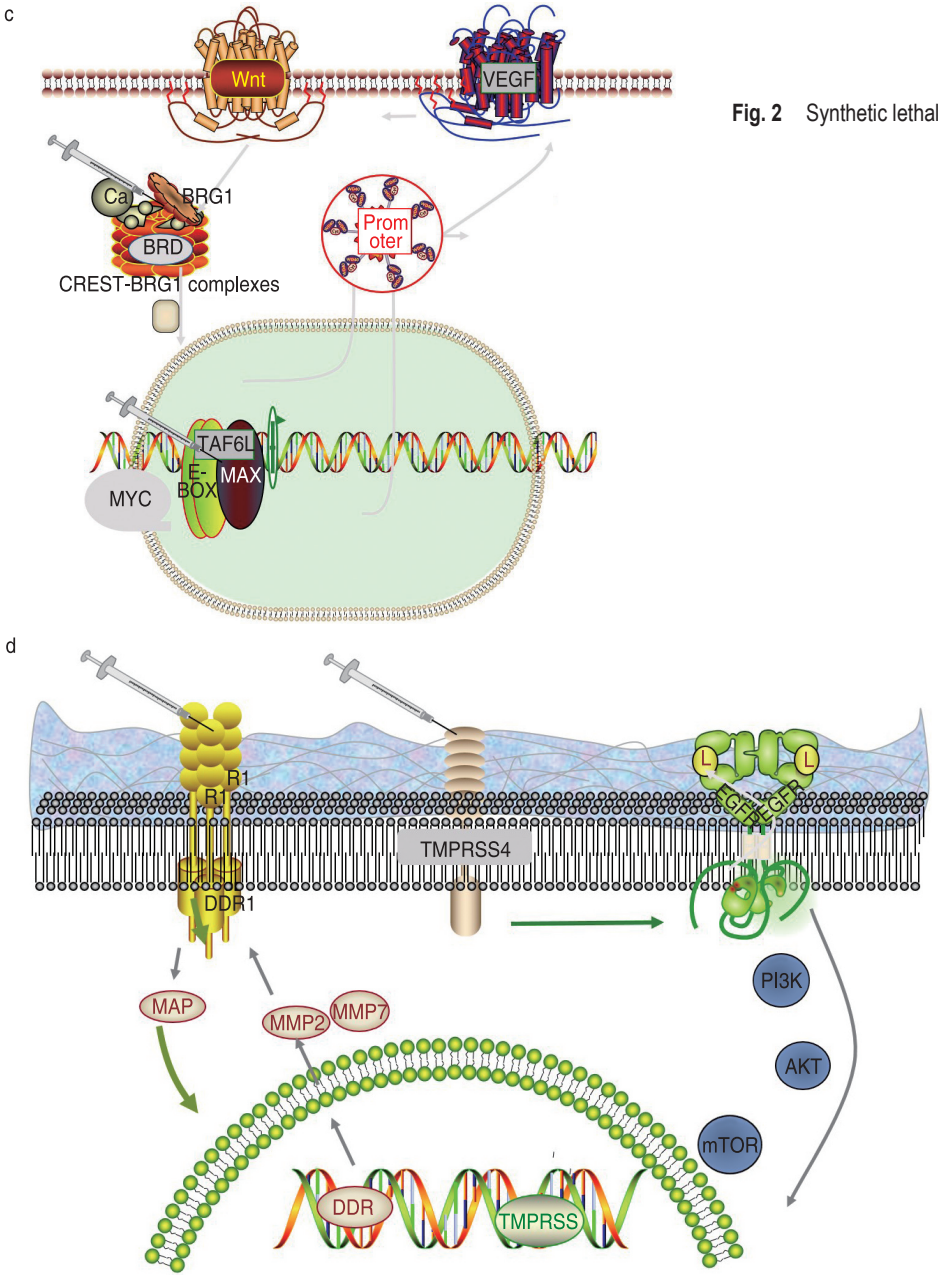

Fig. 2 Synthetic lethal target pair gene signal pattern diagram

is involved in transcriptional activation and repression of selected genes through chromatin remodeling (alterations in DNA-nucleosome topology). Components of the SWI/SNF chromatin remodeling complex perform key enzymatic activities to alter chromatin structure by altering DNA-histone contacts in the nucleosome in an ATP-dependent manner. The recruitment of CREBBP to the promoter is increased by a CREST-dependent mechanism, which leads to transcriptional activation. During cell differentiation, the role of KRAS and CDK4 in regulating cell proliferation is very important, and the addition of CDK cell cycle inhibitors to KRAS monophasic blockade can effectively arrest the growth of cancer cells [21] (Fig. 2b).

BRG1-MYC

BRG1 is a downstream protein of SMARCA4 (actin-dependent modulator), and its related pathways include Wnt-mediated regulation of β-catenin signaling and transcription of target genes. The downstream component complex of CREST-BRG1 associated with BRG1, a multiprotein complex, regulates promoter activation by coordinating the release of calcium-dependent

repressor complexes and the recruitment of activator complexes, and inhibition of BRG1 protein inhibits the transcriptional priming program of the genetic material [21]. Its protein bromodomain (BRD) is an epigenetic reader domain that selectively recognizes acetylated lysine residues on histone protein tails and is the only known protein module that can target acetylated lysine residues. The MYC gene is closely related to the inhibition of cell differentiation and tumor transformation. The protein encoded by this gene forms a heterodimer with the related transcription factor MAX [22]. This complex binds to the EboxDNA consensus sequence and regulates transcription of specific target genes together with TAF6L to activate target gene expression by RNA polymerase II pause release (by similarity). Modulators involved in somatic cell reprogramming control the self-renewal of embryonic stem cells [23]. It activates the transcription of genes associated with growth. It binds to the VEGFA promoter and promotes the production of VEGFA and subsequent germination of angiogenesis [24]. It is involved in tumor-associated angiogenesis. There is an antagonistic functional link between BRG1 and MYC and, therefore, non-compliance to RA and GC via BRG1 inactivation involves deregulation of MYC activity. Mechanistically, some of these roles are mediated by binding of BRG1 to MYC and MYC target promoters [25]. BRG1-MYC co-targets inhibition from the promoter to lead to tumor cell suppression [26] (Fig. 2c).

TMPRSS4-DDR1

Transmembrane serine protease [27] (TMPRSS4) encodes a protein that binds together with an N-terminal anchor sequence and a glycosylated extracellular region containing a serine protease domain. Discoidin domain receptor tyrosine kinase (DDR) encodes a protein belonging to the subfamily of tyrosine kinase receptors, which regulates cell attachment to the extracellular matrix, remodeling of the extracellular matrix, cell migration, differentiation, and cell proliferation, and plays an important role in tumor cell invasion. There is a consistent co-expression between TMPRSS4 and DDR1 [28]. Like TMPRSS4, the DDR1 [29] promoter is hypomethylated in NSCLC, while hypomethylation is an independent prognostic factor for disease-free survival. Treatment with 5-azacytidine increased DDR1 levels in the cell lines, indicating epigenetic regulation. Cells lacking TMPRSS4 are highly sensitive to the cytotoxic effects of dasatinib, a DDR1 inhibitor [30]. TMPRSS4/DDR1 double knockout (KD) units, but none of the KD cells suffered G0/G1 cell cycle arrest, loss of E2F1 and cyclins A and B, elevated p21 levels as well as massive apoptosis. Studies have shown in vivo tumor regression in mice injected with double KD. A synthetic lethal interaction between DDR1 and TMPRSS4 has been identified resulting in a new vulnerability in NSCLC (Fig. 2d).

Breast cancer and ovarian cancer

Breast cancers have gradually become the malignant tumors with the highest incidence in the world in recent years, which is still a complex link in pathogenesis, but gene mutation is still an important factor in tumorigenesis, with the increase of the affected population and the extension of survival. The evidence for mutation continuation and accumulation through offspring is increasing, and inhibition of breast and ovarian cancer is an example of synthesis leading to persuasive and clinical validation.

BRCA-PARP

Most breast and ovarian cancers of BRCA-PARP are accompanied by BRCA gene mutation [31]. The BRCA1/2 gene, as a common tumor suppressor gene, accounts for about 40% of hereditary breast cancers and more than 80% of hereditary breast and ovarian cancers. BRCA1/2 mainly encodes DNA damage repair-related proteins as well as other tumor suppressors, which combine with DNA damage sensors and signal transducers to form a large multi-subunit protein complex [32], and also mediates the control of R-loop-related genomic instability involved in double-strand break repair and/or homologous recombination [33]. Members of the PARP gene (poly (ADP-ribose) polymerase) family (PARP1, PARP2, PARP3, etc.) are common nuclear proteins with similar main roles in gene function and are involved in the regulation of various important cellular processes [34]. The BRCA gene requires phosphorylation of the encoded substrate for normal cell cycle progression from G2 to mitosis upon posttranslational modification. PARP1-dependent PARP9-DTX3L-mediated ubiquitination [35] can promote the rapid and specific recruitment of BRCA1 to sites of DNA damage [36]. In the case of BRCA1 mutations affecting BARD1 heteromerization, PARP inhibitors will reduce PAR formation and the rapid recruitment to DNA damage sites by the BRCA1/BARD1 complex, thereby inhibiting HR-mediated repair and inducing cell death. The current combination of breast and ovarian cancer patients with germline lesions can effectively inhibit breast and ovarian cancer [37–39] (Fig. 3).

Colon cancer

An important point in the tendency of colon cancer to be younger may be related to its continuous repair defect of gene instability. Normal mismatch repair plays an extremely important role in body cells, and the loss of this function leads to complex changes in other signaling activities of cells. Inhibition of colon cancer tumor cells requires multiple pathways.

PLK1-RAS

The PLK1 gene belongs to the CDC5/Polo subfamily,

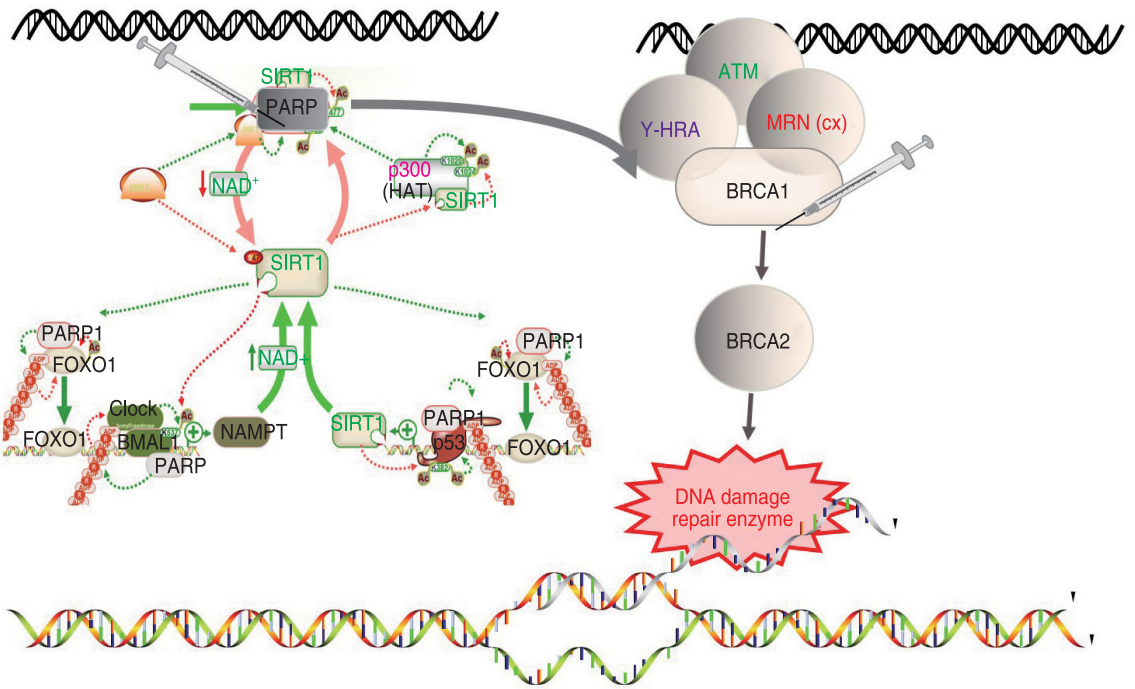

Fig. 3 Synthetic lethal target pair gene signal pattern diagram

and highly conserved structural protein kinases are closely related to cell cycle progression, mitosis, and DNA damage. It is highly expressed during mitosis and performs several important functions throughout the M phase of the cell cycle [40], including regulation of centrosome maturation and spindle assembly, inhibition of anaphase-promoting complex/ring inactivation (APC/C), and regulation of mitotic exit and cytokinesis by phosphorylating adhesin subunits (e. g., STAG2/SA2) to regulate adhesin dissociation from chromosomes. Phosphorylated SGO1: SGO1 isomer 3 is required for spindle pole localization and plays a role in regulating its centriolar cohesion function [41]. It mediates the phosphorylation of FBXO5/EMI1 (a negative modulator of the APC/C complex) during prophase, leading to FBXO5/EMI1 ubiquitination and degradation by the proteasome. It also acts as a negative modulator of p53 family members and phosphorylates TOPORS, thereby inhibiting the sulfonylation of p53/TP53 and simultaneously enhancing the ubiquitination and subsequent degradation of p53/TP53. It phosphorylates the transactivation domain of the transcription factor p53/TP53, thereby inhibiting p53/TP53-mediated transcriptional activation and pro-apoptotic functions [42]. Combined blockade of PLK1-KRAS effectively inhibits colon cancer [43]. However, relevant studies on clinical application are still in progress (Fig. 4a).

PLK1-TP53

PLK1 is highly expressed during mitosis, and TP53, when associated with the CAK complex in response to DNA damage, prevents CDK7 kinase activity and thus cell cycle progression. Isoform 2 enhances the transactivation activity of isoform 1 of some, but not all, TP53-inducible promoters [44]. Isotype 4 inhibits transactivation activity and weakens growth inhibition mediated by isotype 1. Isotype 7 inhibits isotype 1-mediated apoptosis [45]. TP53TG1 can regulate PLK1. Yang Ping [46] could induce OCI-ly1 and OCI-ly3 cells to arrest in G2 phase and reduce cell migration and invasion by up-regulating lncRNATP53TG1 in OCI-ly1 cells and down-regulating lncRNATP53TG1 in OCI-ly3 cells, and the mechanism may be through the regulation of PLK1. Application of PLK1 inhibitors blocks the signaling of TP53 and inhibits tumorigenesis [47] (Fig. 4b).

Prostate cancer

Prostate cancer plays an important role in new tumors in men, and its related research progress is becoming more and more extensive.The relevant combinations currently inhibiting prostate cancer with a synthetic lethal strategy are as follows.

BCL2-PTEN

BCL2 is a protein-coding gene. Its encoded protein regulates cell death by controlling mitochondrial membrane permeability. Its associated pathways include apoptosis regulation as well as T cell and Nur77 signaling. PTEN antagonizes the PI3K-AKT/PKB signaling pathway by dephosphorylating phosphoinositides [48], thereby regulating cell cycle progression and cell survival [49]. The unphosphorylated form cooperates with

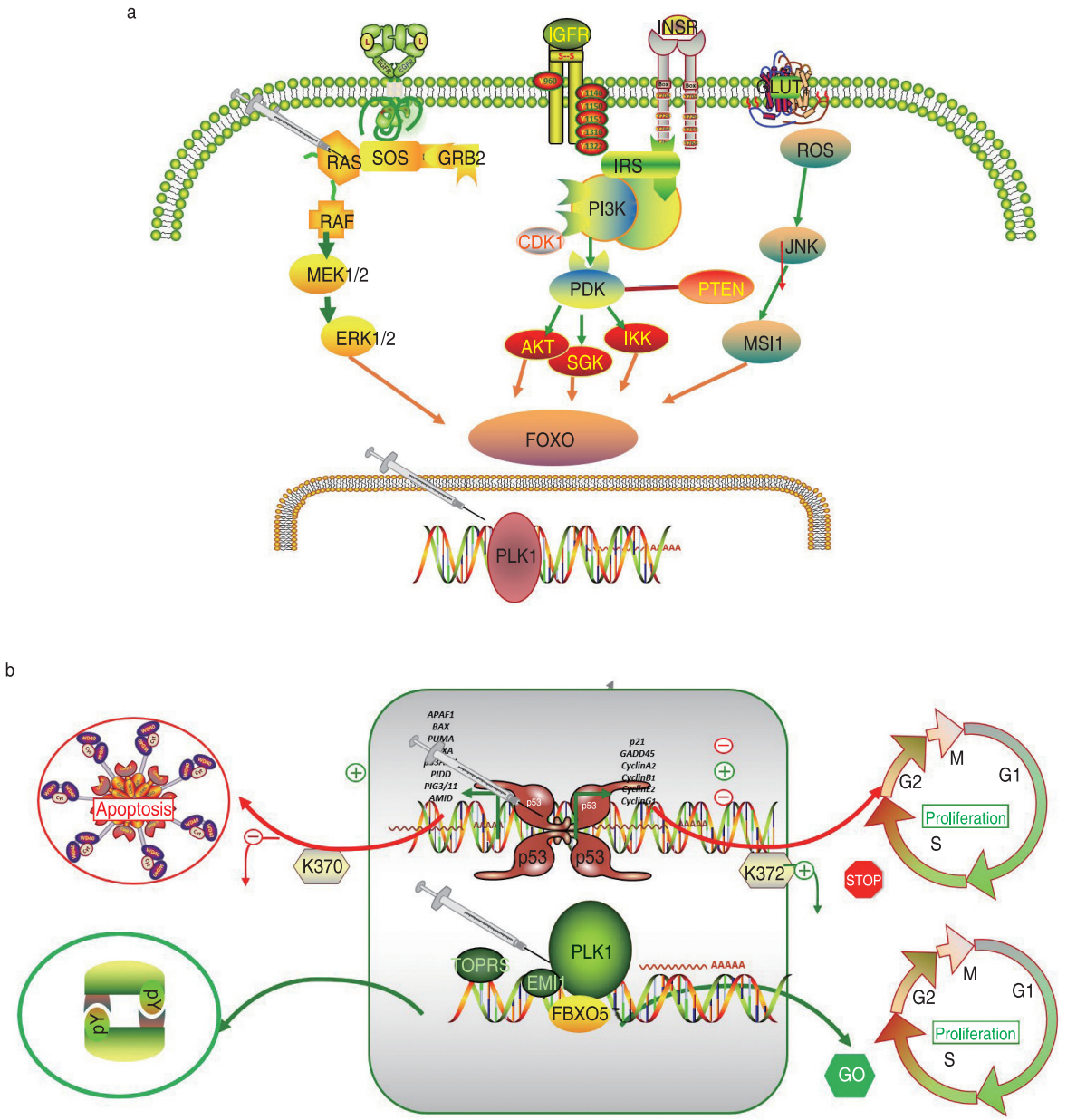

Fig. 4 Synthetic lethal target pair gene signal pattern diagram

AIP1 to inhibit AKT1 activation. It dephosphorylates tyrosine-phosphorylated focal adhesion kinase and inhibits cell migration as well as integrin-mediated cell spreading and focal adhesion formation, acting as a key modulator of the AKT-mTOR signaling pathway. Among several genetic alterations involved in prostate cancer development, BCL2 is an important target molecule after ablation or castration of androgen-independent prostate cancer (AIPC) [50]. BCL-2, implicated in proandrogen-related signaling during the progression of androgen-independent prostate cancer (ADPC), is a survival molecule, while BCL-2 upregulation, PTEN loss, PI3K/AKT phosphorylation and receptor tyrosine kinase (RTK) activation are mainly associated with AIPC. Guccini [51] showed that PTEN deficiency or chemotherapy-driven aging limited the progression of prostate cancer in mice. The nucleo-monoubiquitinated [52] form of PTEN has apoptotic potential, while the cytoplasmic non-ubiquitinated form induces weaker tumor inhibition (Fig. 5a).

CHD1-PTEN

Loss of the CHD1-PTEN gene encoding the chromatin remodeler CHD1 is the most common

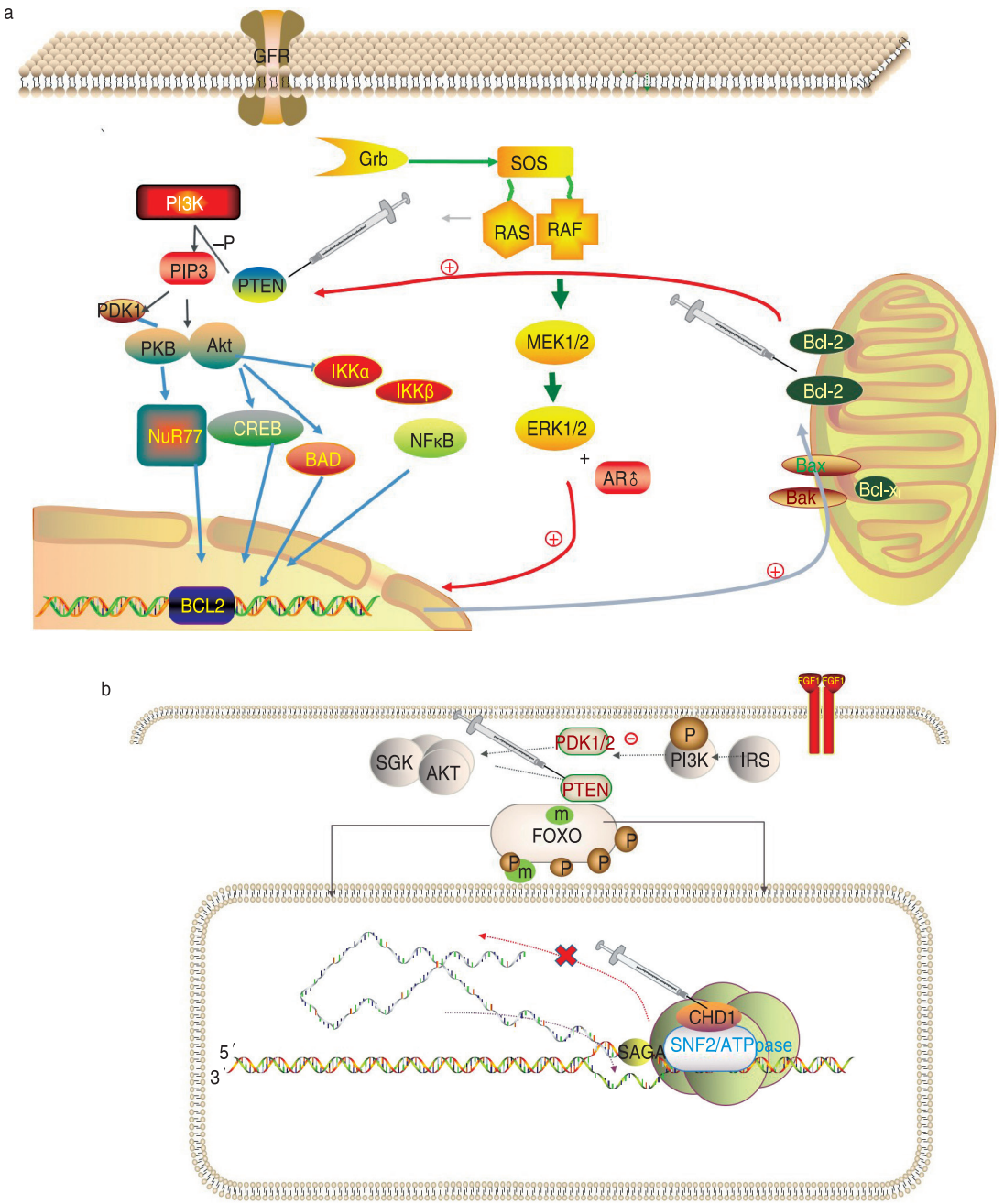

Fig. 5 Synthetic lethal target pair gene signal pattern diagram

alteration in prostate cancer. The CHD protein family is characterized by a chromatin domain and a SNF2 [53] -associated helicase/ATPase domain. CHD genes may alter gene expression by modifying chromatin structure, thereby negatively regulating the transcription of their chromosomal DNA templates. Augello [54] demonstrated that CHD1 occupies a prostate-specific enhancer and is rich in androgen receptor (AR) and lineage-specific cofactors. Prostate tumors with loss of CHD1 appear to be highly sensitive to abiraterone treatment [55]. CHD1ATP-dependent chromatin remodelers regulate the transcription of polymerase II. They can act as a substrate recognition component of the transcriptional regulatory histone acetylation (HAT) complex SAGA [56]. Efficient transcription by RNA polymerase I, and more specifically, the polymerase I transcription termination step, is also required to negatively regulate DNA replication. CHD1 is not only involved in transcription-associated chromatin remodeling, but also requires the maintenance of specific chromatin configurations throughout the genome. CHD1

is also associated (by similarity) with histone deacetylase (HDAC) activity. CHD1 is required to bridge the SNF2, FACT complex, PAF complex, and the U2snRNP complex to H3K4me3. CHD1 regulates the function of pre-mRNA splicing efficiency by the physical bridging of some spliceosome components to H3K4me3 [57]. Maintenance of open chromatin and pluripotency in embryonic stem cells is required through similarity. CHD1 is characterized by synthetic lethality with PTEN inhibition of prostate cancer [58] (Fig. 5b).

Other tumors and genes

CHK1

The protein encoded by CHK1,CHK1 gene belongs to the Ser/Thr protein kinase family. Checkpoint-mediated cell cycle arrest is required in response to DNA damage or the presence of unreplicated DNA. The role of this protein is to integrate signals from ATM and ATR, two cyclins involved in the DNA damage response, which are also associated with chromatin in meiotic prophase I. Phosphorylation of CDC25A protein phosphatase by this protein is a double-stranded DNA break necessary for cells to delay cell cycle progression in response.

Its related pathways include p53 signaling and DNA damage ATM/ATRG1/S checkpoint, regulating the phosphorylation of CDC25A at "Ser-178" and "Thr-507" and the phosphorylation of CDC25C at "Ser-216" resulting in binding sites for 14-3-3 proteins, which inhibit CDC25A and CDC25C. The newly synthesized bis (indolyl) thiazole alkaloid analogue, nortopsentin234 (NORA234), resulted in an initial decrease in the proliferation and clonogenic potential of CRC spherical cells (CR-CSphCs), followed by an adaptive response to select CR-CSphC resistance compartments. Cells that were spared by treatment with NORA234 expressed high levels of CD44v6, a synthetic lethal mode caused by constitutive activation of the Wnt pathway.

The Rad51-WEE1

WEE1 gene encodes a nuclear protein, which is a tyrosine kinase belonging to the Ser/Thr family of protein kinases. This protein catalyzes the inhibitory tyrosine phosphorylation of CDC2/cyclin B kinase, and appears to coordinate the transition between DNA replication and mitosis by protecting the nucleus from cytoplasmically activated CDC2 kinase. For Wee1 kinase and Rad51 recombinase in head and neck tumors are two proteins involved in regulating replication stress and homologous recombination repair in cancer cells.

Synergism between Rad51 inhibitor (B02) and Wee1 inhibitor (AZD1775) is associated with forced CDK1 activation and decreased Chk1 phosphorylation, leading to excessive DNA damage and replication stress, ultimately leading to abnormal mitosis and apoptosis.

NRN1

NRN1 protein contains a consensus cleavage signal protein found in glycosylphosphatidylinositol (GPI) -anchored protein quality. It promotes neurite growth and arborization and has a role in promoting neurogenesis. Overexpression of the encoded protein may be associated with astrocytoma progression. Neuroprotein 1 (NRN1) is involved in the PI3K-Akt-mTOR pathway, and studies have shown that NRN1 expression is frequently inhibited by methylation of promoter regions in human esophageal cancer cells. NRN1 was methylated in 50.4% of primary esophageal cancer samples, and NRN1 inhibited colony formation, cell proliferation, migration, and invasion, and induced apoptosis and G1/S arrest in esophageal cancer cells.NRN1 inhibits the growth of esophageal cancer *in vitro* and *in vivo* by inhibiting PI3K-Akt-mTOR signaling.Methylation of NRN1 is a novel synthetic lethal marker of PI3K-Akt-mTOR and ATR inhibitors in human esophageal cancer.

CREBBP or EP300

CREBBP genes play key roles in embryonic development, growth control, and homeostasis by combining chromatin remodeling with transcription factor recognition.

CREBBP proteins have intrinsic histone acetyltransferase activity and also act as scaffolds to stabilize the interaction of additional proteins with transcriptional complexes. It acetylates histones and non-histones. The protein shares very high sequence similarity regions with protein p300 in its bromodomain, cysteine-histidine-rich region, and histone acetyltransferase domain.

The EP300 gene encodes an adenoviral E1A-associated cellular p300 transcriptional co-activator protein. It functions as a histone acetyltransferase and regulates transcription through chromatin remodeling and is important during cell proliferation and differentiation. It mediates cAMP gene regulation by specifically binding to phosphorylated CREB proteins. This gene has also been identified as a coactivator of HIF1A (hypoxia-inducible factor 1α) and therefore plays a role in the stimulation of hypoxia-inducible genes such as VEGF. Synthetic lethality using the mutation status of CREBBP/EP300 as a biomarker for the use of CARM1 small molecule inhibitors in DLBCL and other cancers.

WRN-MSI

DNA helicase WRN is a target for the synthesis of lethal cancer cells with microsatellite instability (MSI), a form of genetic hypermutation caused by impaired mismatch repair. Depletion of WRN induces extensive

DNA double-strand breaks in MSI cells, leading to cell cycle arrest and/or apoptosis. WRN-encoded nuclear proteins are important in maintaining genomic stability and play roles in DNA repair, replication, transcription, and telomere maintenance. It contains an N-terminal 3 'to 5' exonuclease domain, an ATP-dependent helicase domain, and an RQC (RecQ helicase conserved region) domain in its central region, as well as a C-terminal HRDC (helicase RNaseDC end) domain and nuclear localization signal. It preferentially binds DNA substrates containing alternative secondary structures, such as replication forks and Holliday junctions. It may play an important role in the dissociation of joint DNA molecules that can emerge as products of homologous recombination, replication fork stalling, or during DNA repair. It alleviates the arrest of DNA polymerase at the site of DNA damage. TA-dinucleotide repeats are very unstable in MSI cells, and undergo large-scale expansion, which is different from insertion or deletion mutations of several nucleotides described previously. Extended TA repeats form non-BDNA secondary structures that stall replication forks, activate ATR checkpoint kinases, and require WRN helicase unwinding. In the absence of WRN, the extended TA-dinucleotide repeat is readily cleaved by the MUS81 nuclease, resulting in massive chromosome fragmentation. The synthetic lethal dependence of WRN in MSI and supports the development of therapeutic agents for WRN against MSI-associated cancers.

CYP2S1-BRAF

CYP2S1 gene is in the epidermis and may contribute to the oxidative metabolism of all-trans retinoic acid. For this activity, molecular oxygen is used to insert one oxygen atom into the substrate, and then the second oxygen atom is reduced to a water molecule, and the two electrons are passed by NADPH through cytochrome P450 reductase (NADPH-hemoprotein reductase). In addition, peroxidase and isomerase activities were shown for various oxygen-containing eicosanoids such as prostaglandin H2 (PGH2) and hydroperoxyeicosatetraenoate (HPETE). CYP2S1 is highly expressed in papillary thyroid carcinoma (PTC), especially in conventional PTC (CPTC) and high-cell PTC (TCPTC), and its expression is positively correlated with BRAF mutations. The BRAF-mediated MAPK/ERK cascade upregulates CYP2S1 expression through an AHR-dependent pathway, whereas CYP2S1 in turn enhances the transcriptional activity of AHR through its metabolites.This AHR/CYP2S1 feedback loop strongly amplifies the oncogenic role of BRAF in thyroid cancer cells, which leads to the fatal interaction between synthetic CYP2S1 and BRAF.

TET2

TET2 dioxygenase catalyzes the conversion of the modified genomic base 5-methylcytosine (5mC) to 5-hydroxymethylcytosine (5hmC) and plays a key role in active DNA demethylation. 5-hydroxymethylcytosine is favored in CpG motifs. It also mediates the subsequent conversion of 5hmC to 5-formylcytosine (5fC) and the conversion of 5fC to 5-carboxycytosine (5caC). The conversion of 5mC to 5hmC, 5fC, and 5caC may be the first step in cytosine demethylation. Methylation at the C5 position of cytosine bases is an epigenetic modification of mammalian genomes and plays an important role in transcriptional regulation. In addition to its role in DNA demethylation, it is also involved in recruiting O-GlcNAc transferase OGT to CpG-rich transcriptional start sites of active genes, thereby promoting inactivating mutations in histone H2BGlcNAcylationTET2 through OGT is the initial genetic damage for hematopoietic stem and progenitor cell (HSPC) transformation, and the mechanism of selective killing of TET2 mutant blood cells is due to abnormally low levels of tyrosyl DNA phosphodiesterase 1 (TDP1), an enzyme important for the removal of TOP1 cleavage complex (TOP1 cc). Low TDP1 levels confer sensitivity to TOP1-targeting agents or PARP1 inhibitors, and are unable to remove the TOP1 cleavage complex, leading to DNA double-strand breaks and cell death.

IDH

Mutations in IDH 1 have been observed in a variety of cancer types, including sarcoma, hematologic malignancies, colon cancer, and brain cancer. Mutations in two isocitrate dehydrogenases involved in the conversion of α-ketopentanoic acid to D-2-hydroxypentanoic acid by the cytoplasm (IDH 1) and mitochondria (IDH 2) have been described as mutually exclusive in many of these cancer types. The most common mutations involve R132 (IDH 1) and R172 (IDH 2) involving the active site and resulting in new variant enzymatic activity. The impact of mutations in this gene varies by cancer type. In myelodysplastic syndromes and acute myelogenous leukemia (AML), IDH1 mutations are associated with worse outcome, shorter overall survival, and normal karyotype. However, in glioblastoma and astrocytoma, patients with IDH 1 mutations show better overall survival than patients with wild-type IDH 1. Unlike the association with cytogenetically normal AML, in glioblastoma, IDH 1 mutations are associated with specific cytogenetic abnormalities, 1p and 19q deletions. Another approach to target IDH1 mutations is by inducing synthetic lethality of compounds targeted by poly (ADP-ribose) polymerase (PARP), glutamine metabolism, and the Bcl-2 protein family.

Summary and outlook

Tumor synthetic death may be one of the most important advances in modern cancer therapy.

In this paper, the mechanism of action of target genes in common tumors such as lung cancer, breast cancer, ovarian cancer, colorectal cancer, prostate cancer and other uncommon tumors and the principles leading to the occurrence of synthetic lethal effects are systematically discussed. The concept of synthetic lethality has great potential in anticancer drug discovery and may become an important means of inhibiting tumors at the genetic level in guiding cancer therapy in the future. During the initiation of oncogene program, inhibition of multiple signaling pathways and upstream and downstream molecules of signaling may fundamentally inhibit the development of tumors and drug resistance phenomena during treatment. We proposed the concept of synthetic lethality half a century ago, and cancer gene-targeted drug research in the 21st century was precisely based on NGS and CRISPR gene editing technologies. With the mining of CRISPR gene technology, more and more target genes are discovered in tumors, and humans inevitably face the application of synthetic lethality to inhibit tumors during anti-tumor. Whether some tumors can be accurately and efficiently cured in the future still has the way to go. In this paper, we enumerate the choice of drugs in common tumors under the theory of synthetic lethality, and more updated studies still need to be further validated and summarized.

Conflicts of interest

The authors indicated no potential conflicts of interest.

References

1. Topatana W, Juengpanich S, Li S, *et al*. Advances in synthetic lethality for cancer therapy: cellular mechanism and clinical translation. J Hematol Oncol, 2020, 3, 13: 118.
2. Akimov Y, Aittokallio T. Re-defining synthetic lethality by phenotypic profiling for precision oncology. Cell Chem Biol, 2021, 28: 246–256.
3. Kong YW, Dreaden EC, Morandell S, *et al*. Enhancing chemotherapy response through augmented synthetic lethality by co-targeting nucleotide excision repair and cell-cycle checkpoints. Nat Commun, 2020, 17, 11: 4124.
4. Akimov Y, Aittokallio T. Re-defining synthetic lethality by phenotypic profiling for precision oncology. Cell Chem Biol, 2021, 28: 246–256.
5. Pilié PG, Tang C, Mills GB, *et al*. State-of-the-art strategies for targeting the DNA damage response in cancer. Nat Rev Clin Oncol, 2019, 16: 81–104.
6. Shen JP, Ideker T. Synthetic lethal networks for precision oncology: promises and pitfalls. J Mol Biol, 2018, 430 (18 Pt A): 2900–2912.
7. Schick S, Rendeiro AF, Runggatscher K, *et al*. Systematic characterization of BAF mutations provides insights into intracomplex synthetic lethalities in human cancers. Nat Genet, 2019, 51: 1399–1410.
8. Seton-Rogers S. Prioritizing synthetic lethal targets with functional genomics. Nat Rev Drug Discov, 2019, 18: 418.
9. Chang HR, Jung E, Cho S, *et al*. Targeting non-oncogene addiction for cancer therapy. Biomolecules, 2021, 11: 129.
10. Runkle KB, Kharbanda A, Stypulkowski E, *et al*. Inhibition of DHHC20-mediated EGFR palmitoylation creates a dependence on EGFR signaling. Mol Cell, 2016, 62: 385–396.
11. Lu C, Mi LZ, Grey MJ, *et al*. Structural evidence for loose linkage between ligand binding and kinase activation in the epidermal growth factor receptor. Mol Cell Biol, 2010, 30: 5432–5443.
12. Habib AA, Chatterjee S, Park SK, *et al*. The epidermal growth factor receptor engages receptor interacting protein and nuclear factor-kappa B (NF-kappa B)-inducing kinase to activate NF-kappa B. Identification of a novel receptor-tyrosine kinase signalosome. J Biol Chem, 2001, 276: 8865–8874.
13. Serra RW, Fang M, Park SM, *et al*. A KRAS-directed transcriptional silencing pathway that mediates the CpG island methylator phenotype. Elife, 2014, 3: e02313.
14. Derrien A, Druey KM. RGS16 function is regulated by epidermal growth factor receptor-mediated tyrosine phosphorylation. J Biol Chem, 2001, 276: 48532–48538.
15. Ghosh P, Beas AO, Bornheimer SJ, *et al*. A G{alpha}i-GIV molecular complex binds epidermal growth factor receptor and determines whether cells migrate or proliferate. Mol Biol Cell, 2010, 21: 2338–2354.
16. Yang MH, Nickerson S, Kim ET, *et al*. Regulation of RAS oncogenicity by acetylation. Proc Natl Acad Sci U S A, 2012, 109: 10843–10848.
17. Serra RW, Fang M, Park SM, *et al*. A KRAS-directed transcriptional silencing pathway that mediates the CpG island methylator phenotype. Elife, 2014, 3: e02313.
18. Unni AM, Harbourne B, Oh MH, *et al*. Hyperactivation of ERK by multiple mechanisms is toxic to RTK-RAS mutation-driven lung adenocarcinoma cells. Elife, 2018, 7: e33718.
19. Hussain MS, Baig SM, Neumann S, *et al*. CDK6 associates with the centrosome during mitosis and is mutated in a large Pakistani family with primary microcephaly. Hum Mol Genet, 2013, 22: 5199–5214.
20. Palma F, Affinito A, Nuzzo S, *et al*. miR-34c-3p targets CDK1 a synthetic lethality partner of KRAS in non-small cell lung cancer. Cancer Gene Ther, 2021, 28: 413–426.
21. Zhou J, Zhang S, Chen X, *et al*. Palbociclib, a selective CDK4/6 inhibitor, enhances the effect of selumetinib in RAS-driven non-small cell lung cancer. Cancer Lett, 2017, 408: 130–137.
22. Sanchez JC, Zhang L, Evoli S, *et al*. The molecular basis of selective DNA binding by the BRG1 AT-hook and bromodomain. Biochim Biophys Acta Gene Regul Mech, 2020, 1863: 194566.
23. Sun X, Yu W, Li L, *et al*. ADNP controls gene expression through local chromatin architecture by association with BRG1 and CHD4. Front Cell Dev Biol, 2020, 8: 553.
24. Shi Y, Xu X, Zhang Q, *et al*. tRNA synthetase counteracts c-Myc to develop functional vasculature. Elife, 2014, 3: e02349.
25. Romero OA, Setien F, John S, *et al*. The tumour suppressor and chromatin-remodelling factor BRG1 antagonizes Myc activity and promotes cell differentiation in human cancer. EMBO Mol Med, 2012, 4: 603–616.
26. Zhang H, Pandey S, Travers M, *et al*. Targeting CDK9 reactivates epigenetically silenced genes in cancer. Cell, 2018, 175: 1244–1258.
27. Katopodis P, Kerslake R, Davies J, *et al*. COVID-19 and SARS-CoV-2 host cell entry mediators: Expression profiling of TMRSS4 in health and disease. Int J Mol Med, 2021, 47: 64.
28. Villalba M, Redin E, Exposito F, *et al*. Identification of a novel synthetic

lethal vulnerability in non-small cell lung cancer by co-targeting TMPRSS4 and DDR1. Sci Rep, 2019, 9: 15400.
29. Exposito F, Villalba M, Redrado M, *et al*. Targeting of TMPRSS4 sensitizes lung cancer cells to chemotherapy by impairing the proliferation machinery. Cancer Lett, 2019, 453: 21–33.
30. Doki C, Nishida K, Saito S, et al. Microtubule elongation along actin filaments induced by microtubule-associated protein 4 contributes to the formation of cellular protrusions. J Biochem, 2020, 168: 295–303.
31. Hiraike H, Wada-Hiraike O, Nakagawa S, *et al*. Identification of DBC1 as a transcriptional repressor for BRCA1. Br J Cancer, 2010, 102: 1061–1067.
32. Xie S, Mortusewicz O, Ma HT, *et al*. Timeless interacts with PARP-1 to promote homologous recombination repair. Mol Cell, 2015, 60: 163–176.
33. Bhatia V, Barroso SI, García-Rubio ML, *et al*. BRCA2 prevents R-loop accumulation and associates with TREX-2 mRNA export factor PCID2. Nature, 2014, 511: 362–365.
34. Wu-Baer F, Ludwig T, Baer R. The UBXN1 protein associates with autoubiquitinated forms of the BRCA1 tumor suppressor and inhibits its enzymatic function. Mol Cell Biol, 2010, 30: 2787–2798.
35. Lee Y, Chou TF, Pittman SK, *et al*. Keap1/Cullin3 Modulates p62/SQSTM1 Activity via UBA Domain Ubiquitination. Cell Rep, 2017, 19: 188–202.
36. Zhao WX, Claudia W, Youngho K, *et al*. The BRCA tumor suppressor network in Chromosome damage repair by homologous recombination. Annu Rev Biochem, 2019, 88(undefined): 221–245.
37. Yar MS, Haider K, Gohel V, *et al*. Synthetic lethality on drug discovery: an update on cancer therapy. Expert Opin Drug Discov, 2020, 15: 823–832.
38. Rumford M, Lythgoe M, McNeish I, *et al*. Oncologist-led BRCA 'mainstreaming' in the ovarian cancer clinic: A study of 255 patients and its impact on their management. Sci Rep, 2020, 10: 3390.
39. Yusoh NA, Leong SW, Chia SL, *et al*. Metallointercalator [Ru(dppz)2(PIP)]2+ renders BRCA wild-type triple-negative breast cancer cells hypersensitive to PARP inhibition. ACS Chem Biol, 2020, 15: 378–387.
40. Yang MH, Nickerson S, Kim ET, *et al*. Regulation of RAS oncogenicity by acetylation. Proc Natl Acad Sci USA, 2012, 109: 10843–10848.
41. Liu T, Deng M, Li J, *et al*. Phosphorylation of right open reading frame 2 (Rio2) protein kinase by polo-like kinase 1 regulates mitotic progression. J Biol Chem, 2011, 286: 36352–36360.
42. Queralt B, Cuyàs E, Bosch-Barrera J, *et al*. Synthetic lethal interaction of cetuximab with MEK1/2 inhibition in NRAS-mutant metastatic colorectal cancer. Oncotarget, 2016, 7: 82185–82199.
43. Pang X, Liu M. Defeat mutant KRAS with synthetic lethality. Small GTPases, 2017, 8: 212–219.
44. Xu Y, Wan W, Shou X, *et al*. TP53INP2/DOR, a mediator of cell autophagy, promotes rDNA transcription via facilitating the assembly of the POLR1/RNA polymerase I preinitiation complex at rDNA promoters. Autophagy, 2016, 12: 1118–1128.
45. Bang S, Kaur S, Kurokawa M. Regulation of the p53 family proteins by the ubiquitin proteasomal pathway. Int J Mol Sci, 2019, 21: 261.
46. Liu K, Zheng MY, Zhao Q, *et al*. Different p53 genotypes regulating different phosphorylation sites and subcellular location of CDC25C associated with the formation of polyploid giant cancer cells. J Exp Clin Cancer Res, 2020, 39: 83.
47. Cunningham CE, MacAuley MJ, Vizeacoumar FS, *et al*. The CINs of polo-Like kinase 1 in cancer. Cancers (Basel), 2020, 12: 2953.
48. Ren W, Joshi R, Mathew P. Synthetic lethality in PTEN-Mutant prostate cancer is induced by combinatorial PI3K/Akt and BCL-XL inhibition. Mol Cancer Res, 2016, 14: 1176–1181.
49. Costa HA, Leitner MG, Sos ML, *et al*. Discovery and functional characterization of a neomorphic PTEN mutation. Proc Natl Acad Sci U S A, 2015, 112: 13976–13981.
50. Kim JH, Lee H, Shin EA, *et al*. Implications of Bcl-2 and its interplay with other molecules and signaling pathways in prostate cancer progression. Expert Opin Ther Targets, 2017, 21: 911–920.
51. Guccini I, Revandkar A, D'Ambrosio M, *et al*. Senescence reprogramming by TIMP1 deficiency promotes prostate cancer metastasis. Cancer Cell, 2021, 39: 68–82.
52. Lee Y, Chou TF, Pittman SK, *et al*. Keap1/Cullin3 Modulates p62/SQSTM1 Activity via UBA Domain Ubiquitination. Cell Rep, 2017, 19: 188–202.
53. Pyziak K, Sroka-Porada A, Rzymski T, *et al*. Potential of enhancer of zeste homolog 2 inhibitors for the treatment of SWI/SNF mutant cancers and tumor microenvironment modulation. Drug Dev Res, 2021 Feb 9.
54. Augello MA, Liu D, Deonarine LD, *et al*. CHD1 loss alters AR binding at lineage-specific enhancers and modulates distinct transcriptional programs to drive prostate tumorigenesis. Cancer Cell, 2019, 35: 603–617.
55. Boysen G, Rodrigues DN, Rescigno P, *et al*. SPOP-mutated/CHD1-deleted lethal prostate cancer and abiraterone sensitivity. Clin Cancer Res, 2018, 24: 5585–5593.
56. Zhao D, Lu X, Wang G, *et al*. Synthetic essentiality of chromatin remodelling factor CHD1 in PTEN-deficient cancer. Nature, 2017, 542: 484–488.
57. Liu H, Zhang H, Wu X, *et al*. Nuclear cGAS suppresses DNA repair and promotes tumorigenesis. Nature, 2018, 563: 131–136.
58. Stone L. Prostate cancer: Fatal interaction: a new target identified. Nat Rev Urol, 2017, 14: 258–259.

DOI 10.1007/s10330-021-0490-0
Cite this article as: Zhang YH, Xu P. Mechanism of tumor synthetic lethal-related targets. Oncol Transl Med, 2021, 7: 183–194.

中国科技核心期刊

（中国科技论文统计源期刊）

收录证书

CERTIFICATE OF SOURCE JOURNAL

FOR CHINESE SCIENTIFIC AND TECHNICAL PAPERS AND CITATIONS

ONCOLOGY AND TRANSLATIONAL MEDICINE

经过多项学术指标综合评定及同行专家评议推荐，贵刊被收录为“中国科技核心期刊”（中国科技论文统计源期刊）。

特颁发此证书。

中国科学技术信息研究所

Institute of Scientific and Technical Information of China

北京复兴路 15 号 100038　　www.istic.ac.cn

2020年12月

证书编号：2019-G616-0093

有效期至：2021年12月